PhD-FSTC-2016-19
The Faculty of Sciences, Technology and Communication

DISSERTATION

Defense held on 03/06/2016 in Luxembourg

to obtain the degree of

DOCTEUR DE L'UNIVERSITÉ DU LUXEMBOURG

EN PHYSIQUE

by

Rick DANNERT
Born on 02 September 1988 in Schkeuditz, (Germany)

DYNAMICS OF VISCOELASTIC COLLOIDAL SUSPENSIONS

Dissertation defense committee

Dr Roland Sanctuary, dissertation supervisor
Professor, Université du Luxembourg

Dr Jörg Baller
Université du Luxembourg

Dr Andreas Michels, Chairman
Associate Professor, Université du Luxembourg

Dr Henning Winter
Professor, University of Massachusetts Amherst

Dr Christian Wagner, Vice Chairman
Professor, Universität des Saarlandes

„Theorien sind gewöhnlich Übereilungen eines ungeduldigen Verstandes, der die Phänomene gern lossein möchte und an ihrer Stelle deswegen Bilder, Begriffe, ja oft nur Worte einschiebt."

Johann Wolfgang von Goethe

Für meine Oma Erna Jacob

Abstract

DYNAMICS OF VISCOELASTIC COLLOIDAL SUSPENSIONS

Dipl. Phys. Rick Dannert

University of Luxembourg, 2016

Supervisor: Prof. Dr. Roland Sanctuary

Co-Supervisor: Dr. Jörg Baller

The influence of different types of nanoparticles on the dynamics of glass forming matrices has been studied by small oscillatory shear rheology. Experimental measurements reveal that besides the glass transition process of the matrix an additional relaxation process occurs in presence of nanoparticles. The latter is identified as the macroscopic signature of the microscopic temporal fluctuations of the intrinsic stress and is called Brownian relaxation. Besides the fact that Brownian relaxation has so far not been observed in colloidal suspensions with a matrix exhibiting viscoelastic behaviour in the frequency range of the experimental probe, the study reveals another important feature to be highlighted: the evolution of the Brownian relaxation times depends non-monotonously on the filler concentration. This finding challenges the use of the classical Peclet-time as a characteristic timescale for Brownian relaxation. Literature defines the Peclet-time as the specific time needed by a particle to cover –via self-diffusion- a distance comparable to its own size. As a main result it will be shown that after replacing the particle size which is relevant for the Peclet time by the mean interparticle distance depending on the filler content the non-monotonic evolution of the relaxation times can be fully described. Moreover, the introduction of the new characteristic length scale allows to include data from literature into the phenomenological description.

Table of Contents

I. Introduction

According to Mewis and Wagner [1] a "colloid refers to the dispersed phase of a two-component system in which the elements of the dispersed phase are too small to be easily observed by an optical microscope and whose motion is affected by thermal forces". In the frame of the present thesis only colloid suspensions are considered where the suspended particles are solid and the suspending medium is a liquid. Besides alimental, pharmaceutical and technological applications colloidal suspensions are of great relevance in research, since the influence of heterogeneities on suspending medium properties are still not completely understood. The complexity of colloidal suspensions arises from the high number of influencing parameters, many-body effects as well as the small size of the colloids. Especially the size of the heterogeneities make it difficult to link macroscopic effects to microscopic origins, since a direct visualization (e.g. by microscopy) is complicated.

Rheology represents an efficient tool to investigate the dynamics of colloidal suspensions and to provide useful information to establish links between structure formation and macroscopic behaviour of the samples.

In a colloidal suspension shear fields can disturb the equilibrium distribution of the fillers resulting in a shear-induced stress. In the past, many authors have reported on the rheological behaviour of colloidal suspensions of rigid spherical particles with hard-sphere potential under steady and oscillatory shear [2-5]. Steady shear experiments revealed the occurrence of shear thinning, which was attributed to the loss of the shear-induced stress contribution to the steady shear viscosity [6, 7]. Generally the transition from Newtonian behaviour to shear-thinning can be described using the classical Peclet number which is known to characterize the relative importance of the contributions of shear flow and Brownian motion to the steady shear viscosity [3].

As shown by van der Werff, et al. [5] and Shikata and Pearson [4] shear induced stress also contributes to the shear moduli measured on colloidal systems under oscillatory shear. At sufficiently low frequencies e. g. the relaxation of shear-induced stress can be detected. The corresponding process is called in the following Brownian relaxation. As an important result the evolution of the relaxation time of shear-induced stress with changing filler content has been shown to correspond to the evolution of the Peclet time [4]. This characteristic scale measures the time needed by a suspended particle to cover a distance equal to its own size by self-diffusion. All of the experimental results described here above stem from investigations performed on colloidal suspensions with matrices which behave as Newtonian liquids in the shear rate/frequency range covered by the probe. Moreover, the samples used for the studies are semi-dilute or concentrated suspensions. The lack of information on the

behaviour of dilute or ultra-dilute suspensions can probably be explained by an argument published in the theoretical work of Lionberger and Russel [8]. According to these authors the strength of the Brownian relaxation scales with a^{-3} (*a:* radius of the suspended particles) and with the volume concentration of suspended particles. To the very best knowledge of the author of the present thesis all of the experiments related to Brownian relaxation described in literature deal with particles with average sizes larger than $40\ nm$. Hence a limitation is imposed on the smallest concentration of nanoparticles for which Brownian relaxation can be resolved by the experimental probe.

Surprisingly, so far no information is available on the relaxation of the shear induced stress in colloidal suspensions where the matrix exhibits viscoelastic behaviour in the frequency range covered by the experimental probe. In this context it is interesting to raise the question whether Brownian relaxation continues to manifest itself, and if so, how it competes with the viscoelastic behaviour of the matrix. Moreover, it is exciting to meet the scientific challenge consisting in the configuration of a highly diluted suspension with the potential to render Brownian relaxation observable. Finally, assuming that Brownian relaxation can be explored throughout the whole range spanning from ultra-dilute to concentrated suspensions, does the Peclet-time remain the adequate time-scale for the description of the phenomenon?

The oligomer Diglycidil ether of Bisphenol A (DGEBA) is a prominent glass former playing an important role for instance as a resin for technologically relevant epoxies used as adhesives or coatings. To enhance the mechanical properties of the epoxies, generally inorganic fillers (SiO_2, Al_2O_3 e.g.) are dispersed in the resin [9-13]. A systematic improvement of the mechanical properties of the nanocomposites requires a deeper understanding of their elastic-, viscoelastic- and flow behaviours. Beside the technological aspects of these behaviours there exists a fundamental interest in the relationship between the mechanical properties of the nanocomposites, the matrix/filler [14] or filler/filler interactions [15] and the associated structure modifications (e.g. network formation [16], interphase formation [17]). At the Laboratory for Physics of Polymers (LPM) of the University of Luxembourg, where the present thesis project was carried out, a lot of research efforts focus on the physical properties of DGEBA and nanocomposites using the oligomer as a matrix. For instance, the investigation of the influence that nanoparticles take on the thermal or dynamical glass transition represents a useful approach to shed light on the mentioned structure-property relationship. In this context calorimetric investigations [18-20] have been realized on DGEBA-SiO_2 composites up to a nanoparticle concentration of 40 weight %: almost no influence of the fillers on the glass transition of the DGEBA matrix has been found. In contrast the same type of measurements carried out on DGEBA-Al_2O_3 suspensions [21] with a maximum filler content of 25 weight % revealed a substantial slowing down of the α-process. While in case of the hydrophobic silica particles matrix-filler interactions seem play a negligible role, DGEBA molecules stick to the hydrophilic alumina aggregates resulting in an increased hydrodynamic radius of the latter. Dynamic shear

experiments [22] reveal a rather simple relaxation behaviour of the matrix: increasing the shear angular frequency at constant temperature yields a direct transition from the terminal regime to the dynamically frozen state.

The original aim of the present PhD project was to investigate the influence of different types of nanoparticles (hydrophobic SiO_2, hydrophilic Al_2O_3) on the viscoelastic behaviour of the oligomer DGEBA. Thereby, at the beginning of the project, the DGEBA/ SiO_2- Al_2O_3 systems were considered as nanocomposites rather than as colloidal suspensions where Brownian relaxation processes could play a role. A first effort therefore consisted in identifying an unexpected low-frequency feature observed in the viscoelastic behaviour of DGEBA-SiO_2 nanocomposites as Brownian relaxation. After this identification, a systematic investigation of Brownian relaxation in various types of colloidal suspensions using DGEBA as a matrix was carried out. Thereby all of the questions and challenges described here above could be tackled. A major concern of the author was to communicate the history of the creation of knowledge in the course of the project to the interested reader.

The thesis is organized as follows: In chapter II some elementary notions of rheology will be presented together with background knowledge on colloidal suspensions. Chapter (III) deals with the materials and experimental tools used for the present study. Chapter (IV) starts with the rheological characterization of the glass former DGEBA, followed by a detailed investigation of the influence of silica particles on the rheological behaviour of the matrix. Next the findings related to the DGEBA/SiO_2 suspension are compared to modified suspensions (suspensions with polymerized DGEBA and systems with alumina nanoparticles instead of silica). Finally, all of the results are compared to data reported in literature. This comparison allows a look at a common relaxation behaviour shared by numerous colloidal suspensions.

II. Theory

The present dissertation focuses on the rheological investigation of colloidal dispersions based on viscoelastic fluids, so-called viscoelastic colloidal suspensions. To give a brief introduction to the topic, the present chapter is divided into two main sections. In the first part elementary notions of rheology are introduced and applied to viscoelastic fluids, especially glass forming materials. The second part describes the dynamics of colloidal particles in a fluid matrix, with special regard to the particles' concentration, interaction potential and shape.

II.1. Rheology of viscoelastic fluids

II.1.1. Introduction to Rheology

Rheological investigations are used for studying the flow behaviour of materials, which are mainly but not only restricted to the liquid state. Rheology is a very powerful tool to investigate the microstructure of soft matter with complex structures such as suspensions, polymers, foods and biological materials [23].

i) Basic notions

Rheology attempts to link a force applied to a material to the resulting deformation or flow [1]. The basic experimental set-up is schematically shown in Figure II-1: a sample is placed between two parallel plates of surface *S*, which are separated by the distance *h.* The lower plate is fixed.

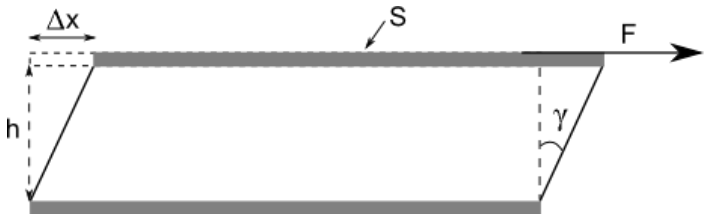

Figure II-1: Schematic representation of the basic idea of Rheology: Two parallel plates of surfaces S separated by h. While the lower plate is fixed, the upper plate is moving due to an applied force F. The resulting stress (force divided by the surface of the upper plate) leads to a deformation γ of the investigated sample.

A tangential force *F* applied to the upper plate leads to a stress

$$\sigma = \frac{F}{S} \qquad (2.1.1.1)$$

and a relative displacement Δx between the upper and the lower plate [23]. The applied stress results in a deformation or strain

$$\tan(\gamma) = \frac{\Delta x}{h} \qquad (2.1.1.2)$$

of the sample. For small deformations ($\Delta x \ll h$) the strain can be approximated by

$$\gamma \approx \frac{\Delta x}{h}. \qquad (2.1.1.3)$$

The shear rate is defined as

$$\dot{\gamma} = \frac{d\gamma}{dt} = \frac{V}{h}, \qquad (2.1.1.4)$$

where *V* represents the velocity of the upper plate, the so-called shear velocity [1, 23, 24].

ii) Perfect solids and fluids under shear

In the last section we have introduced key parameters playing a role in rheological experiments. However the answer of a certain material to an applied stress, strain or shear rate depends on the characteristics of the investigated sample. Therefore in the following section it will be reviewed how samples such as perfect solids and fluids behave under shear deformation.

Perfect solids under deformation

A constant deformation γ of a perfect solid results in a constant shear stress σ for the duration of the experiment (see Figure II-2) [23]. For sufficiently low deformations, Hooke's law is valid:

$$\sigma = G\gamma \qquad (2.1.1.5)$$

where the factor of proportionality between stress and strain is the elastic modulus *G*. Hook's law can be modelled by a spring showing an elongation γ when submitted to a stress σ (see Figure II-3).

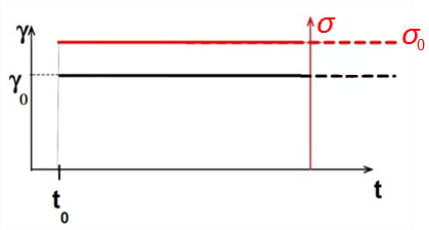

Figure II-2: Strain-step experiment carried out on a perfect solid. At $t = t_0$ a constant deformation γ_0 (black solid line) is applied resulting in a constant stress σ_0 (red solid line)

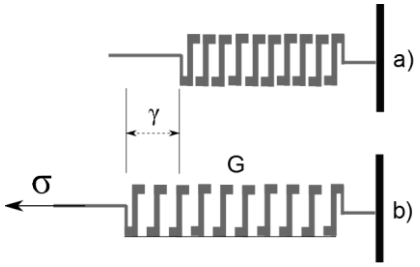

Figure II-3: Schematic representation of the spring model. In case a) no stress is applied to the spring. When a stress σ is applied to the spring the latter will be deformed by γ(case b)

Perfect fluids under deformation

If a strain step experiment (constant deformation for $t \geq t_0$) is performed on a perfect fluid the resulting shear stress is rapidly decaying for times $t \geq t_0$ (see Figure II-4). This behaviour is described by Newton's law

$$\sigma = \eta \dot{\gamma} \qquad (2.1.1.6)$$

indicating that the shear stress is proportional to the shear rate [1]. The proportionality factor corresponds to the fluid viscosity η. The reaction of a perfect fluid to an applied shear stress can be modelled by a dashpot (see Figure II-5). If a stress is applied to a dashpot filled with a liquid of viscosity η, the piston in the dashpot will be displaced at a constant velocity $\dot{\gamma}$ since friction forces oppose the applied external force. In contrast to the behaviour of a perfect solid, the deformation γ imposed by the applied shear stress will remain even after the stress has been removed.

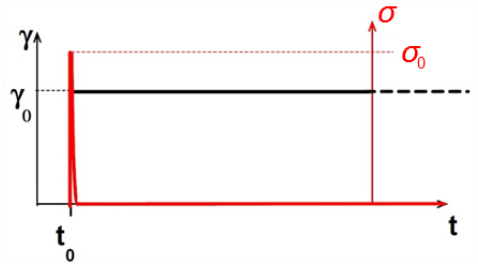

Figure II-4: Strain-step experiment carried out on a perfect fluid. A constant strain γ_0 (black solid line) applied at $t = t_0$ to a perfect liquid sample results in an instantaneously decaying stress σ (red solid line)

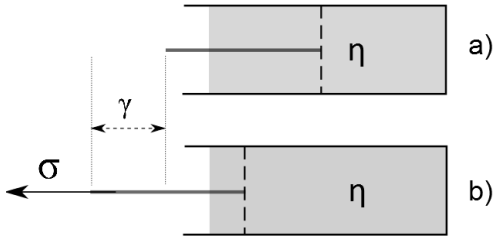

Figure II-5: Schematic representation of the dashpot model. In case a) no stress is applied to the dashpot. When a stress σ is applied to the dashpot the latter will move at constant velocity $\dot{\gamma}$ (case b)

II.1.2. Introduction to viscoelastic fluids

In the following section the concept of viscoelasticity will briefly be introduced. In addition the behaviour of a viscoelastic fluid in simple strain step experiments will be discussed.

i) Definition of viscoelastic fluids

As the name suggests viscoelastic fluids represent a special class of materials which, once submitted to a deformation, exhibit elastic as well as viscous properties [25]. Best known examples of viscoelastic fluids are polymers. When polymers are subject to a deformation, the molecules flow (viscous part) and simultaneously deform (elastic part).

ii) Relaxation modulus

The response of a viscoelastic fluid to a constant deformation can schematically be represented as done in Figure II-6. The application of a constant strain γ_0 results in a monotonously decaying stress. In contrast to Newtonian fluids where the stress decay is instantaneous (see Figure II-4) the stress needs a finite time to decrease from the initial value σ_0 at time point t_0 to zero. The stress decay is described by the relaxation modulus $g(t)$ [25, 26].

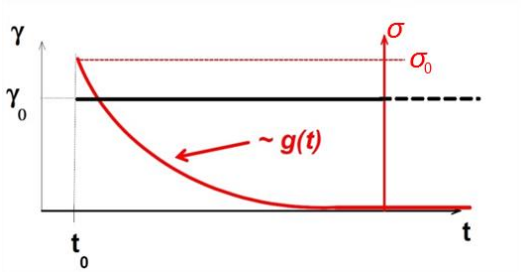

Figure II-6: Strain-step experiment carried out on a viscoelastic fluid. By applying a constant strain γ_0 (black solid line) the stress monotonously decreases from σ_0 at time point t_0 to zero (red solid line). The stress decay is described by the relaxation modulus $g(t)$.

iii) Boltzmann superposition principle

As pointed out in the last paragraph the stress relaxation which can be observed for viscoelastic fluids undergoing a constant deformation γ occurs on finite timescales. Therefore, in case of a viscoelastic sample subjected to subsequent deformations the stress $\sigma(t)$ depends on the entire deformation history (Figure II-7). Especially, in the stress-time diagram (Figure II-7, graph on the right) the difference between the solid black line ($\sigma(t)$ corresponding to subsequent strain-steps at t_0, t_1, t_2 and t_3) and the green line ($\sigma(t)$ associated to a single strain-step at t_1 without any shear history before) illustrates that the stress behaves differently depending on the history.

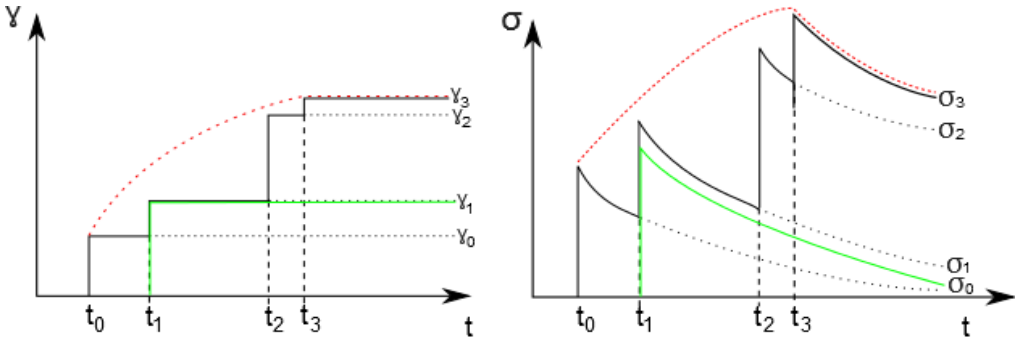

Figure II-7: Illustration of the Boltzmann superposition principle. The left graph illustrate different strain steps, which generate shear stresses (see right graph). The green line indicates the stress relaxation for a single strain step at time t_1 without a strain step at t_0. If a large number of strain steps are applied (red dotted line) the induced stress follows the red dotted line in the right graph

In case of an infinite number of deformations (see red dotted lines in Figure II-7) the shear stress $\sigma(t)$ can be determined by the Boltzmann superposition principle [26]

$$\sigma(t) = \int_{-\infty}^{t} g\left(t - t'\right) \frac{d\gamma}{dt'} dt' , \qquad (2.1.2.1)$$

It has to be noted that the Boltzmann superposition principle in equation (2.1.2.1) relies on linear response theory, which means that the relaxation modulus is independent of the applied strain γ.

iv) Maxwell-model

Until now the relaxation modulus has only been introduced in a phenomenological way. In the following a simple model for viscoelastic fluids is presented. This model allows for a deeper understanding of the relaxation modulus.

To model the behaviour of a viscoelastic fluid Maxwell suggested a serial connection of a spring and a dashpot as schematically represented in Figure II-8 [25, 26].

In case of a serial connection each component is submitted to the same stress σ. If σ_S represents the stress on the spring and σ_D the stress on the dashpot:

$$\sigma = \sigma_S = \sigma_D \qquad (2.1.2.2)$$

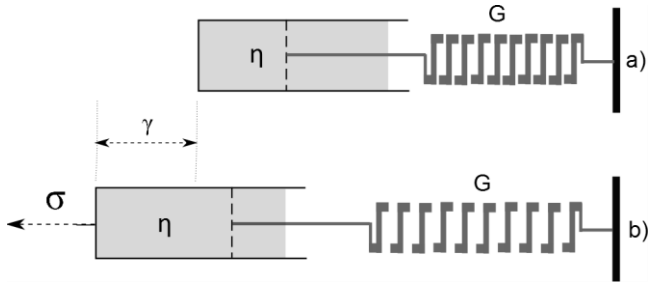

Figure II-8 Schematic representation of the Maxwell model. A spring is connected in series to a dashpot. Case a) shows the serial connection without any stress applied, while for case b) a stress σ is applied to the serial connection resulting a deformation γ

In contrast the resulting deformation γ is the sum of the deformation γ_S of the spring and the deformation γ_D of the dashpot:

$$\gamma = \gamma_S + \gamma_D \qquad (2.1.2.3)$$

The time derivative of equation (2.1.2.3) leads to

$$\frac{d\gamma}{dt} = \frac{d\gamma_S}{dt} + \frac{d\gamma_D}{dt} . \qquad (2.1.2.4)$$

Using Hooke's and Newton's laws (equation (2.1.1.5) and (2.1.1.6)), relation (2.1.2.4) can be written as

$$\frac{d\gamma}{dt} = \frac{1}{G}\frac{d\sigma}{dt} + \frac{\sigma}{\eta} , \qquad (2.1.2.5)$$

with the solution

$$\sigma(t) = G\int_{-\infty}^{t} e^{-G\frac{t-t'}{\eta}} \frac{d\gamma}{dt'} dt' \quad . \tag{2.1.2.6}$$

A comparison of equation (2.1.2.6) with the Boltzmann superposition principle (equation (2.1.2.1)) yields a mathematical expression for the relaxation modulus

$$g(t-t') = Ge^{-\frac{t-t'}{\tau}}, \tag{2.1.2.7}$$

where the characteristic relaxation time τ is defined as

$$\tau = \frac{\eta}{G}. \tag{2.1.2.8}$$

The relaxation modulus in equation (2.1.2.7) can only be used in the case that the relaxation of the shear stress can be described by a single relaxation time τ. This limits the applicability of the Maxwell model to ideal viscoelastic fluids. In real systems, relaxation processes are often broad and generally correspond to a superposition of many modes with characteristic relaxation times and therefore can be described by a so-called generalized Maxwell model. The latter corresponds to a parallel connection of *n* single Maxwell models with a relaxation modulus [27]

$$g(t-t') = \sum_i G_i e^{\frac{t-t'}{\tau_i}} . \tag{2.1.2.9}$$

With equation (2.1.2.9) the shear stress relaxation of any viscoelastic fluid can be described, even if different relaxation processes are involved. However the disadvantage of the generalized Maxwell model is that for each relaxation mode two parameters i.e. G_i and τ_i are needed which rapidly leads to a high number of parameters to describe real systems [28].

v) Special form of viscoelastic fluids: Glass-formers

A special class of viscoelastic fluids are glass forming liquids. When such materials are cooled they exhibit a transition from the liquid to the glassy state, the so-called thermal glass transition. The temperature at which this transition takes place is called glass transition temperature T_g . A material in the glassy state behaves like a solid without possessing translation symmetry such as crystals. When a susceptibility of a material is determined with a dynamic measurement, a liquid-to-solid transition can also be observed for temperatures $T > T_g$, when the experimental timescale (t_{exp}) crosses the intrinsic characteristic timescale τ_α. τ_α is the characteristic time needed by a material to restore the equilibrium state after a perturbation (e.g. by a change of temperature). This transition is called dynamic glass transition.

Intrinsic characteristic timescale τ_α

For strong glass former (in thermodynamic equilibrium) the temperature dependency of the relaxation time τ_α obey to the Arrhenius law

$$\tau_\alpha = \tau_{\alpha,0} e^{\frac{\Delta G}{k_B T}}, \qquad (2.1.2.10)$$

with $\tau_{\alpha,0}$ the relaxation time at infinite temperatures, k_B the Boltzmann constant and ΔG the activation enthalpy [29]. In contrast for fragile glass formers the relaxation times τ_α scale with the Vogel-Fulcher-Tammann (VFT) equation (see Figure II-9)

$$\tau_\alpha = \tau_{\alpha,0} e^{\frac{\Delta G}{k_B (T - T_V)}}, \qquad (2.1.2.11)$$

where T_V represents the Vogel temperature [30]. For a dynamic experiment at temperatures above the thermal glass transition, we can distinguish three cases:

i) In case of $t_{exp} \gg \tau_\alpha$ the molecules are able to react to the perturbation. The measured susceptibility is the one of the liquid state.

ii) In case of $t_{exp} \ll \tau_\alpha$ the molecules cannot follow the perturbation. The susceptibility of the solid state will be measured.

iii) For experiments where $t_{exp} \approx \tau_\alpha$, the susceptibility shows relaxation behaviour.

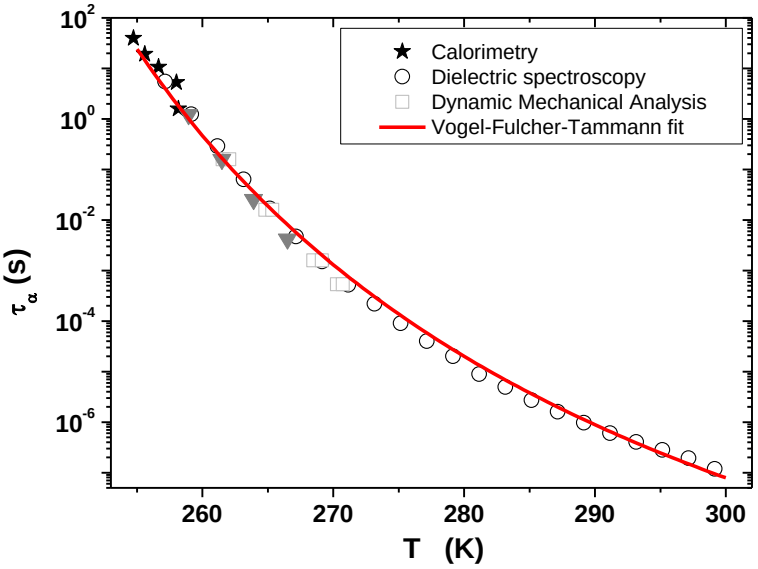

Figure II-9: Activation diagram $\tau_\alpha(T)$ of Diglycidyl Ether of Bisphenol A (DER331) obtained from measurements using different methods as calorimetry, dielectric spectroscopy and dynamic mechanical analysis. The red solid line represents the Vogel-Fulcher-Tammann law from equation (2.1.2.11) with parameters $\Delta G = 204 \frac{J}{mol}, \tau_{0,\alpha} = 8.36 \cdot 10^{-15} s$ and $T_V = 211K$.

Glass transition temperature T_g

A unique definition and determination of the glass transition temperature is difficult since T_g depends on the cooling rate and in case of dynamic measurements on the applied frequency. One of the most used methods for detection of T_g is differential scanning calorimetry (DSC). This method is based on the measurement of the increase in specific heat of the material as it passes from the glassy to the liquid state. Furthermore mechanical methods like oscillatory shear rheology can be used. By measuring the temperature evolution of the viscosity the glass transition temperature is defined as the temperature at which $\eta = 10^{12.3} Pa.s$ [31].

II.1.3. Dynamic rheology of viscoelastic fluids

In the last section viscoelastic fluids and their relaxation behaviour in simple strain step experiments has been introduced. In the following part the discussion will be extended to the relaxation behaviour of viscoelastic fluids subjected to oscillatory strain experiments.

i) Dynamic rheology

Dynamic rheology is referred to rheological investigations where a time dependent oscillatory strain

$$\gamma(t) = \gamma_0 \sin(\omega t) \tag{2.1.3.1}$$

is applied to the sample. In equation (2.1.3.1) γ_0 represents the strain amplitude and ω the angular frequency[1]. From equation (2.1.3.1) follows the shear rate

$$\dot{\gamma}(t) = \gamma_0 \omega \cos(\omega t). \tag{2.1.3.2}$$

When $\gamma_0 \ll 1$, the relaxation modulus is independent of the strain amplitude: the Boltzmann superposition principle can be applied (linear response). In this case the linear viscoelastic properties of the sample are investigated and the rheological measurement method is referred to as Small Amplitude Oscillatory Shear (SAOS).

From the Boltzmann superposition principle (equation (2.1.2.1)) it follows that in case of an oscillating strain the time dependency of the stress can be described by

$$\sigma(t) = \omega \gamma_0 \int_{-\infty}^{t} g(s) \cos(t-s) ds. \tag{2.1.3.3}$$

with $s = t - t'$. Using $\cos(x-y) = \sin(x) \cdot \sin(y) + \cos(x) \cdot \cos(y)$ equation (2.1.3.3) transforms into [1]

$$\sigma(t) = G'(\omega) \gamma_0 \sin(\omega t) + G''(\omega) \gamma_0 \cos(\omega t), \tag{2.1.3.4}$$

where

[1] From now –for reasons of simplicity- ω is called frequency.

$$G'(\omega) = \omega \int_0^{+\infty} g(s)\sin(\omega s)ds \qquad (2.1.3.5)$$

is the shear storage modulus, and

$$G''(\omega) = \omega \int_0^{+\infty} g(s)\cos(\omega s)ds \qquad (2.1.3.6)$$

represents the shear loss modulus. Inspection of equation (2.1.3.4) yields that the storage modulus $G'(\omega)$ is related to the stress term which oscillates in phase with the strain, whereas $G''(\omega)$ is linked to the stress term oscillating in phase with the shear rate. Consequently $G'(\omega)$ and $G''(\omega)$ characterize the elastic and the viscous response respectively of the investigated material [1, 23, 24, 28]. The viscoelastic behaviour of a sample can also be described by the complex shear viscosity defined as

$$\eta^*(\omega) = \eta'(\omega) + i\eta''(\omega) \qquad (2.1.3.7)$$

where the real part

$$\eta'(\omega) = \frac{G''(\omega)}{\omega} = \int_0^{+\infty} g(s)\cos(\omega s)ds \qquad (2.1.3.8)$$

is linked to the loss shear modulus and the imaginary part

$$\eta''(\omega) = \frac{G'(\omega)}{\omega} = \int_0^{+\infty} g(s)\sin(\omega s)ds \qquad (2.1.3.9)$$

to the storage shear modulus.

ii) Viscoelastic fluids: Modelling of results from SAOS experiments

Maxwell-Model

The Maxwell model introduced in section II.1.2 yields an exponentially decaying relaxation modulus *g(s)* (equation (2.1.2.7)). Substituting *g(s)* into equations (2.1.3.5) and (2.1.3.6) leads to

$$G'(\omega) = G\frac{(\omega\tau)^2}{1+(\omega\tau)^2} \qquad (2.1.3.10)$$

and

$$G''(\omega) = G\frac{\omega\tau}{1+(\omega\tau)^2}. \qquad (2.1.3.11)$$

The frequency dependencies of the shear moduli $G'(\omega)$ and $G''(\omega)$ from equation (2.1.3.10) respectively (2.1.3.11) are shown in Figure II-10 for the case $\tau \stackrel{\text{def}}{=} 1\ s$ and $G \stackrel{\text{def}}{=} 1\ Pa$ (double logarithmic representation).

For $\omega\tau \ll 1$ equations (2.1.3.10) and (2.1.3.11) yield the power laws

$$G'(\omega) \propto \omega^2 \qquad (2.1.3.12)$$

$$G''(\omega) \propto \omega \qquad (2.1.3.13)$$

describing the low frequency tails of the shear moduli. This specific behaviour, which is characteristic for viscoelastic fluids and therefore independent of the used model, is called terminal regime behaviour.

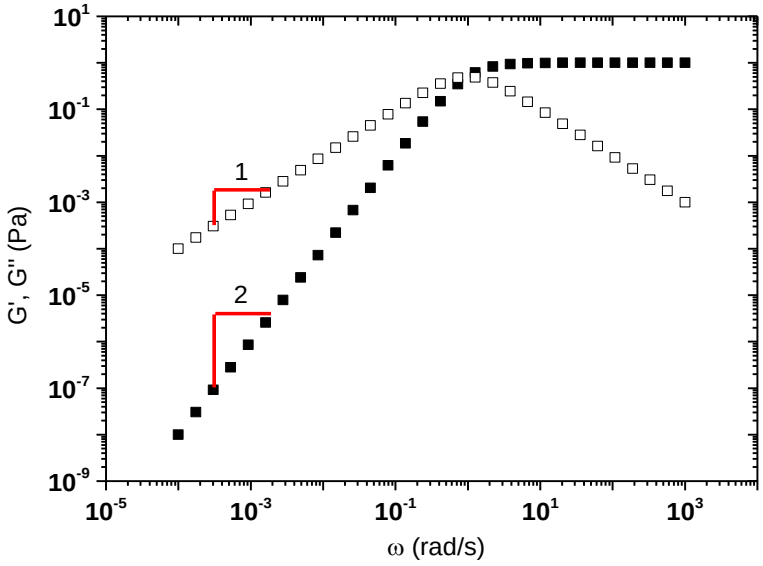

Figure II-10: Double logarithmic representation of the shear moduli $G'(\omega)$ (closed symbols) and $G'(\omega)$ (open symbols) as function of the frequency obtained by the Maxwell model using $\tau \stackrel{\text{def}}{=} 1\ s$ and $G \stackrel{\text{def}}{=} 1\ Pa$. For $\omega \ll 1\ rad/s$ (e.g $\omega\tau \ll 1$) the Maxwell model predicts a fluid-like behaviour as $G''(\omega) > G'(\omega)$, whereas for $\omega \gg 1\ rad/s$ ($\omega\tau \gg 1$) a solid-like behaviour ($G''(\omega) < G'(\omega)$) is observed

Generalized Maxwell-Model

If materials with complex relaxation behaviours are studied the Maxwell model is not useful for the description of the relaxation or shear moduli. However it has been shown that a superposition of single Maxwell relaxations (generalized Maxwell model) can describe any material [27]. Using the generalized relaxation modulus from equation (2.1.2.9) the shear moduli can be written as

$$G'(\omega) = \sum_i G_i \frac{(\omega\tau_i)^2}{1+(\omega\tau_i)^2} \qquad (2.1.3.14)$$

and

$$G''(\omega)=\sum_i G_i \frac{\omega\tau_i}{1+(\omega\tau_i)^2}\,. \qquad (2.1.3.15)$$

Similar to the relaxation modulus the generalized shear moduli are superposition of shear moduli obtained from single Maxwell models [32]. Equations (2.1.3.14) and (2.1.3.15) can be used to fit experimental data. The parameters G_i and τ_i yielded by the fit can be represented in a G_i -τ_i plot leading to a so-called parsimonious spectrum (see black points in Figure II-11) [33].

Baumgärtel-Schausberger-Winter (BSW)-Model

Similar to the approach for the generalized Maxwell model the shear moduli can be written as integrals of shear moduli corresponding to the Maxwell model [33-36]

$$G'(\omega)=\int_0^\infty \frac{H(\tau)}{\tau}\frac{(\omega\tau)^2}{1+(\omega\tau)^2}d\tau \qquad (2.1.3.16)$$

$$G''(\omega)=\int_0^\infty \frac{H(\tau)}{\tau}\frac{\omega\tau}{1+(\omega\tau)^2}d\tau\,, \qquad (2.1.3.17)$$

where $H(\tau)$is the relaxation time probability distribution function. Baumgaertel and Winter [33] showed that for several materials the parsimonious spectrum can be described by a power-law

$$H(\tau)=\frac{G}{n}\left(\frac{\tau}{\tau_{\max}}\right)^n \qquad (2.1.3.18)$$

where $0<n<1$ represents the power-law exponent and τ_{max} the longest relaxation time in the parsimonious spectrum [37] (see graph (a) in Figure II-11). As the distribution function in equation (2.1.3.18) monotonously increases and diverges for $\tau \to \infty$, the upper integration limits in equations (2.1.3.16) and (2.1.3.17) have to be replaced by τ_{max}. As a consequence the mode with the characteristic time $\tau = \tau_{max}$ yields the highest contribution to the shear moduli. For some materials the parsimonious spectrum exhibits a maximum (see graph (b) in Figure II-11). To properly describe these materials Baumgaertel and Winter [33] have extended $H(\tau)$ to a stretched exponential power-law distribution function

$$H(\tau)=\frac{G}{n}\left(\frac{\tau}{\tau_{\max}}\right)^n e^{-\left(\frac{\tau}{\tau_{\max}}\right)^\beta}\,, \qquad (2.1.3.19)$$

with $0<\beta<1$ [37]. In contrast to the power-law given by equation (2.1.3.18) the stretched exponential power-law function converges to zero for $\tau \to \infty$. This implies that equations (2.1.3.16) and (2.1.3.17) can be used with infinity as an upper integration limit.

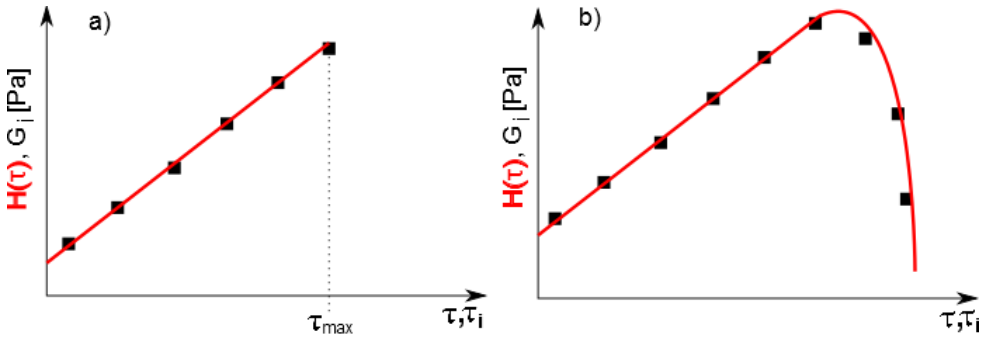

Figure II-11: Schematic representation of parsimonious spectra (black points), as well as the attributed distribution functions $H(\tau)$. The left graph a) shows a material, for which the relaxation time distribution is given by a power-law expression, whereas the right graph b) represents a system with a relaxation process following a stretched exponential power-law function as relaxation time distribution

II.1.4. Frequency-Temperature-Superposition principle

In the last section the discussion of the shear moduli G' and G'' has been restricted to the frequency dependency. However the shear moduli depends also - via the elastic modulus G and the relaxation time τ - on the temperature T. To illustrate the influence of temperature on the shear moduli the analytic expressions for G' and G'' obtained from the Maxwell model (equations (2.1.3.10) and (2.1.3.11)) can be used leading to

$$G'(\omega,T)=G(T)\frac{(\omega\tau(T))^2}{1+(\omega\tau(T))^2} \tag{2.1.4.1}$$

and

$$G''(\omega,T)=G(T)\frac{\omega\tau(T)}{1+(\omega\tau(T))^2}\,. \tag{2.1.4.2}$$

Both temperature dependent quantities $\tau(T)$ and $G(T)$can be replaced by

$$\tau(T)=a_T\tau(T_{ref}) \tag{2.1.4.3}$$

and

$$G(T)=b_T G(T_{ref})\,, \tag{2.1.4.4}$$

where $\tau(T_{ref})$ and $G(T_{ref})$ stand for the relaxation time respectively the elastic modulus at a certain reference temperature T_{ref} and

$$a_T=\frac{\tau(T)}{\tau(T_{ref})} \tag{2.1.4.5}$$

as well as

$$b_T=\frac{G(T)}{G(T_{ref})} \tag{2.1.4.6}$$

are material dependent parameters. Consequently the shear moduli can be written as

$$G'(\omega,T)=b_T G(T_{ref})\frac{\left(a_T\omega\tau(T_{ref})\right)^2}{1+\left(a_T\omega\tau(T_{ref})\right)^2}=b_T G'\left(a_T\omega,T_{ref}\right) \qquad (2.1.4.7)$$

and

$$G''(\omega,T)=b_T G(T_{ref})\frac{a_T\omega\tau(T_{ref})}{1+\left(a_T\omega\tau(T_{ref})\right)^2}=b_T G''\left(a_T\omega,T_{ref}\right). \qquad (2.1.4.8)$$

The latter expressions clearly illustrate that shear moduli G' and G'' measured at a temperature *T* and frequency ω are equivalent to shear moduli $b_T G'$ and $b_T G''$ at reference temperature T_{ref} and frequency $a_T\omega$. The relation between temperature and frequency is the main statement of the frequency-temperature-superposition (FTS-) principle. The FTS-principle is especially useful to obviate experimental technique limitations, which arise due to the restricted frequency window of conventional rheometers. In fact commercial rheometer cover in general 2-3 decades, whereas relaxation processes of glass formers or polymeric systems can extent over much more frequency (time) decades [28]. Therefore in order to artificially extend the frequency window, shear moduli can be measured at different temperatures within the available frequency window of the rheometer and, via the parameters a_T and b_T, merged together into single curves of shear moduli at a certain reference temperature but over a wide frequency range.

The technical meaning of a_T and b_T becomes clear, when reformulating equations (2.1.4.7) and (2.1.4.8) in a double logarithmic way:

$$\log\left[G'(\log(\omega),T)\right]=\log\left[b_T\right]+\log\left[G'\left(\log\left(a_T\right)+\log\left(\omega\right),T_{ref}\right)\right] \qquad (2.1.4.9)$$

and

$$\log\left[G''(\log(\omega),T)\right]=\log\left[b_T\right]+\log\left[G''\left(\log\left(a_T\right)+\log\left(\omega\right),T_{ref}\right)\right]. \qquad (2.1.4.10)$$

According to equations (2.1.4.9) and (2.1.4.10) $log(b_T)$ reflects a vertical shift, while $log(a_T)$ indicates a horizontal shift on the frequency axis [28, 38].

In general the exact analytical expressions of a_T and b_T depend on the considered material [38, 39]. However if fragile glass formers are studied the expression for the horizontal shift factor a_T follows the William-Landau-Ferry (WLF) equation [26]

$$\log\left(a_T\right)=-C_1\frac{T-T_{ref}}{C_2+T-T_{ref}}, \qquad (2.1.4.11)$$

with $C_1 = \log(e)\frac{\Delta G}{R\left(T_{ref} - T_V\right)}$ and $C_2 = T_{ref} - T_V$. In contrast the expression of the vertical shift factor b_T arises directly from the definition of the elastic modulus G:

$$\log\left(b_T\right) = \log\left(\frac{\rho\left(T_{ref}\right)T_{ref}}{\rho(T)T}\right) \qquad (2.1.4.12)$$

with ρ the mass density.

Albeit the temperature dependency of G' and G'' has been illustrated on the shear moduli obtained from the Maxwell model, the equivalence between frequency and temperature can be generalized to any material, for which the shear moduli can be described by the generalized Maxwell model as the latter represents a sum a single Maxwell modes.

II.2. Colloidal suspensions

II.2.1. Introduction to colloidal suspensions

Colloidal suspensions are two-component systems, where the dispersed phase is usually referred to as colloid and the continuous phase as suspending medium [1]. By definition colloids are mesoscopic objects with dynamics generally affected by Brownian motion [30]. Colloidal suspensions play a role in foods, coatings or biological systems. Some examples of daily life products are milk, ink, blood, or mayonnaise.

The following sections will provide some basic information on solid particles suspended in Newtonian or viscoelastic liquids. First a single sphere embedded in a Newtonian liquid is considered.

The motion of a single sphere within a Newtonian liquid is determined by the forces acting on the particle. If a particle is immerged in a liquid it is first of all subjected to gravity. Taking into account buoyancy the apparent gravitational force F_g acting on a sphere with radius a and density ρ_p can be written as [2]

$$F_g = \frac{4}{3}\pi\left(\rho_p - \rho_m\right)a^3 g \qquad (2.2.1.1)$$

where ρ_m is the medium density and g the gravitational acceleration. Thus, if $\rho_p > \rho_m$ and no other forces are acting, the particle will settle. However, for a particle moving in a fluid environment, frictions between the particle and the fluid lead to Stokes' drag

$$F_H = 6\pi\eta_m aV\,, \qquad (2.2.1.2)$$

where V stands for the velocity of the sphere [1]. Since hydrodynamic forces act contrary to the velocity direction of the particle, they retard the particle sedimentation.

However if a colloid is considered sedimentation is generally avoided due to the balancing action of the Brownian force

$$F_B = \frac{k_B T}{a} \tag{2.2.1.3}$$

which for colloidal particles is of the same order of magnitude as F_g. The Brownian force arises from permanent collisions between medium molecules and the particle leading to a non-directional diffusive motion of the sphere. Einstein and Smoluchowski independently of each other showed that the mean square displacement $\langle \Delta l^2 \rangle$ of the particle increases linearly with time (see Figure II-12) [40, 41]:

$$\left\langle \Delta l^2 \right\rangle = 6 D_0 t \tag{2.2.1.4}$$

In equation (2.2.1.4) D_0 represents the Einstein-Smoluchowski diffusion coefficient, which for a spherical particle can be written as [41]

$$D_0 = \frac{k_B T}{6\pi \eta_m a} \tag{2.2.1.5}$$

with η_m the matrix viscosity.

II.2.2. Colloids in Newtonian liquids

In the last section the exemplary case of a single sphere embedded in a fluid matrix has been discussed. However the situation becomes much more complex when several colloids are embedded in a liquid, since in that case, interactions between particles can affect the particle dynamics. The motion of a particle will be affected by direct interparticle interactions e.g. by collisions with surrounding colloids. Moreover the motion of neighbouring particles leads to hydrodynamic interactions. Clearly these interactions as well as the interplay between them depend on parameters as the particle concentration, the interaction potentials and the shape of the particles.

For the general introduction of the topic the particles are assumed to be electrically neutral hard spheres of radius *a*: two particles only interact directly when the distance between their center is equal to 2a. Direct collisions between particles affect the Brownian motion of a tagged particle in the colloidal suspension and lead to different diffusive regimes as shown in Figure II-12 [42-44]. To illustrate the regimes, a simple thought experiment can be considered.

At $t = 0$ the particles are supposed to be well dispersed. Therefore at short times the tagged particle will exhibit a diffusive motion (region I in Figure II-12) without any direct collisions with the other particles leading to a mean square displacement

$$\left\langle \Delta l^2 \right\rangle_{t \ll \tau_i} = 6 D_S t \tag{2.2.2.1}$$

where D_S is the short-time self-diffusion coefficient (equation 2.2.1.5) [44]. Even without particle-particle collisions, the tagged particle feels the hydrodynamic

interactions of the surrounding particles. Albeit the exact description of hydrodynamic interactions is still a matter of research [45-49], it is known that they disturb the diffusive motion of the tagged particle. Their effect becomes visible in the suspension viscosity

$$\eta_{HI} = \eta_m f_{HI}(x) \qquad (2.2.2.2)$$

where '*HI*' refers to included hydrodynamic interactions, η_m describes the matrix viscosity and $f_{HI}(x)$ is a function depending on the filler concentration [50-52]. The exact expression of $f_{HI}(x)$ will be discussed in subsection i) of this chapter.

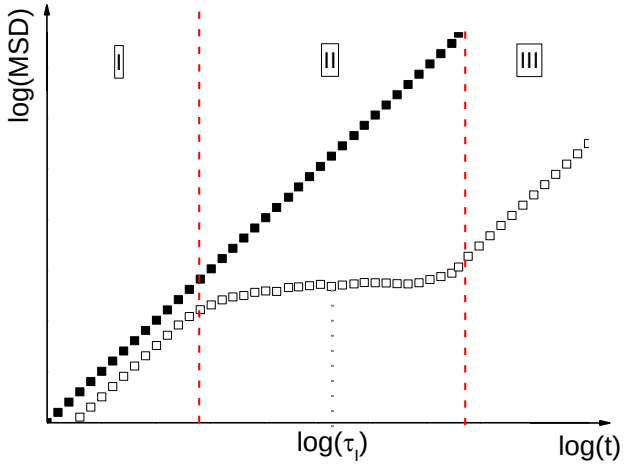

Figure II-12: Schematic representation of the logarithmic mean square displacement (MSD) $log(\langle \Delta l^2 \rangle)$ as a function of the logarithmic timescale $log(t)$. The open symbols represent the expected mean square displacement of a tagged particle embedded in a bath of surrounding particles, whereas the close symbols indicate the time evolution of the MSD for a single particle in a liquid [43, 44, 46]. The grey dotted line indicates the characteristic time $log(\tau_I)$(see text)

The short-time self-diffusion coefficient in equation (2.2.2.1) is expressed by the Stokes-Einstein-relation [53]

$$D_S = \frac{k_B T}{6\pi\eta_{HI} a}. \qquad (2.2.2.3)$$

The Stokes-Einstein relation corresponds to the expression of the Einstein-Smoluchowski self-diffusion coefficient (equation 2.2.1.5) with the exception that the matrix viscosity η_m is replaced by the suspension viscosity η_{HI} . After a characteristic time τ_I (see Figure II-12) inter-particle collisions start to hinder the tagged particle to move on substantially: it is trapped in a cage formed by surrounding particles (cage effect).The zone II in Figure II-12 represents the sub-diffusive motion regime [43]. For $t \gg \tau_I$, the tagged particle has enough time available to escape the cage formed by the neighbouring particles and enters in a diffusive motion regime again (long-time self-diffusion regime III in Figure II-12). In this regime the mean square displacement of the tagged particle obeys to

$$\left\langle \Delta l^2 \right\rangle_{t \gg \tau_i} = 6 D_L t \qquad (2.2.2.4)$$

with D_L the long-time self-diffusion coefficient [54]. As in regime III the tagged particle permanently undergoes collisions, D_L is generally smaller than the short-time self-diffusion coefficient D_S [55, 56]. In a first approach the long-time self-diffusion coefficient is expressed by the Stokes-Einstein-relation

$$D_L = \frac{k_B T}{6 \pi \eta_0 a} \qquad (2.2.2.5)$$

where η_0 represents the zero shear viscosity [57]. η_0 can be written as the sum of two terms

$$\eta_0 = \eta_{HI} + \eta_B . \qquad (2.2.2.6)$$

While the first term represents the contribution of equation (2.2.2.2) to the zero shear viscosity, the second term is referred in literature as Brownian contribution [1].

i) Influence of the particle concentration

There are different ways to express the amount of particles in a system. As a first approach the mass concentration of particles

$$x_m = \frac{m_p}{m_p + m_f} \qquad (2.2.2.7)$$

can be used, where m_p stands for the particle and m_f for the fluid mass. The mass concentration can directly be determined using the masses of the particles. However for a better comparison between different suspensions the volume concentration

$$x_V = \frac{V_p}{V_p + V_f} \qquad (2.2.2.8)$$

is often used in literature, with V_p the particle and V_f the fluid volume.

It has been shown that colloidal suspensions undergo different phases depending on the volume concentrations [1]. As can be seen in Figure II-13 until the particle glass transition concentration $x_{V,g} \approx 0.58$ hard sphere dispersions exhibit a fluid behaviour. Around this concentration the dynamics of the particles especially long-time self-diffusion behaviour start to freeze due to the lack of possible cage escaping of the particles. However a glass with liquid-like behaviour can persist until a maximum packing fraction of $x_{V,rcp} \approx 0.638$ [1]. Above this concentration no places for further particles are available when a random packing is performed.

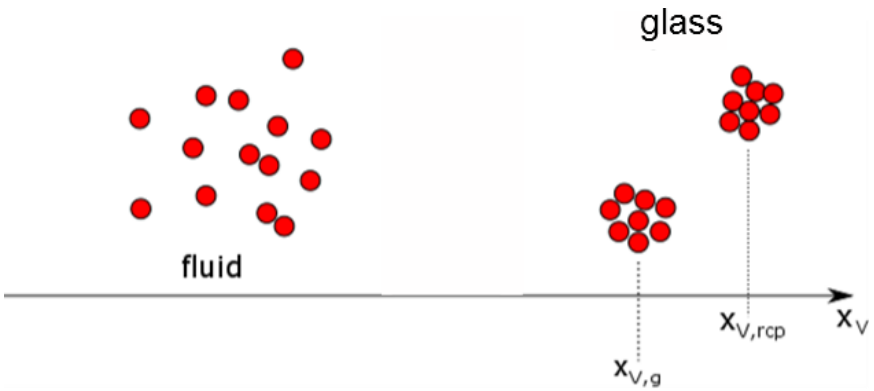

Figure II-13: Hard sphere dispersion phase diagram, $x_{V,g}$ and $x_{V,rcp}$ stand for the particle glass transition respectively the randon close packing limits

As mentioned in the last paragraph η_{HI} and η_0 are quantities which strongly depend on the volume concentration. A semi-empirical representation was introduced by Krieger-Dougherty predicting that the volume concentration dependency of the viscosities can be written as [1, 52]

$$\eta_i = \eta_m \left(1 - \frac{x_V}{x_{V,\max,j}} \right)^{-[\eta] x_{V,\max,j}}, \qquad (2.2.2.9)$$

where $[\eta]$ stands for the so-called intrinsic viscosity [1], *i* for the index defining the considered viscosities η_{HI} or η_0 and *j* for an index referring to the maximum packing limits $x_{V,g}$ or $x_{V,rcp}$. In case of hard sphere dispersions the exponent $[\eta]. x_{V,max,j}$ has been shown to be equal to 2.5 [1, 58]. Equation (2.2.2.9) shows that the viscosities η_{HI} and η_0 increases with the volume concentration until a well-defined concentration $x_{V,max,j}$, at which they diverge. It has been shown that the viscosity η_{HI} diverges at the random close packing concentration $x_{V,rcp}$, whereas the zero-shear viscosity diverges at the particle glass transition concentration $x_{V,g}$ [51, 57]. The difference in the divergence behaviour of the viscosities arises from the increasing importance of the Brownian contribution η_B to the zero shear viscosity. Theoretical calculations [59], Mode-coupling-theory (MCT) [60] and experimental results [61] predict that η_B diverges at the particle glass transition concentration $x_{V,g}$ because of the jamming associated with random close packing i.e. particles become arrested due to an infinite long cage effect. In addition Brady [62] predicted that η_B scales with the square of the volume concentration i.e $\eta_B \propto {x_V}^2$.

Depending on the volume concentrations, dispersions are defined as dilute, semi-dilute or concentrated. The definition of a dilute dispersion is attributed to the concentration range for which the Krieger-Dougherty relation can be linearized [63], leading to Einstein's prediction [2, 51]

$$\eta_i = \eta_m \left(1 - 2.5 x_V \right) \qquad (2.2.2.10)$$

Equation (2.2.2.10) holds true for volume concentrations below 0.02. In this concentration range the viscosities η_{HI} and η_0 are similar, as contributions with higher

orders in the volume concentration ($\mathcal{O}(x_V^2)$) i.e. the contribution η_B can be neglected. The classification of concentrated suspensions is not such concrete. Often concentrated dispersions are referred to suspensions where the viscosities are strongly increasing with the volume concentration and where non-Newtonian effects such shear-thinning are quite relevant [63]. Therefore in literature the concentration range of concentrated dispersions is tentatively defined by $x_V \geq 0.25$. In between i.e. $0.02 \leq x_V \leq 0.25$ suspensions are called semi-dilute.

ii) Influence of interparticle interactions

In the last subsection dispersions with hard spheres have been discussed i.e. no particle-particle interactions (except for the hard sphere potential, i.e. collisions) have been considered. However, in many suspensions interactions between particles cannot be neglected.

In fact even for electrically neutral spheres the sheer approach of two small particles leads to short-range attractive van-der-Waals interactions, which can result in aggregation or even flocculation [64, 65]. Also the chemical composition of the particles' surfaces plays a role for the formation of aggregates [51]. For technical applications, a good dispersion of the filler particles in the suspensions is generally desired. In order to avoid aggregation, the particles are often electrostatically charged or enclosed by a steric layer [66]. As a consequence, the excluded volume which is inaccessible for other particles increases, which in turns leads to the introduction of so-called effective volume concentrations. The expression

$$x_{V,eff} = x_V \left(\frac{a_{eff}}{a} \right)^3 \tag{2.2.2.11}$$

is often used assuming the particles to be hard spheres with an effective radius $a_{eff} = a + \Delta$, where Δ describes the thickness of the repulsive interaction layer [51]. Since the values for Δ are mostly unknown, the divergence of the viscosity as a function of particle concentration can be used to determine the relation between x_V and $x_{V,eff}$:

$$\frac{x_{V,eff}}{x_V} = \frac{x_{V,eff,\max,j}}{x_{V,\max,j}} \tag{2.2.2.12}$$

where $x_{V,max,j}$ is the volume concentration at which the viscosity (η_{HI} or η_0) diverges in measurements and $x_{V,eff,max,j}$ stands for the volume concentration at which the viscosities should theoretically diverge ($x_{V,eff,rcp} \approx 0.638$ and $x_{V,eff,g} \approx 0.58$).

iii) Influence of the particle shape

Until now the discussion has been restricted to spherical particles. But even in dispersions with spherical particles, aggregation due to surface interactions or flocculation generated from attractive interparticle forces can lead to complex fractals, which can no longer be treated as spherical particles.

First concerning the suspension viscosity the intrinsic viscosity $[\eta]$ will be strongly dependent on the fractal dimension of the particles and can become indefinitely large depending on the kind of aggregates [67]. In addition the viscosities have been shown to diverge at much smaller volume concentrations $x_{V,max,j}$. This effect results first from the aggregation process, which increases the volume concentration with respect to the nominal concentration x_V of the primary particles. Second above a critical concentration called percolation threshold the clusters interconnect leading to a solid like behaviour [51]. However it has been shown that these clusters can also be assimilated to effective spheres [68] (see Figure II-14), which generates again an effective volume concentration

$$x_{V,eff} = x_V \left(\frac{R}{a} \right)^{3-f}, \qquad (2.2.2.13)$$

where *a* stands for the radius of primary particles, *R* for the radius of the assimilated sphere including the cluster and *f* for the fractal dimension [51]. For chemical reaction limited cluster aggregation *f* is typically equal to *2.1.* Again the transition from a nominal to an effective concentration can be obtained using equation (2.2.2.12) if no detailed knowledge of the cluster sizes is available.

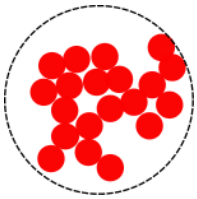

Figure II-14: Schematic representation of a cluster of aggregated primary particles (red spheres) with radius a. The black dashed line indicates the assimilation of the cluster to a sphere of radius R.

Besides the effects on the concentration dependency of the suspension viscosity, the particle shape influences also the diffusion behaviour of the particles. In case of non-spherical particles, the latter exhibit rotational diffusion processes additionally to translational. Similar to the time dependency of the mean square displacement in case of translational diffusion a mean square angle rotation can be defined $\langle \theta^2 \rangle = 6D_r t$ with

$$D_r = \frac{k_B T}{8\pi\eta R^3} \qquad (2.2.2.14)$$

the rotational diffusion coefficient for a cluster assimilated to a sphere of radius *R* [69].

III. Materials and Experimental setup

III.1. Materials

III.1.1. Suspending matrices

The low-molecular weight glass former Diglycidyl ether of Bisphenol A (DGEBA) is a basic component of the matrix in all of the colloidal suspensions investigated in this project. The chemical structure of the molecule is shown in Figure III-1. At both extremities the DGEBA molecule possesses a reactive epoxy group (-$OCHCH_2$: oxiran ring). The degree of polymerization *n* defines the number of hydroxyl groups (-OH).

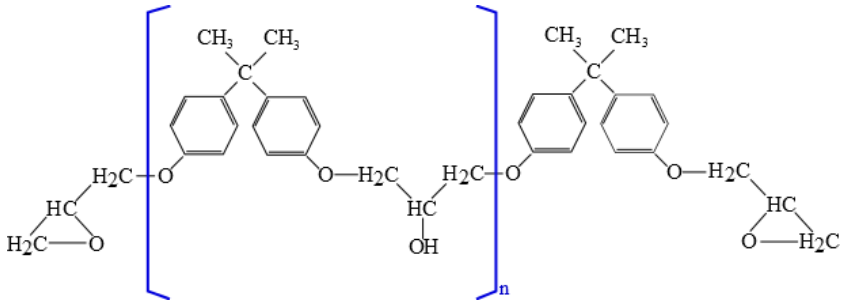

Figure III-1: Chemical structure of a Diglycidyl ether of Bisphenol A (DGEBA) molecule. n represents the degree of polymerization

The number average molecular weight of DGEBA is given by [28]

$$M_n = 340 + 248n \text{ [g/mol]}. \qquad (3.1.1.1)$$

DGEBA matrices

A part of the experimental investigations has been realized with a DGEBA matrix with a degree of polymerization $n \to 0$. Thus the corresponding samples are mainly formed by DGEBA monomers (see Figure III-3). Depending on the nature of the nanoparticles which have been dispersed in the DGEBA matrix the oligomer was purchased either from (see section III.1.2)

- DOW plastics (Germany, DER331) or
- Nanoresins AG (Germany, DER distilled)

Even if the resins stem from different companies both, their thermic and rheological properties are similar [28]. Therefore in the following no differentiation will be made between the two types of matrices. It has been shown that both types of matrices behave as a simple viscoelastic fluid undergoing a glass transition around $T_g \approx 257K$ [18].

Polymerized DGEBA matrices

By curing DGEBA monomers with Bisphenol A (BPA), DGEBA matrices with a higher degree of polymerization can be obtained. The chemical structure of a Bisphenol A molecule is shown in Figure III-2. The two primary hydroxyl groups (-OH) of BPA are able to react with the epoxy groups (-$OCHCH_2$) of the DGEBA molecules. For curing temperatures below *423K* the chemical reaction of DGEBA with BPA leads to an oligomer with mostly linear chains and increased molecular weight [70]. An exact description of the evolution of the reaction between DGEBA and BPA can be found in [71].

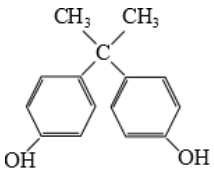

Figure III-2: Chemical structure of a Bisphenol A (BPA) molecule

Bisphenol A ($M_n = 248\ g.mol^{-1}$) with a degree of purity larger than 99% and a melting temperature of about *431 K* has been provided by Aldrich Chemistry. The following procedure was applied to prepare the samples: In a first step a planetary mixer is used to homogeneously disperse the appropriated amounts of BPA (crystalline at room temperature) inside distilled DGEBA. Next the samples are kept at 393 K until all of the BPA has reacted with DGEBA. The amount of Bisphenol A is represented by the mass ratio

$$r_{BPA} = \frac{m_{BPA}}{m_{DGEBA}}, \qquad (3.1.1.2)$$

where m_{BPA} designates the mass content of BPA and m_{DGEBA} the mass of DGEBA. In this project matrices with mass ratios r_{BPA} of *0.3, 0.5 and 0.7* were studied. The effect of curing on the weight average molecular weight of DGEBA is shown in Figure III-3. Obviously curing DGEBA with BPA leads to molecules with higher molecular weights. However, irrespective of the mass ratio r_{BPA}, DGEBA monomers represent the main part of the molecules in the samples (see peak I in Figure III-3). With the knowledge of the molecular weights of DGEBA and BPA, the peaks (II-V) can be attributed to different DGEBA/BPA products with fair accuracy. Peak II was tentatively attributed to DGEBA molecules with a degree of polymerization $n = 2$ ($340\ g.mol^{-1} + 2 \times 248\ g.mol^{-1} = 836\ g.mol^{-1}$ see equation (3.1.1.1)). In contrast the peaks (III-V) rather seem to represent contributions of branched DGEBA/BPA molecules to the weight average molecular weight. This means that branching processes could not be completely avoided. Nevertheless in any case the weight average molecular weight of the DGEBA/BPA molecules with n = 2 exceeds the weight average molecular weight of the DGEBA molecules with n = 2 by a factor of about 40.

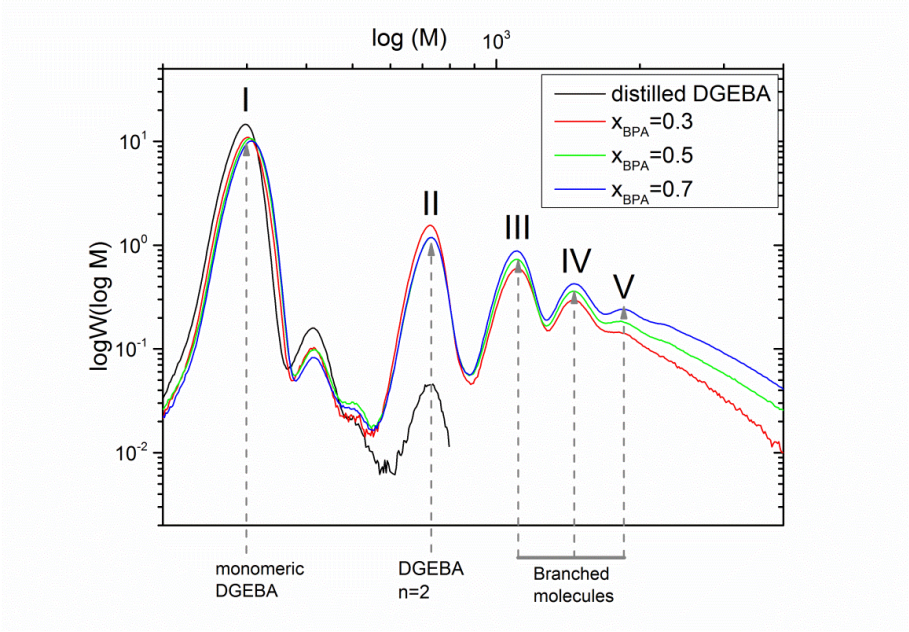

Figure III-3: Weight molecular weight distributions for DGEBA (DER distilled) as well as for the DGEBA/BPA matrices cured with different mass ratios x_{BPA} of BPA. The molecular weight distributions have been obtained by Gel Permeation Chromatography (GPC).

III.1.2. Colloidal suspensions

i) DGEBA/SiO_2 suspensions

The silica nanocomposites are based on a master batch of DGEBA (DER distilled) filled with 40 mass % of silica nanoparticles (Nanopox A410, Nanoresins AG, Germany). The quasi-spherical silica particles have an average radius of about *12.5 nm* (with an approximated standard deviation of about 4 nm) including a hydrophobic silane layer, which prevents particle aggregation [18, 19]. Figure III-4 shows the silica fillers embedded in a DGEBA matrix. Obviously the size distribution of the homogeneously dispersed nanoparticles is rather narrow [19].

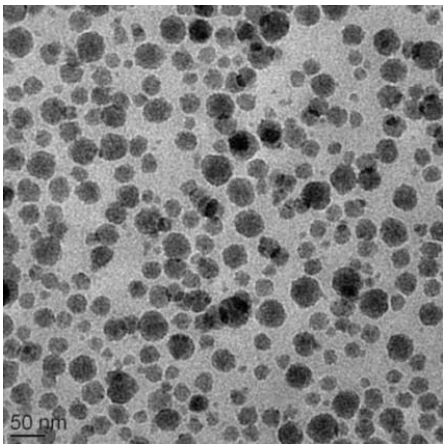

Figure III-4: TEM-picture of a DGEBA-40 mass % SiO_2 sample

The DGEBA/SiO_2 systems with different mass concentrations ($x_m = 0.01, 0.02, 0.05, 0.1, 0.2, 0.3$ and 0.4) are obtained by adequately diluting the master batch with the same distilled DGEBA contained in the master batch. From the mass

concentration x_m the volume concentration x_V can be calculated using the mass densities $\rho_{DGEBA} = 1.16 g.cm^{-3}$ and $\rho_{SiO_2} = 2.28 g.cm^{-3}$. Table 1 shows the correspondence between volume and weight concentrations for the samples investigated in the present thesis.

Table 1: Weight concentrations x_m and corresponding volume concentrations x_V of the investigated DGEBA/SiO_2 nanocomposites.

x_m	0.01	0.02	0.05	0.1	0.2	0.3	0.4
x_V	0.005	0.010	0.026	0.054	0.11	0.18	0.25

ii) DGEBA/SiO_2/BPA suspensions

DGEBA/SiO_2/BPA nanocomposites are obtained by curing DGEBA/SiO_2 suspensions with BPA using the same procedure as for the DGEBA/BPA systems described above. Hence the silica nanoparticles are already embedded in one of the reactants before the polymerization takes place. For a DGEBA/SiO_2 sample with an original mass concentration $x_{m,bm}$ of silica particles, the addition of BPA decreases the effective mass concentration of the fillers. Therefore in order to obtain the same mass concentrations as for the DGEBA/SiO_2 suspensions, the mass concentration $x_{m,bm}$ has to be adapted depending on the desired final mass concentration x_m and on the mass ratio r_{BPA} of Bisphenol A, using

$$x_m = \frac{x_{m,bm}}{1+(1-x_{m,bm})\cdot r_{BPA}} . \qquad (3.1.2.1)$$

In the present project DGEBA/SiO_2/BPA suspensions with the same mass concentrations as for the DGEBA/SiO_2 nanocomposites, are produced (except $x_m = 0.4$). For the determination of the volume concentrations the mass densities of DGEBA and SiO_2 used in paragraph i) has been used[2].

iii) DGEBA/Al_2O_3 suspensions

The DGEBA/ Al_2O_3 suspensions are obtained from a master batch of DGEBA (DER331) filled with 29 mass % of alumina particles. The latter has been produced and characterized by the "Institut für Verbundwerkstoffe" (IVW Kaiserslautern, Germany). The primary alumina particles have an average radius of around 13 nm. Figure III-5 shows TEM-pictures of a DGEBA+ 5 mass % Al_2O_3 suspension. In contrast to the silica particles the primary alumina particles tend to aggregate: the TEM pictures show a dispersion incorporating fractal aggregates with a mean radius of around 50 nm.

To obtain different mass concentrations of alumina particles in DGEBA the master batch is diluted using DER 331. In the frame of the present project suspensions with mass concentrations $x_m = 0.03, 0.04, 0.05, 0.1, 0.15, 0.2 \text{ and } 0.25$ are prepared and investigated. The volume concentrations of the alumina suspensions are calculated

[2] This approximation leads certainly to some uncertainties in the volume concentration. This point will be adressed in section IV.3.1.ii).

using the mass densities $\rho_{DGEBA} = 1.16g.cm^{-3}$ and $\rho_{Al_2O_3} = 3g.cm^{-3}$. Table 2 shows the mass and volume concentrations of the DGEBA/ Al_2O_3 suspensions.

Table 2: Weight concentrations x_m and corresponding volume concentrations x_V of the investigated DGEBA/Al_2O_3 suspensions

x_m	0.03	0.04	0.05	0.1	0.15	0.2	0.25
x_V	0.012	0.016	0.02	0.04	0.06	0.09	0.11

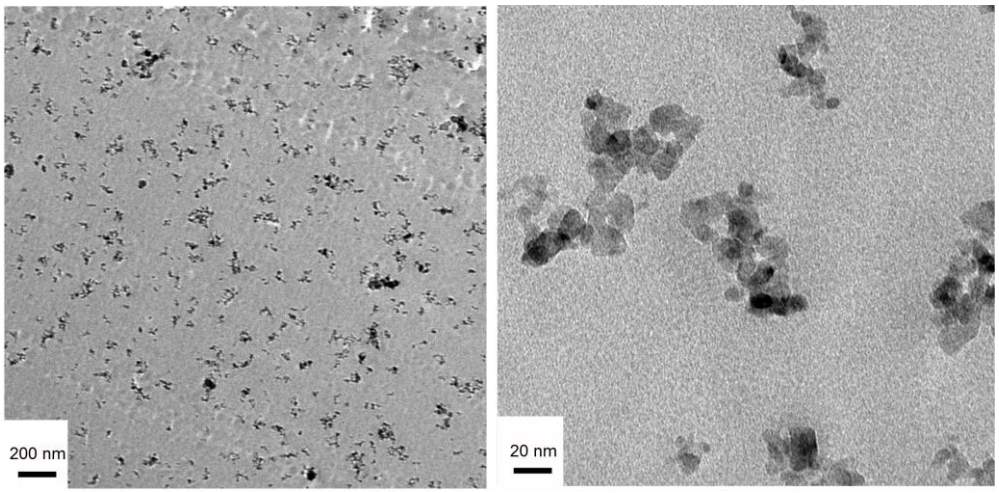

Figure III-5: TEM-pictures of a DGEBA-5 mass % Al_2O_3 samples with different magnifications

III.2. Experimental Method

III.2.1. The rheometer

i) General setup

The rheological measurements have been carried out using rheometers from Thermo Fisher (Haake Mars II) and Anton Paar (MCR 302). A typical experimental setup is depicted in Figure III-6.

The measuring cell (Figure III-6 b) and Figure III-7) comprises two parallel and horizontal metallic plates. The gap between the plates is filled by the sample to be investigated. The gap width can be controlled by the instrument. While the lower plate is fixed, the upper plate is free to turn around or oscillate depending on the measuring protocol. The motion of the axis of the upper plate is controlled by the motor located at the top of the rheometer (see Figure III-6 a)). In addition the rheometer is equipped with a liquid nitrogen cryostat operated by a temperature control unit. Both the Haake Mars II and MCR 302 rheometer cover a temperature range extending from *193 K* to *473 K* with an accuracy of $\pm 0.5K$. More details on the rotational rheometers used during this thesis can be found in the work of Thomassey [28].

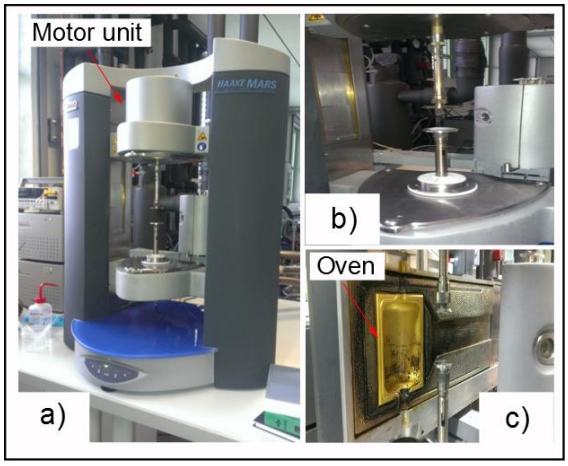

Figure III-6: Experimental setup for rheology a) Haake Mars II rotational rheometer; b) measuring cell (plate-plate configuration); c) the heating/cooling unit

ii) Controlled stress (CS) and controlled deformation (CD) modes

Depending on the rheometer's pre-setting and on the properties of the sample different measuring modes can be exploited. In the controlled stress mode (CS) the motor of the instrument applies a constant torque on the vertical axis of the upper plate and measures the rotation angle of the axis by means of an optical encoder. In contrast, in the controlled deformation mode (CD) the instrument measures the magnitude of the torque needed to impose a given deformation on the sample. The CS-mode is usually exploited for the investigation of low-viscous liquids. The CD-mode can be applied to high-viscous or stiff materials. It has to be stressed that the rheometers used in this project are pre-set to the CS mode. The latter can be switched to CD-mode by adequate software implemented in the rheometer [72].

iii) Measuring cell geometry: Plate-Plate configuration

Depending on the sample or application different geometries of the measuring cell can be used (plate-plate, cone-plate, Couette, etc.). However, in the frame of the present PhD project, all of the measurements have been carried out with a plate-plate configuration, a setup comprising two parallel and horizontal disks of radius *R* separated by a gap with width *h* (see Figure III-7).

General remarks on plate radii and plate distances

The chosen plate radius usually depends on the resistance opposed by the sample to a deformation. In case of samples with low viscosity it is advantageous to rely on plates with large radius: the area of the interface between the sample and the plates increases and so does the signal transferred to the evaluation unit of the rheometer. In contrast if a high-viscous sample fills the gap between the plates with an oversized diameter, the maximum torque, which can be applied by the rheometer, risks to be exceeded. To avoid such a situation plates with smaller radii are used. Usually a gap width $h = 1mm$ is respected when using the plate-plate configuration [73]. All of the measurements presented in this thesis are carried out using plate-plate geometry (plate radii of 8 mm, 25 mm and 50 mm) and respecting a gap width $h = 1\ mm$.

Determination of shear stress and strain

Generally a rheometer measures a torque M_e and a deformation angle ϕ, whereas rheological properties are defined in terms of shear stress σ , strain γ or strain rate $\dot{\gamma}$ (see Figure III-7).

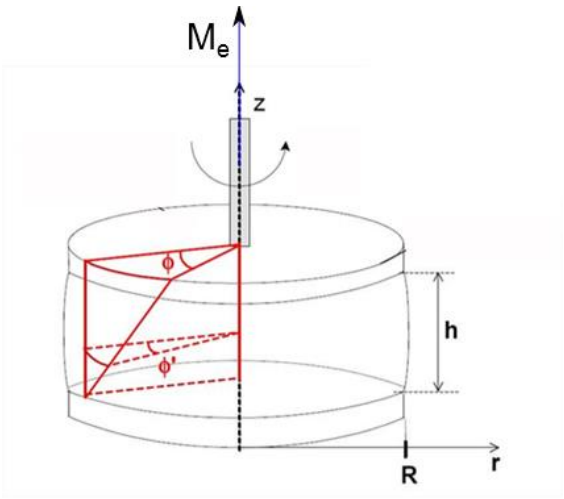

Figure III-7: Schematic representation of the plate-plate geometry (plate radius R; gap width h) The axis of the upper plate is submitted to a torque M_e leading to a rotation of the axis and hence of the upper disc by an angle ϕ The lower plate does not move

The conversion of the applied torque M_e to the shear stress $\sigma(r)$ and of the measured rotation angle ϕ to the strain $\gamma(r)$ and the rate $\dot{\gamma}(r)$ is provided by the rheometer software. In case of the plate-plate geometry strain and strain rate at a distance $r \leq R$ (with R the plate radius) from the axis are calculated using [24]

$$\gamma(r) = \frac{r}{h}\phi \qquad (3.2.1.1)$$

and

$$\dot{\gamma}(r) = \frac{r}{h}\dot{\phi}. \qquad (3.2.1.2)$$

Obviously for the plate-plate configuration the strain and the rate are not homogeneous along the radial direction. In fact at $r = 0$ the strain is zero whereas at $r = R$ it is maximal. The radial dependency of the shear stress induced by the applied torque is given by

$$\sigma(r) = \frac{M_e}{2\pi r^3}\left(3 + \frac{\partial ln(M_e)}{\partial ln(\dot{\gamma}(r))}\right), \qquad (3.2.1.3)$$

where the second term on the right side stands for the Rabinowitsch-Mooney coefficient [74]. The values of the strain, rate and stress displayed by the Rheometer are calculated using equations (3.2.1.1), (3.2.1.2) and (3.2.1.3) with $r = R$.

III.2.2. Dynamic rheology

In case of an oscillatory shear experiment the strain obeys to $\gamma(t) = \gamma_0 sin(\omega t)$. If the sample is viscoelastic the stress can be written as

$$\sigma(t) = \sigma_0 sin(\omega t + \delta), \qquad (3.2.2.1)$$

In CD mode, an oscillatory strain with amplitude γ_0 and frequency ω is applied to the sample. The stress amplitude σ_0 as well as the phase shift δ are measured. Equation (3.2.2.1) can be converted in

$$\sigma(t) = \sigma_0 cos(\delta) sin(\omega t) + \sigma_0 sin(\delta) cos(\omega t). \qquad (3.2.2.2)$$

Comparing the latter expression to equation (2.1.3.4) yielded by the Boltzmann superposition principle, the shear moduli $G'(\omega)$ and $G''(\omega)$ can be written as

$$G'(\omega) = \frac{\sigma_0}{\gamma_0} cos(\delta) \quad \text{and} \quad G''(\omega) = \frac{\sigma_0}{\gamma_0} \sin(\delta). \qquad (3.2.2.3)$$

The angular phase shift is given by

$$\delta = arctan\left(\frac{G''(\omega)}{G'(\omega)}\right). \qquad (3.2.2.4)$$

If $\delta = 0°$ only the storage shear modulus is different from zero: the sample behaves as a perfect solid. In contrast if $\delta = 90°$ only the loss shear modulus is zero: the sample behaves as a Newtonian liquid. For all values of δ between 0° and 90° the sample shows viscoelastic properties.

III.2.3. The measuring procedure

In the following section the experimental procedure applied to investigate the linear viscoelastic properties of the samples will be described.

i) Amplitude Sweeps

The Boltzmann superposition principle is fundamentally based on linear response of the sample (see section II). Linear response of the sample implies that the relaxation modulus and hence the shear moduli $G'(\omega, T)$ and $G''(\omega, T)$ are independent of the applied strain amplitude. To ensure linear response so-called amplitude sweeps are performed. In such measurements the sample is sheared with constant angular frequency but increasing strain amplitude (see Figure III-8 a)). As can be seen in Figure III-8 b) the shear moduli are constant below a critical strain γ_c (linear regime). Above this critical strain non-linear effects appear leading to shear moduli depending on the strain amplitude. Since the critical strain depends on the temperature and the frequency (see Figure III-8 b)), the amplitude sweeps have to be repeated at several frequencies (usually 3-4 amplitude sweeps covering the whole frequency window of the rheometer) and at all of the temperatures, for which the samples have to be investigated.

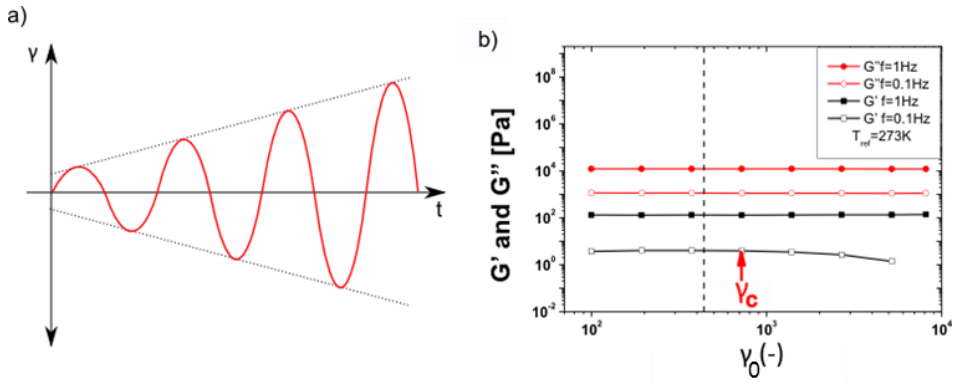

Figure III-8: a) Amplitude sweep at a given frequency; b) shear moduli G' and G'' as a function of the strain amplitude at different frequencies. γ_c is the critical strain amplitude.

ii) Frequency Sweeps

Once a strain amplitude respecting linear regime conditions has been chosen, frequency sweeps can be carried out[3]. In such measurements an oscillatory strain field with constant amplitude but increasing angular frequency is applied to the sample (see Figure III-9). The used frequency window extends from $\omega_{min} = 0.314\, rad/s$ to $\omega_{max} = 62.8\, rad/s$.

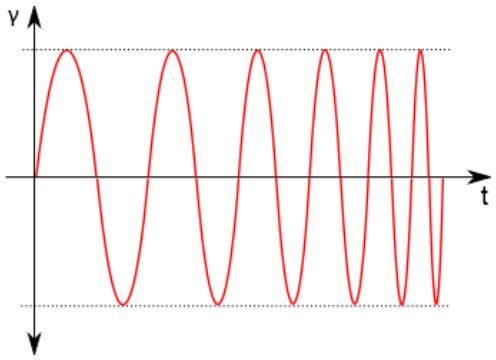

Figure III-9: Frequency sweep with a fixed amplitude.

iii) From frequency sweeps to master curves

Using the frequency-temperature-superposition (FTS-) principle single frequency sweeps at different temperatures can be superposed to a single curve (called master curve) at a reference temperature. The software "Iris" was used for this purpose. After selection of the reference temperature (for the illustration in Figure III-10 $T_{ref} = 273K$), the frequency sweeps can be shifted horizontally and/or vertically alligning them with the frequency sweep measured at the reference temperature. The horizontal and vertical shifts lead to the a_T and b_T factors introduced in section II.1.4. An illustration of the obtained master curve for $G'(\omega)$ is Figure III-10. As in Figure III-10 only the storage modulus is represented one may think that several possibilities for a_T and b_T exist. However Figure III-10 is only restricted to $G'(\omega)$-data for reasons of clarity. Normally both the storage and the loss modulus are represented. The shift of the shear moduli into a master curve is performed simultaneously by the Iris-program,

[3] In this context one has to take care to choose an amplitude strain which is not too small compared to γ_c in order to obtain measurements which are not disturbed due to signal noise.

implying that only one choice of a_T and b_T exists for which both shear moduli data collapse into a master curve.

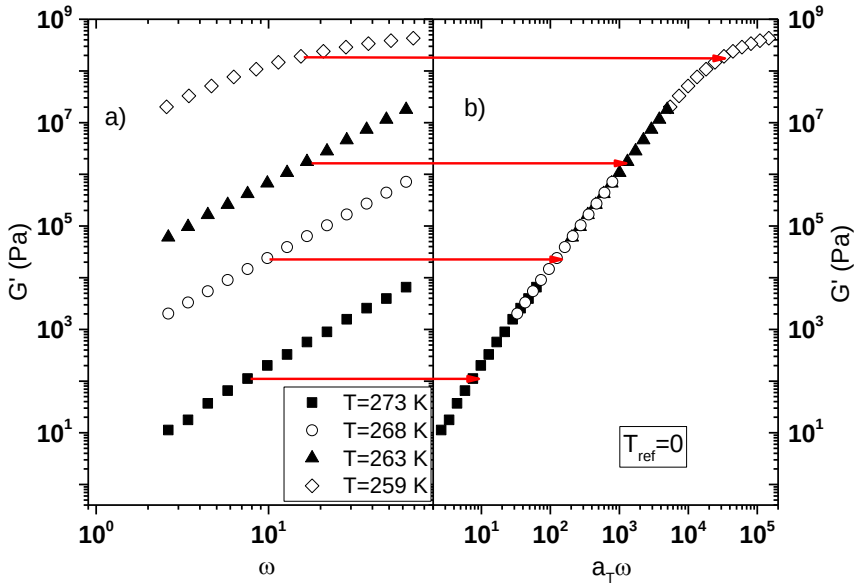

Figure III-10: a) Frequency sweep data of $G'(\omega)$ for different temperatures as well as b) the master curve at the reference temperature $T_{ref} = 273K$ obtained by a horizontal shift of the frequency sweep data. The red arrows indicate the shift procedure of each frequency sweep

IV. Results and discussion

IV.1. Characterization of the linear viscoelastic behaviour of DGEBA

As described in section III.1.1, all of the investigated matrices and suspensions are based on DGEBA. Hence before discussing the linear viscoelastic properties of the modified matrices and suspensions non-polymerized DGEBA needs to be characterized[4]. As pointed out DGEBA is a glass former undergoing dynamic or thermal liquid-to-solid or solid-to-liquid transitions. Both types of transitions have been previously investigated by dynamic rheology [28]. In the frame of the present project the rheological investigations are restricted to the dynamic glass transition implying that the measurements are limited to temperatures above the thermal glass transition temperature of DGEBA i.e. $T_g = 257\ K$ [18].

The viscoelastic behaviour of glass forming materials strongly depends on the complexity of the molecules [75-79]. For low-molecular weight glass formers the linear viscoelastic behaviour is expected to be simple especially due to the absence of an entanglement plateau. Consequently, at a constant temperature $T > T_g$, it is expected that DGEBA shows liquid-like behaviour with terminal regime scaling of the shear moduli in the low frequency regime. At higher frequencies DGEBA is supposed to undergo a dynamic glass transition.

In the following results from isothermal frequency sweeps carried out on a DGEBA sample are shown. Furthermore the master curves obtained from these results (using the frequency-temperature-superposition principle) are discussed.

IV.1.1. Frequency dependency of the shear moduli of DGEBA at different temperatures

Figure IV-1 shows the results from isothermal frequency sweeps carried out on a DGEBA sample in the temperature range extending from $259K$ to $273K$. While the lower limit of the temperature range is dictated by the thermal glass transition of the sample, the upper limit is imposed by the rheometer's resolution limit for measurements of phase angles (see section III.2.2). Obviously, when the temperature increases the storage and loss shear moduli decrease. At temperatures $T \geq 263K$ the loss moduli are higher than the corresponding storage moduli. At $T = 259K$ a crossover between $G'(\omega)$ and $G''(\omega)$ occurs.

[4] The linear viscoelastic properties of polymerized DGEBA will be discussed in section IV.3.1.

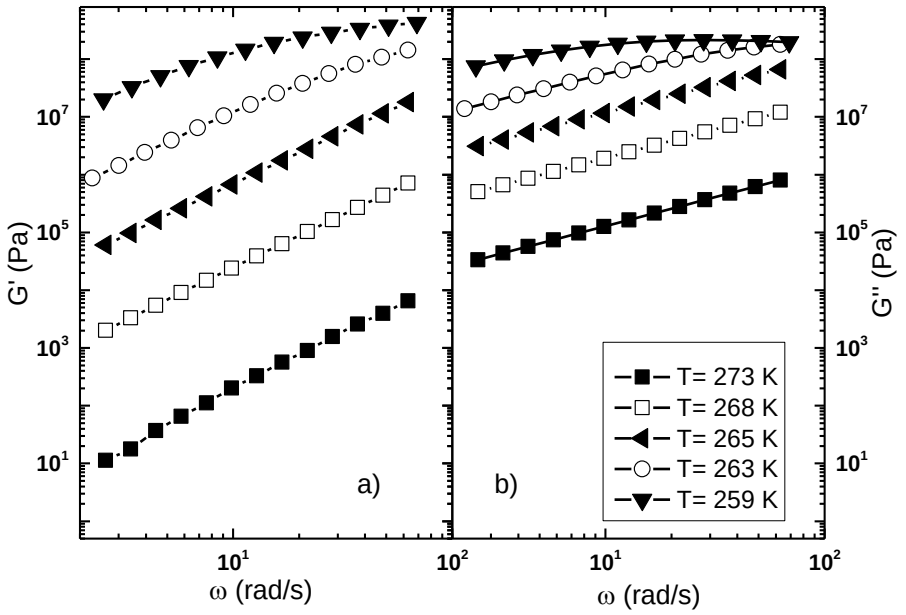

Figure IV-1: a) Storage modulus $G'(\omega)$ and b) loss modulus $G''(\omega)$ of DGEBA (DER distilled) as a function of the angular frequency at different temperatures [80].

IV.1.2. Master curves of the shear moduli of DGEBA

As illustrated in Figure IV-3 the storage and loss shear moduli of DGEBA depicted in Figure IV-1 can be shifted to master curves at the reference temperature $T_{ref} = 273K$ using the frequency-temperature-superposition principle. Figure IV-2 shows the corresponding shift factors $log(a_T)$ and $log(b_T)$ as a function of the temperature. As can be seen the $log(a_T)$ data can fairly be fitted to the William-Landau-Ferry (WLF) model described in section II.1.4. In contrast the vertical shift factor $log(b_T) = 1$ irrespective of the temperature. This means that the master curves can be constructed without any vertical shift.

Obviously DGEBA behaves as a solid at high frequencies and exhibits liquid-like behaviour at low frequencies ($G''(\omega) > G'(\omega)$). In the double-logarithmic representation of Figure IV-3 the low frequency tails of both moduli linearly scale with the frequency. Linear fits yield $G'(\omega) \propto \omega^{1.86}$ and $G''(\omega) \propto \omega^{0.99}$. These power-laws fairly agree with the terminal regime behaviour $G'(\omega) \propto \omega^2$ and $G''(\omega) \propto \omega$ expected for viscoelastic fluids. The master curves in Figure IV-3 correspond to the rheological signature of the α-process in DGEBA. Obviously there is no evidence for an additional relaxation process. At a first glance the data presented in Figure IV-3 suggest that the viscoelastic behaviour of DGEBA can be described by the Maxwell model (see section II.1.3) .Using equation (2.1.3.8) the real part of the complex matrix viscosity can be determined as

$$\eta'_m = \left(\frac{G''(\omega)}{\omega} \right)_{\omega \to 0} \qquad (4.1.2.1)$$

Accordingly, at the reference temperature $T_{ref} = 273K$, the real part of the viscosity of DGEBA can be evaluated to $\eta'_m = 10275\ Pa.s$. As for $\omega \to 0$ the contribution of the storage modulus to the complex viscosity can be neglected, $\eta'_m \approx \eta_m$, η_m representing the zero shear viscosity of the matrix.

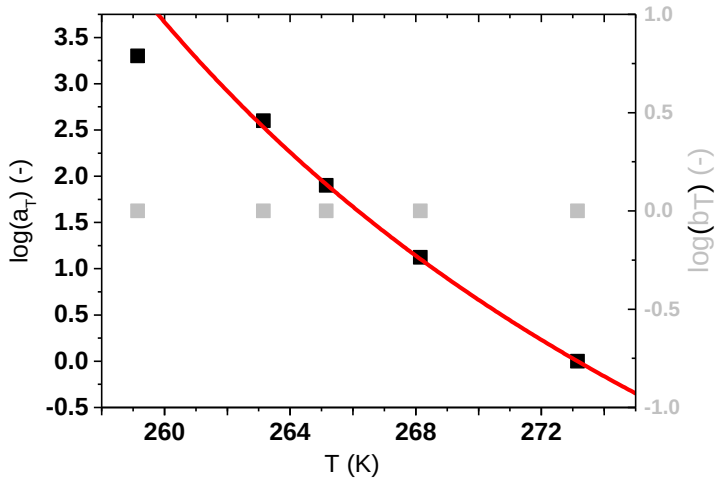

Figure IV-2: Horizontal and vertical shift factors a_T (black symbols) respectively b_T (grey symbols) used for the construction of the master curves (Figure IV-3) of $G'(\omega)$ and $G''(\omega)$ for DGEBA (DER distilled) at the reference temperature $T_{ref} = 273K$. The red line represents a WLF-plot (equation 2.1.4.11) with parameters $C_1 = 8.63$ and $C_2 = 44.08\ K$.

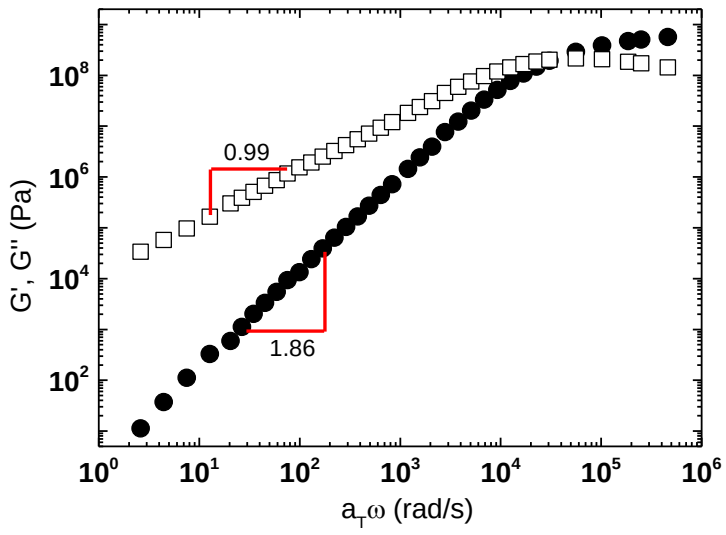

Figure IV-3: Master curves of $G'(\omega)$ and $G''(\omega)$ for DGEBA at a reference temperature of $T_{ref} = 273K$

IV.1.3. Modelling of the linear viscoelastic behaviour of DGEBA

In section II.1.3 different models able to describe linear viscoelastic behaviour have been introduced: the Maxwell model, the generalized Maxwell model and the BSW-model. Figure IV-4 compares the fits of these models to the experimental data shown in Figure IV-3.

Figure IV-4a shows the fit of the Maxwell model (equations (2.1.3.10) and (2.1.3.11)) to the master curves $G'(\omega)$ and $G''(\omega)$ obtained for DGEBA. Obviously the low frequency tails of the data are well described by the Maxwell-model. However the model fails at higher frequencies. Thus the viscoelastic behaviour of DGEBA cannot fully be described by a Maxwell model relying on a single pair (τ,G) of characteristic parameters.

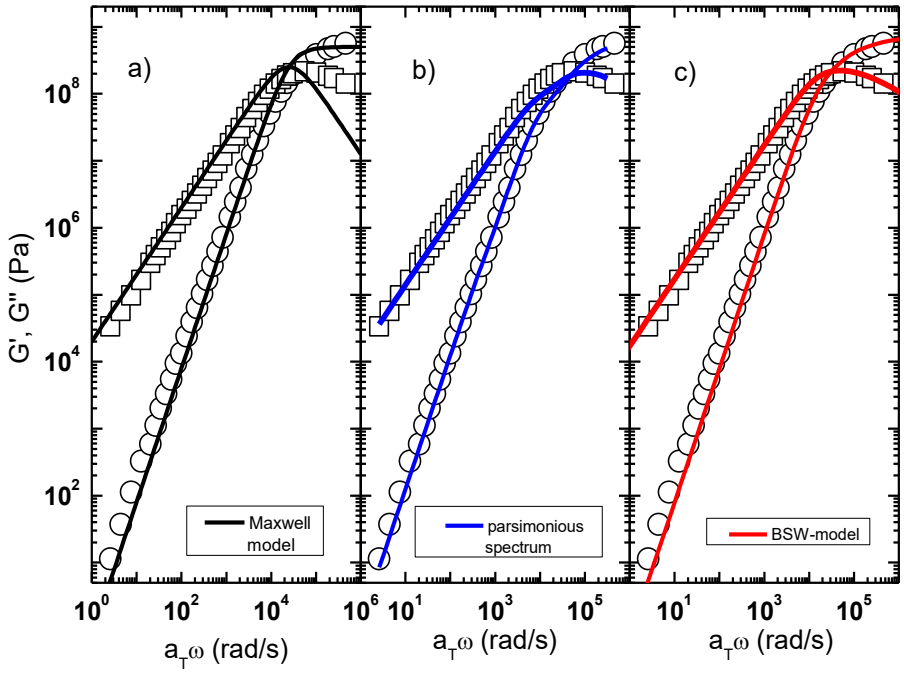

Figure IV-4: Master curves of $G'(\omega)$ and $G''(\omega)$ for DGEBA as well as different models introduced in section II.1.3. a) shows a fit of a simple Maxwell model to the data using the parameter $\tau = 2 \cdot 10^{-5}s$ and $G = 5 \cdot 10^{8}Pa$. b) illustrates the fit of the generalized Maxwell model, where the fit parameters are represented in Figure IV-5. c) represents a fit of the BSW-model to the data using a stretched exponential power-law distribution function with parameters $G = 1 \cdot 10^{8}Pa$; $n = 0.51$; $\tau_{max} = 7.3 \cdot 10^{-5}s$ and $\beta = 0.68$.

Figure IV-4b depicts the fit of the generalized Maxwell model equations (2.1.3.14) and (2.1.3.15)) to the shear moduli of DGEBA. The corresponding relaxation times τ_i and strengths G_i are represented by the parsimonious spectrum shown in Figure IV-5. Obviously the model can be used to adequately describe both, the low frequency tails of the master curves and the dynamic glass transition occurring at higher frequencies. A major drawback of the generalized Maxwell model is that it requests a high number of characteristic parameters (four pairs (τ_i, G_i) in case of DGEBA). One aim of the BSW-model is to reduce the number of parameters needed for the description of the viscoelastic behaviour of a sample [33]. As discussed in section II.1.3 (equations

(2.1.3.16) and (2.1.3.17)) the BSW-model relies on a continuous sum (an integral) of Maxwell modes. The contribution of each term, is thereby weighted by the probability distribution function $H(\tau)$. By using a stretched exponential power-law function for $H(\tau)$ (equation (2.1.3.19)) with parameters $G = 1 \cdot 10^8 Pa; n = 0.51; \tau_{max} = 7.3 \cdot 10^{-5} s$ and $\beta = 0.68$ both the parsimonious spectrum in Figure IV-5 and the linear viscoelastic behavior in Figure IV-4c are well described (see red lines) .

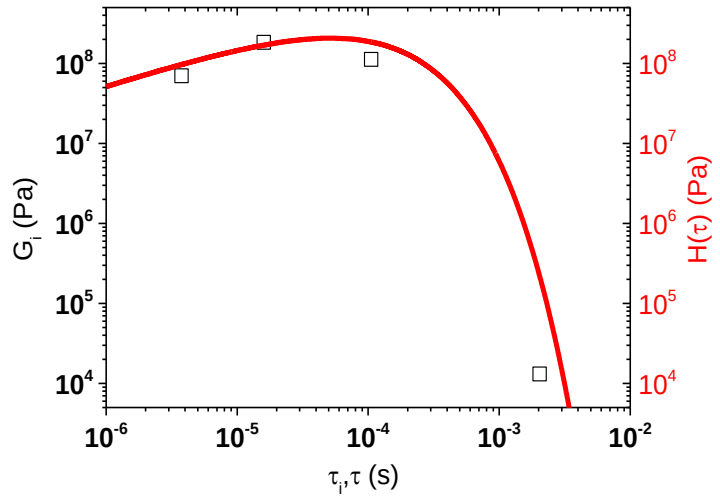

Figure IV-5: Parsimonious spectrum (open symbols) for DGEBA and prediction of the stretched exponential power-law distribution function $H(\tau)$ (red line) with parameters $G = 1 \cdot 10^8 Pa; n = 0.51; \tau_{max} = 4.7 \cdot 10^{-5} s$ and $\beta = 0.68$

IV.2. The linear viscoelastic behaviour of DGEBA/SiO_2 suspensions

Rheological measurements reveal that the linear viscoelastic behaviour of DGEBA can adequately be described by the generalized Maxwell model or the BSW model. Thus, at temperatures above T_g, DGEBA behaves as a Newtonian liquid in the low-frequency regime. At higher frequencies the dynamic glass transition determines the rheological behaviour. The question arises how solid colloids suspended in DGEBA affect the linear viscoelastic behaviour of the matrix. For reason of simplicity in the first part the influence of quasi-spherical silica particles is investigated.

IV.2.1. Highly concentrated DGEBA/Silica suspension

In this section the influence of silica nanoparticles on the linear viscoelastic behaviour of DGEBA will exemplarily be showcased for a given filler fraction. As the filler-induced effects are expected to increase with the content of nanoparticles, a concentrated suspension $(x_V = 0.18)$ of silica in DGEBA is chosen. Even if at a first sight a suspension with $x_V = 0.18$ may not be considered as a concentrated suspension (see section II.2.2), in appendix VI.4.1 the concept of effective volume concentrations is applied clarifying that this suspension is concentrated in terms of the definition given in section II.2.2.

i) Frequency dependency of the shear moduli of a DGEBA/ SiO_2 suspension with a high filler content

Figure IV-6 shows the results from isothermal frequency sweeps performed on the DGEBA/SiO_2 suspension ($x_V = 0.18$) at temperatures ranging from $259K$ to $303K$. At low temperatures the evolutions of the storage and loss shear moduli as a function of the frequency are quite similar to the results found for the neat DGEBA matrix. It can also be observed that at higher temperatures the system behaves like a liquid: generally $G''(\omega) > G'(\omega)$. Most interestingly however, at temperatures $278K \leq T \leq 293K$ especially the evolution of the storage shear modulus is clearly affected by the nanoparticles. A close inspection of Figure IV-6b yields that the loss shear moduli measured at $T = 278K$ and $T = 283K$ also deviate from the terminal behaviour observed for the DGEBA matrix (see Figure IV-1b).

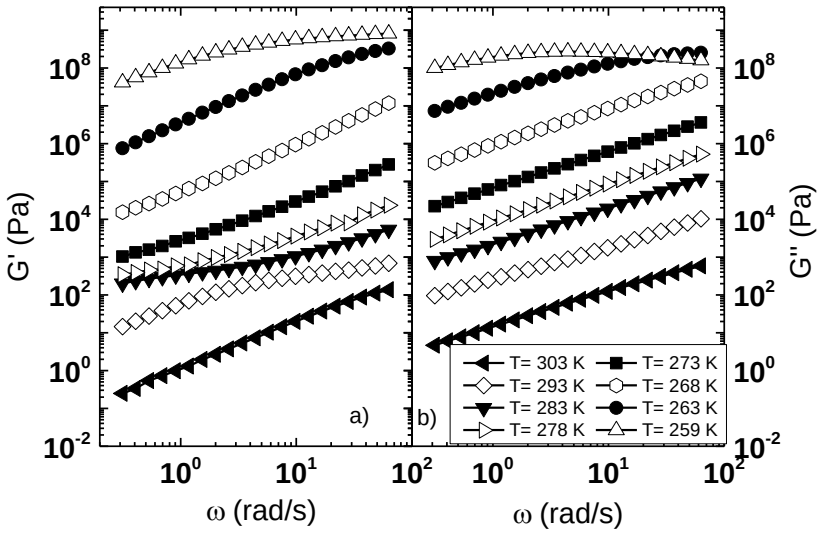

Figure IV-6: a) Storage modulus $G'(\omega)$ and b) loss modulus $G''(\omega)$ of a DGEBA/SiO_2 suspension with $x_V = 0.18$ as a function of the frequency at different temperatures [80]

ii) Master curves of the shear moduli of the DGEBA/SiO_2 suspension ($x_V = 0.18$)

Although the process behind the anomalous behavior of the shear moduli of the suspension is unknown at the moment the frequency-temperature-superposition principle is tentatively applied to construct master curves of $G'(\omega)$ and $G''(\omega)$. Figure IV-7 allows to compare the linear viscoelastic behaviour of pure DGEBA and of the DGEBA/silica suspension ($x_V = 0.18$) at the reference temperature $T_{ref} = 273K$. Obviously both systems behave similarly at high frequencies near the dynamic glass transition. In contrast, at intermediate frequencies, the shear moduli of the filled system considerably deviate from those of DGEBA. The most prominent feature revealed by the filled system is the occurrence of a distinct plateau-like elastic behaviour going along with a small step-like transition of the loss modulus in the same frequency range. However at the lowest frequencies both shear moduli seem to approach again terminal regime scaling.

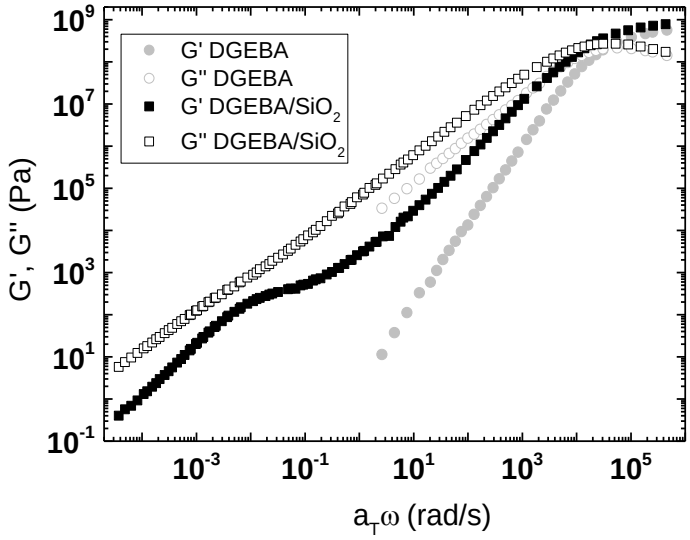

Figure IV-7: Master curves of $G'(\omega)$ and $G''(\omega)$ for a DGEBA/SiO_2 suspension with $x_V = 0.18$ at the reference temperature T_{ref} = 273K . The master curves represented by the grey symbols correspond to the shear moduli of DGEBA (see Figure IV-3)

IV.2.2. Semi-dilute and concentrated DGEBA/SiO_2 suspensions

In the last section two important results concerning the influence of silica nanoparticles on the linear viscoelastic behaviour of DGEBA have been described. First the dynamic glass transition of the matrix appears to be unaffected by the presence of the particles. Second a low-frequency anomaly in the shear moduli has been observed. However neither the influence of the silica particles on the glass transition nor the origin of the low frequency process has been rigorously discussed in the last section. To shed more light on the effects produced by the silica fillers in the following the investigation will be extended to suspensions with different concentrations of silica particles $(0.054 \leq x_V \leq 0.25)$.

Figure IV-8 depicts the master curves of the shear moduli $G'(\omega)$ and $G''(\omega)$ obtained for neat DGEBA and for the DGEBA/SiO_2 suspensions with volume concentrations $x_V = 0.054; 0.11; 0.18;\ 0.25$ at the reference temperature $T_{ref} = 273K$. The isothermal frequency sweeps used for the construction of the master curves can be found in appendix VI.1. Obviously, at least the evolutions of the storage moduli of the investigated suspensions are comparable. All of the $G'(\omega)$ curves seem to converge at the dynamic glass transition, except the one obtained for the sample with the highest filler content ($x_V = 0.25$). Apparently the α-process of the latter system dynamically freezes at a slightly lower frequency. Furthermore the storage moduli of all of the suspensions show the anomaly at intermediate frequencies described in section IV.2.1. While the loss shear moduli of the DGEBA/SiO_2 suspensions with the highest nanoparticle contents ($x_V = 0.18;\ 0.25$) exhibit a step-like transition at intermediate frequencies, the loss shear moduli obtained for the semi-dilute suspensions seem to obey to the same terminal scaling as the DGEBA matrix.

Before discussing the various features revealed by the master curves shown in Figure IV-8, the applicability of the frequency-temperature superposition principle needs to be questioned. The frequency-temperature superposition principle has been successfully exploited for the construction of the master curves shown in Figure IV-7 and in Figure IV-8 . Figure IV-9 shows how the horizontal shift factors a_T depend on the temperature.

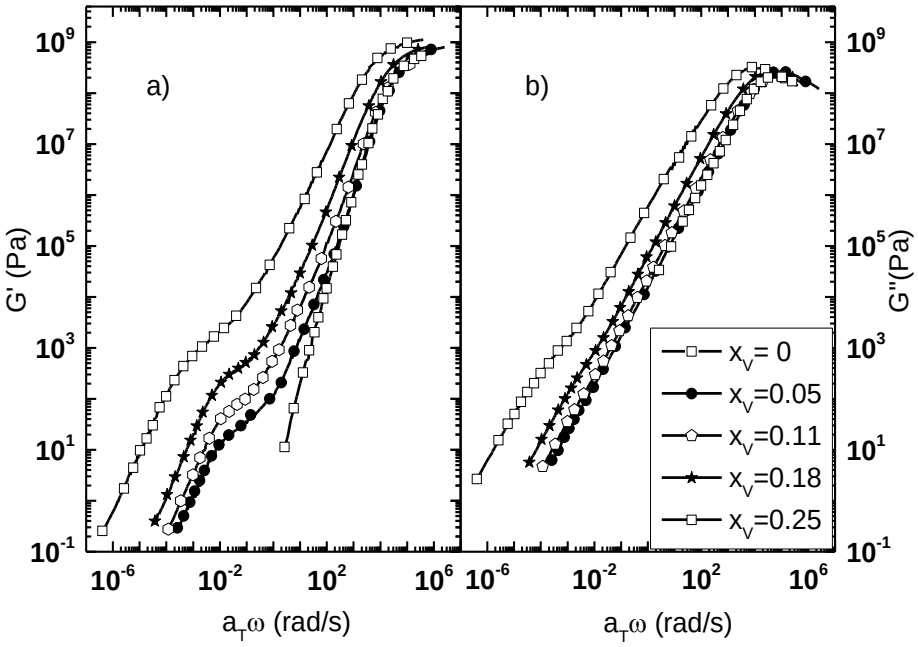

Figure IV-8: Master curves $G'(\omega)$ (a) and $G''(\omega)$ (b) for the various DGEBA/SiO_2 samples at the reference temperature $T_{ref} = 273K$. The lines linking the measured points are guidelines for the eyes (the measured data points lie closer)

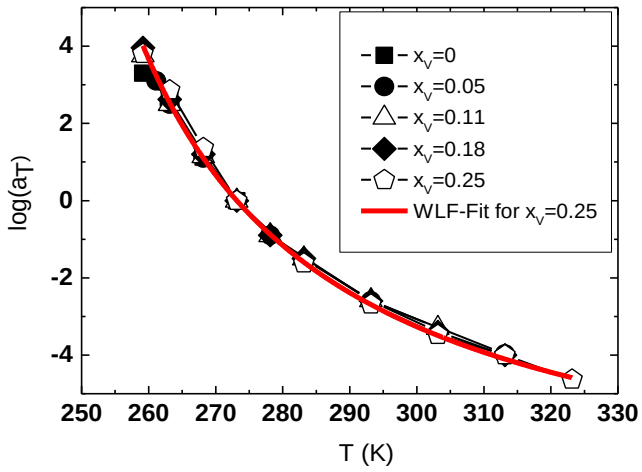

Figure IV-9: Horizontal shift factors $log(a_T)$ used for the construction of the master curves in Figure IV-8. The red line represents the WLF-fit (equation 2.1.4.11) to the shift factors with parameters $C_1 = 8.63$ and $C_2 = 44.08\ K$.

Obviously, in case of the suspensions, the evolution of the shear moduli as a function of frequency is controlled by two different processes. The first one is the well-known α-process. The second one which manifests itself by the anomaly at intermediate frequencies has not yet been identified. The results presented in Figure IV-9 suggest that, irrespective of the investigated sample, all of the shear moduli obtained from isothermal frequency sweeps (at different temperatures) could be merged into continuous master curves by using a unique set of shift parameters. In addition as shown in Figure IV-9 the $log(a_T)(T)$-curves of all of the investigated systems (DGEBA matrix and DGEBA/SiO_2 suspensions) can be described by the same WLF function. The physical background will be provided in paragraph ii) of this section.

i) Influence of silica particles on the glass transition and the viscosity of DGEBA

Concentration dependency of glass transition related parameters: $T_g(x_V)$ and $\tau_\alpha(x_V)$

Previous calorimetric [19] and dielectric measurements (see Figure IV-13) have shown that the glass transition temperature T_g of DGEBA/SiO_2 suspensions is practically independent of the volume concentration. This result was explained by the fact that the silica particles are not interacting with the DGEBA matrix [19]. Figure IV-10 shows the evolution of the relaxation times τ_α as a function of the volume concentration x_V for the different DGEBA/SiO_2 suspensions ($T_{ref} = 273K$). The relaxation times correspond to the α-process and have been obtained by fitting the BSW-model to the high-frequency range (near the dynamic glass transition) of the master curves $G'(\omega)$ and $G''(\omega)$. Obviously τ_α slightly increases with x_V. Does this finding agree with the results obtained for the thermal glass transition temperature T_g of DGEBA/SiO_2 suspensions?

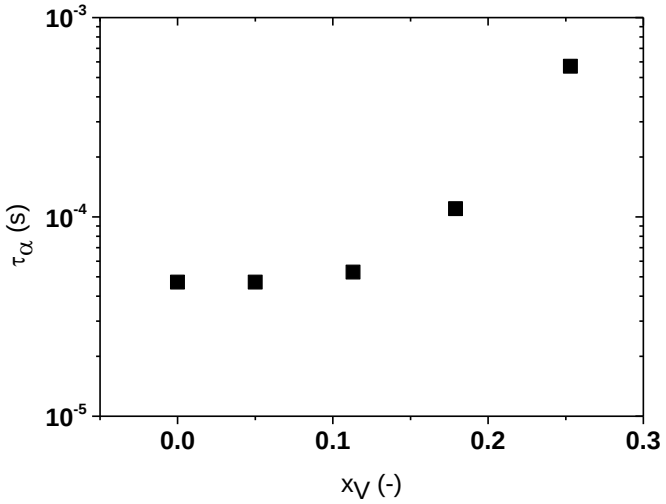

Figure IV-10: Relaxation times τ_α of dynamic glass transition for the various DGEBA/SiO_2 samples. The values are obtained by fitting the frequency region of the master curves (Figure IV-8) near the intersection point between $G'(\omega)$ and $G''(\omega)$.The τ_α-data are listed in Table 3

To answer this question a closer look at the temperature dependency of τ_α is necessary. As discussed in section II.1.2 the empirical Vogel-Fulcher-Tammann law

$$\tau_\alpha = \tau_{\alpha,0} e^{\frac{\Delta G}{k_B(T-T_V)}} \qquad (4.2.2.1)$$

allows to establish a link between the relaxation time τ_α related to the dynamic glass transition and the temperature at which the material dynamically freezes. Unfortunately the evaluation of the master curves $G'(\omega)$ and $G''(\omega)$ of the various suspensions only allows to determine the relaxation time at the reference temperature $T_{ref} = 273K$. Also from the frequency sweeps in appendix VI.1.1 the relaxation times can only be determined for a single temperature. Therefore the temperature dependency of τ_α cannot directly be discussed. But it is known that the temperature dependency of the relaxation time τ_α corresponds also to the temperature dependency of the viscosity (see section II.1.2). Fortunately, for each of the investigated samples, the temperature evolution of the matrix/suspension viscosity can be evaluated from the loss shear moduli obtained from the isothermal frequency sweeps performed at different temperatures. The evaluation is restricted to temperatures at which the loss modulus obeys to terminal regime scaling, i.e. $G''(\omega) \propto \omega^1$. In case of the DGEBA matrix the viscosity used for the evaluation can without any ambiguity be determined using equation (4.1.2.1). In case of the suspensions the situation is more delicate, as one has to differentiate between the regime where the low-frequency anomaly contributes to the suspension viscosity leading to the so called zero-shear viscosity (see sections II.1.3 and II.2.2)

$$\eta_0 = \left(\frac{G''(\omega)}{\omega} \right)_{\omega \to 0} \qquad (4.2.2.2)$$

and the regime where the corresponding process is frozen. The viscosity obtained in this second regime is called high-frequency viscosity and is determined using

$$\eta_{HI} = \left(\frac{G''(\omega)}{\omega} \right)_{\omega \to \infty}, \qquad (4.2.2.3)$$

where $\omega \to \infty$ is restricted to frequencies for which the loss modulus exhibit terminal regime scaling[5]. Figure IV-11 illustrates the procedure to determine the suspension viscosities η_0 and η_{HI} for different temperatures in case of a DGEBA/SiO_2 dispersion ($x_V = 0.25$).

Clearly the high-frequency regime (where the anomaly is not contributing to the suspension viscosity) is relevant for the dynamic freezing of the suspension (α-process). Therefore the high-frequency viscosities $\eta_{HI}(T)$ are represented in Figure

[5] In general the viscosities obtained by this methods represent the real part of the complex viscosities and consequently should be denoted be η'_0 and η'_{HI}. However for reasons of simplicity they are called η_0 and η_{HI}.

IV-12 for all of the investigated suspensions. The red lines in Figure IV-12 correspond to fits of the Vogel-Fulcher-Tammann law to the respective viscosity data. The fit parameters are summarized in Table 3. From Figure IV-12 it becomes clear that the temperature dependencies of the viscosities and hence of τ_α are specific for each fraction of silica particles.

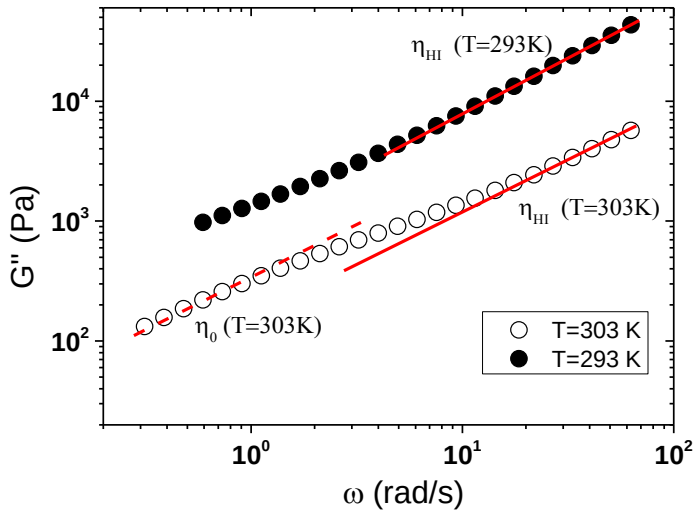

Figure IV-11: Determination of zero-shear and high-frequency viscosities (η_0 and η_{HI}) from isothermal frequency sweeps. The open symbols show the loss modulus obtained from an isothermal frequency sweep of the DGEBA/SiO_2 suspension with $x_V = 0.25$ at $T = 303\ K$. The closed symbols show the loss modulus for the same suspension but a different temperature ($T = 293\ K$) . The red lines illustrate the different viscosities determined using equations (4.2.2.2) and (4.2.2.3).

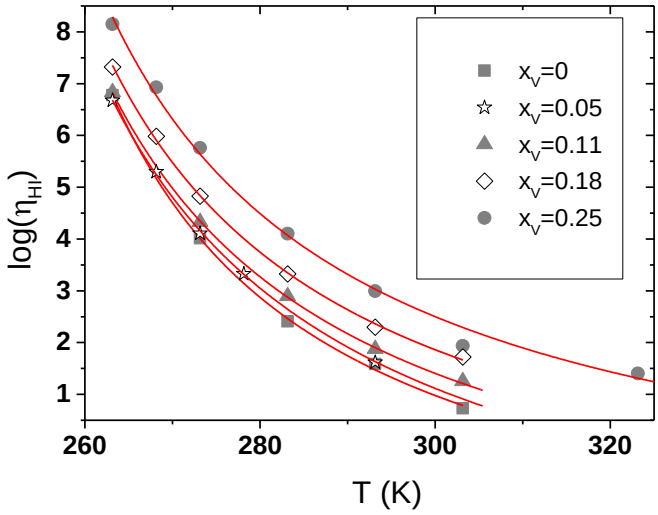

Figure IV-12: DGEBA and DGEBA/SiO_2 high-frequency viscosities (equation (4.2.2.3)) for different volume concentrations and temperatures obtained from the loss modulus of the different frequency sweeps shown in appendix VI.1. The red lines represent Vogel-Fulcher-Tammann fits (equation (4.2.2.4)). The corresponding parameters of the VFT-fits are listed in Table 3

The thermal glass transition temperature T_g can directly be determined from the temperature dependency of the viscosity. Very often, as a convention, T_g corresponds to the the temperature at which $\eta_{HI} = 10^{12.3} Pa.s$. Therefore for each volume concentration the glass transition temperature can be obtained by solving the equation

$$\eta_{HI} = 10^{12.3}\ \mathrm{Pa \cdot s} = \eta_{HI,0} \cdot e^{\frac{\Delta G}{k_B (T - T_V)}} \qquad (4.2.2.4)$$

with the appropriated parameters from Table 3. The thermal glass transition temperatures T_g obtained by this procedure are represented in Figure IV-13 as a function of the filler fraction. It can clearly be observed that the glass transition temperature is practically independent of the volume concentration. Consequently the dependency of T_g on the filler content evaluated by using rheological measurements is in agreement with the results delivered by calorimetry or dielectric spectroscopy. As far as the scattering of T_g values are concerned ($256K$ obtained by calorimetry; around $255K$ by dielectric spectroscopy and $254K$ by rheology) a final conclusion cannot be drawn. First the three experimental probes relied on three different temperature calibrations. Second the evaluation of T_g generally depends on conventions. From the results reported in this section it can definitely be concluded that in the DGEBA/SiO_2 suspensions effects due to particle-matrix interactions can be neglected.

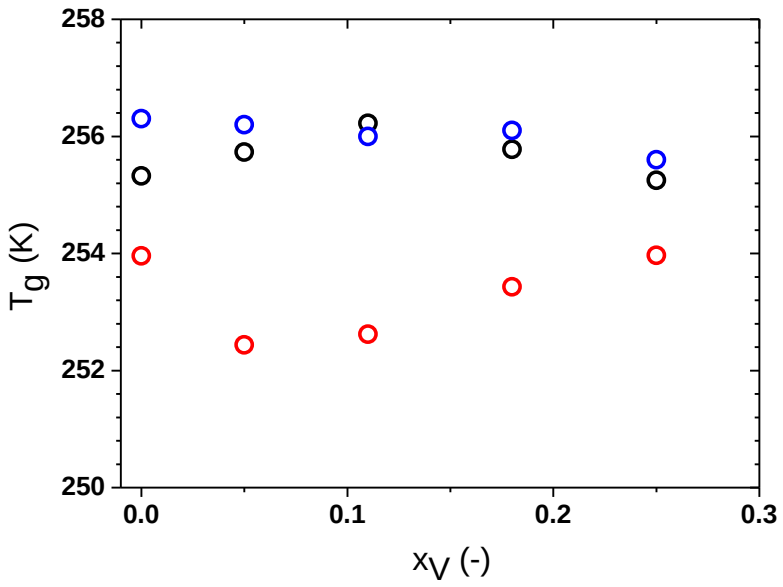

Figure IV-13: Glass transition temperature T_g of DGEBA/ SiO_2 suspensions as a function of the filler fraction. The T_g-values have been obtained by different experimental methods. The red, black and blue symbols represent the data from rheology, dielectric spectroscopy and calorimetry respectively

Table 3: Relaxation times τ_α of dynamic glass transitions and parameters obtained by fitting the viscosity data in Figure IV-12 by the VFT-law (equation (4.2.2.1)) i.e. the viscosity $\eta_{HI,0}$ at $T \to \infty$, the free enthalpie $\Delta G/k_B$ normalized by k_B and the Vogel-temperature T_V all listed for the different volume concentrations x_V. The glass transition temperature T_g for the various DGEBA/SiO_2 samples are obtained from the VFT-parameters (see text).

x_V (-)	τ_α (s)	$\eta_{HI,0}$ (Pa.s)	$\Delta G/k_B$ (K)	T_V (K)	T_g (K)
0	$4.7 \cdot 10^{-5}$	$9.3 \cdot 10^{-4}$	575	237	253.9
0.054	$4.7 \cdot 10^{-5}$	$8.3 \cdot 10^{-4}$	697	233	252.4
0.11	$5.3 \cdot 10^{-5}$	$1.3 \cdot 10^{-3}$	651	234	252.6
0.18	$1.1 \cdot 10^{-4}$	$3.9 \cdot 10^{-3}$	652	234	253.4
0.25	$5.7 \cdot 10^{-4}$	$8 \cdot 10^{-3}$	695	233	253.9

Concentration dependency of the suspension viscosities: $\eta_0(x_V)$ and $\eta_{HI}(x_V)$

Identically to the temperature evolution of the viscosities η_0 and η_{HI} equations (4.2.2.2) and (4.2.2.3) can be used to study the volume concentration dependency of the latter. From the master curves in Figure IV-8 the viscosities η_0 and η_{HI} can be determined for the different concentrations of silica particles ($T_{ref} = 273K$). Both types of viscosities are listed in Table 4 and represented in Figure IV-14 as a function of the volume concentration x_V. Obviously both viscosities increase with growing filler fraction. Thereby the zero-shear viscosity η_0 is increasing faster than the high-frequency viscosity η_{HI}. Figure IV-14 reveals that both viscosities are well described by the Krieger-Dougherty relation (equation (2.2.2.9)). The parameters delivered by the Krieger-Dougherty fits are listed in Table 4. Although the Krieger-Dougherty model seems to provide an adequate description the evolution of the viscosities as a function of the filler content both, η_0 and η_{HI}, are predicted to diverge at filler fractions ($x_{V,max} = 0.26$ in case of η_0 and $x_{V,max} = 0.28$ in case of η_{HI}), which are small compared to the volume concentrations (around $x_{V,max} = 0.58 - 0.63$) expected for colloidal suspensions of hard spheres.

Albeit this behaviour is surprising, it nevertheless can be understood when thin repulsive interaction layers existing around the particles are considered. In section II.2.2 it has been shown that such interaction layers due e. g. to electrostatic repulsion lead to effective particle radii and hence to effective volume concentrations. The conversion from volume fractions x_V into effective volume concentrations is postponed to section IV.4. In contrast to the $x_{V,max}$ values, the exponents $[\eta] \cdot x_{V,max}$ delivered by the Krieger-Dougherty fits are in good agreement with the prediction of Einstein ($\left[[\eta] \cdot x_{V,max}\right]_{theo} = 2.5$). It follows that the silica particles can be considered as spheres.

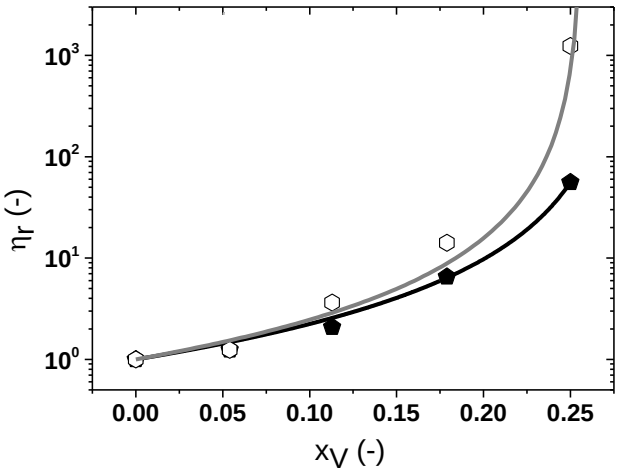

Figure IV-14: Relative viscosities $\eta_r = \eta_{HI}/\eta_m$ (closed symbols) and $\eta_r = \eta_0/\eta_m$(open symbols) for DGEBA/SiO_2 suspensions as a function of the volume concentration x_V. The black and grey lines correspond to fits of the Krieger-Dougherty relation (equation (2.2.2.9)) to the measured viscosities η_{HI} respectively η_0 delivering parameters $x_{V,max} = 0.28$ and $[\eta] \cdot x_{V,max} = 1.83$ for η_{HI} and $x_{V,max} = 0.26$ and $[\eta] \cdot x_{V,max} = 1.83$ for η_0

Table 4: Zero-shear and high frequency viscosity (η_0, η_{HI}) for the different volume concentrations x_V. The values of the viscosities were determined from equations (4.2.2.2) and (4.2.2.3). For both viscosities the used fit parameters for the Krieger-Dougherty relation are also listed.

Krieger-Dougherty Parameter	x_V (-)	η_{HI} ($\cdot 10^5$Pa.s)	η_0 ($\cdot 10^5$Pa.s)
	0	1.02	1.02
	0.05	1.27	1.27
	0.11	2.13	3.74
	0.18	6.71	14.5
	0.25	57.5	1270.4[6]
$\mathbf{x_{V,max}}$		0.28	0.26
$[\boldsymbol{\eta}] . \mathbf{x_{V,max}}$		1.83	1.83

ii) The low-frequency process

In the last subsection the influence of the silica particles on the glass transition behaviour of the matrix and the related viscosity has been discussed. However the nature of the low-frequency process observed in the last section is still unclear.

Available information on the low-frequency process

First of all it is important to note that the low-frequency process emerges in the master curves $G'(\omega)$ of all of the suspensions represented in Figure IV-8. While at the two highest concentrations the elastic quasi-plateau-like behaviour is accompanied by a transition in the loss shear modulus $G''(\omega)$, the latter cannot be observed at the lowest filler fractions. Therefore first clarification is needed whether the low-

[6] This viscosity has been determined using a different method (see appendix VI.3) than this described by equations (4.2.2.2) and (4.2.2.3)

frequency anomaly can be attributed to an additional relaxation process (beside the α-process). A first piece of answer is delivered by the Kramers-Kronig relation claiming that a relaxation process should manifest itself in both, the real and imaginary part of a susceptibility. This is clearly established for the complex shear moduli of the suspensions with volume concentrations $0.11 \leq x_V \leq 0.25$ (see Figure IV-15). This can be better illustrated by introducing the reduced moduli $G'_{red}(\omega)$ and $G''_{red}(\omega)$ as shown in Figure IV-15. The reduced shear moduli are obtained by extrapolating the high frequency tail of the master curves (in the frequency range between α-process and low-frequency anomaly) towards the lowest frequencies and subtracting it from the actually measured values.

Inspection of Figure IV-15 a)-c) yields that the behaviour of the reduced moduli resembles to a Maxwell-model:

- linear increase of both moduli fairly obeying to terminal regime conditions ;
- $G'_{red}(\omega) < G''_{red}(\omega)$in the terminal regime;
- Crossing of $G'_{red}(\omega)$ and $G''_{red}(\omega)$ at specific frequencies;

At the lowest filler contents the loss shear moduli appear to rigorously obey to terminal power-law scaling: there is no experimental evidence for a transition going along with the plateau-like behaviors of the corresponding storage shear moduli. As the effect of the fillers on $G''(\omega)$ already fades out with decreasing nanoparticle content at the highest concentrations it is surmised that at the lowest silica fractions the transition is no longer resolvable by the experimental probe. All of the arguments provided so far lead to the preliminary conclusion that the low-frequency anomaly is due to the occurrence of an additional relaxation process.

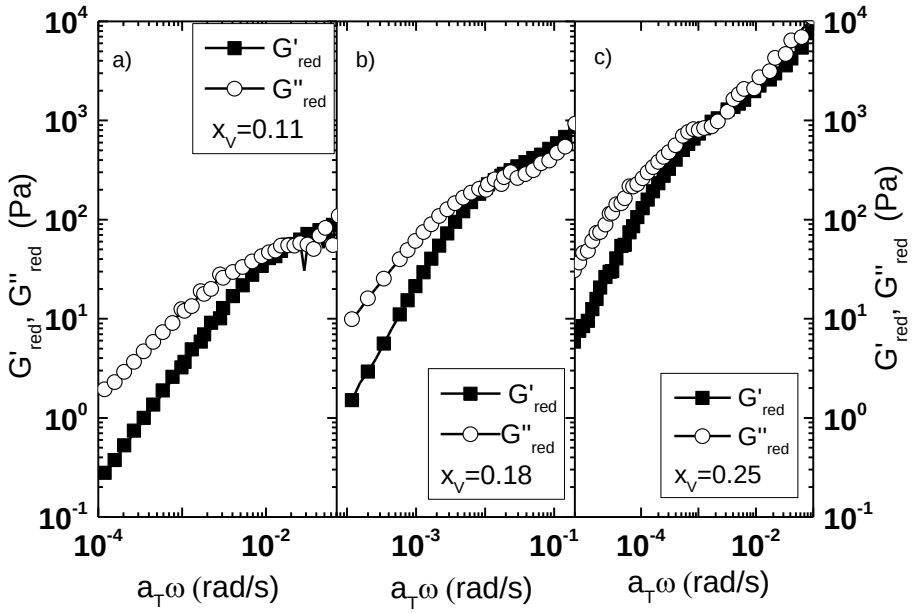

Figure IV-15: Representation of reduced shear moduli $G'_{red}(\omega)$ and $G''_{red}(\omega)$ at a reference temperature of $T_{ref} = 273K$ for DGEBA/SiO_2 suspensions with concentration range $0.11 \leq x_V \leq 0.25$

Secondly it is worth to stress that the low-frequency process appears only in presence of nanoparticles. Although the terminal regime of the pure matrix could so far only be investigated at frequencies higher then $10^0 rad/s$, there is no experimental evidence for the occurrence of an additional relaxation process. To the very best knowledge of the author of the present thesis there is also no hint in literature for the existence of a low-frequency relaxation process occurring in low molecular weight DGEBA which is slower than the α-process.

Astonishingly the low-frequency anomaly detected in the DGEBA/SiO_2 suspensions could not be observed by experimental methods like calorimetry, dielectric spectroscopy or refractometry. Apparently the low-frequency process mainly couples to the shear stress or disturbances caused by shearing. This does not necessarily mean that the low-frequency anomaly is shear-induced.

The last information helping to characterize the low-frequency process, regards the horizontal shift factors used to construct the master curves in Figure IV-8. From Figure IV-9 it becomes clear that all of the $log(a_T)(T)$ curves superpose irrespective of the filler content and temperature. As a matter of fact a single WLF-fit can be used to describe all of the $log(a_T)(T)$ curves. This leads to an interesting conclusion: The temperature dependency of the low-frequency relaxations should be similar to that of the alpha relaxations, which is a first hint that the relaxation times of the low frequency process are related to the suspension viscosity.

Interpretation of the low-frequency relaxations

Before coming up with a final interpretation of the low frequency relaxation process in the colloidal DGEBA/SiO_2 suspensions findings from literature will be reviewed. With all the knowledge on the low-frequency process compiled so far, only relaxation processes occurring in the presence of fillers have to be considered.

Literature indeed yields information on low-frequency relaxation processes occurring in colloidal suspensions [4, 81-83]. Two key mechanisms can be retained: (i) deformation relaxation of the suspended particles and (ii) relaxation of shear-induced perturbations of the particle distributions inside the suspensions. Both effects have individually been reported to occur in suspensions with silica particles.

(i) Vignaux-Nassiet, et al. [82] observed low-frequency behaviours of G' and G'' similar to those reported in this project on polybutadiene melts filled with micro-sized spherical silica. Using appropriated models the authors justify that the low-frequency relaxation is linked to deformation relaxation of a thin layer of polymer chains weakly interacting with the silica surfaces via Van der Waals dispersion forces. Due to the large size of the suspended particles Brownian diffusion effects could be neglected.

(ii) The investigation of linear viscoelastic behaviour of concentrated submicron silica suspensions in supercooled ethylene glycol/glycerol mixtures [4, 81] also revealed the existence of a low-frequency relaxation process. The authors attribute the process to the relaxation of shear-induced

perturbations of the particle distribution by diffusion processes resulting from Brownian motion. It has to be stressed that in the temperature range where the investigation took place the low-frequency relaxation was obviously not in competition with the dynamic glass transition of the ethylene glycol/glycerol mixture.

Basically both relaxation processes are possible in DGEBA/SiO_2 suspensions. Mechanism (i) relies on the presence of deformable layers around the nanoparticles. From section III.1.2 it is known that the silica particles are coated with ultra-thin silane layers (thickness *0.6 nm – 2 nm* (private communication of Dr. Sprenger from Evonik Hanse GmbH, Germany)). Due to the very small thickness a relaxation of this layer can be excluded. Adsorption of DGEBA molecules at the silica surfaces has to be excluded too. The related slow-down of the α-process of the matrix should –at least for high filler fractions of particles- be observable by other experimental probes working in the same frequency regime as the oscillatory shear rheology presented in this work. As already mentioned calorimetry (TMDSC) and refractometry failed to provide evidence for the low-frequency anomaly. In contrast relaxation of shear-induced perturbations of the particle distribution fits to all of the information previously provided. Moreover, as the shear-induced perturbation is balanced by Brownian motion, the characteristic timescales are expected to by coupled to the viscosity via diffusion processes (see equation (2.2.2.3)).

In the following the low-frequency anomaly occurring in the rheological measurements of the DGEBA/SiO_2 suspensions will tentatively be interpreted as a relaxation of the shear-induced perturbation of the particle distribution. Hereafter the process will be referred to as Brownian relaxation. In the following further striking arguments will be delivered fortifying the latter interpretation. However, firstly, the physical mechanism driving Brownian relaxation will be discussed.

Origin of Brownian relaxation

In colloidal suspensions at rest the stress – the stress due to interparticle forces (per example due to hydrodynamic interactions) - fluctuates since the colloids are subjected to Brownian motion (even if the time average is zero) [84]. In case that a small mechanical perturbation (as it is the case for small amplitude oscillatory shear experiments) is applied to the suspension, the particle distribution is slightly disturbed and additional hydrodynamic interactions appear due to the shearing motion of the colloids resulting in an artificially created stress called in the following shear-induced stress. The same microscopic mechanism, which leads to the temporal intrinsic stress fluctuations in suspensions at rest (i.e. Brownian motion of the colloids), tries to disintegrate the shear-induced stress. Hence this process is not instantaneous the shear-induced stress decay depends on the experimental timescale. In case of oscillatory shear experiments the timescale is pretended by the inverse of the angular frequency. Therefore at low frequencies (long times) the shear-induced stress has enough time to decay, while at high frequencies the experimental time window is too small resulting in the storage of the shear-induced stress.

Timescale of Brownian relaxation

In the previous sections the low-frequency process was interpreted as Brownian relaxation. So far however no convincing experimental argument was delivered helping to establish Brownian relaxation as the origin of the low-frequency process observed in Figure IV-8. Remaining doubts are justified as, to the author's very best knowledge, Brownian relaxation has never been observed in a colloidal suspension with a viscoelastic matrix.

A meticulous literature research only provided information on Brownian relaxation occurring in concentrated colloidal suspensions with Newtonian liquids as matrices [4, 50, 81]. All of the contributions found in literature have in common that they use the same timescale for the description of the low-frequency anomaly: the Peclet-time τ_p defined as

$$\tau_p = \frac{a^2}{6D}. \qquad (4.2.2.5)$$

τ_p describes the time needed by a spherical particle of radius a to cover a distance comparable to its own radius by diffusion. The right choice of the diffusion coefficient D is an ongoing matter of debate. Some authors use the short-time self-diffusion coefficient D_S [4, 5], while other claim that the long-time self-diffusion coefficient D_L is more appropriate [57, 84]. To keep the line at this place, the discussion on the diffusion coefficients is postponed to section IV.2.3. Relying on the work of Shikata and Pearson [4] the short-time self-diffusion coefficient D_S is tentatively used in this section. According to the Stokes-Einstein relation (equation (2.2.2.3)) D_S can be linked to the viscosity η_{HI} and the Peclet-time can be rewritten as

$$\tau_p = \frac{\pi \eta_{HI} a^3}{k_B T}. \qquad (4.2.2.6)$$

From equation (4.2.2.6) it becomes clear that, at a given temperature, the Peclet-time increases with the viscosity η_{HI} and hence with the filler fraction. The mean particle radius of the silica particles is $a = 12.5\ nm$ (see section III.1.2) and the temperature is $T_{ref} = 273K$. The measured viscosities η_{HI} are listed in Table 4. The related Peclet frequencies

$$\omega_p = \tau_p^{-1} \qquad (4.2.2.7)$$

are listed in Table 5 for all filler fractions and represented by red arrows in Figure IV-16. Obviously the Peclet-frequencies ω_p fit quite well to the respective onsets of the quasi-plateau like sections of the master curves $G'(\omega)$ represented in Figure IV-16.

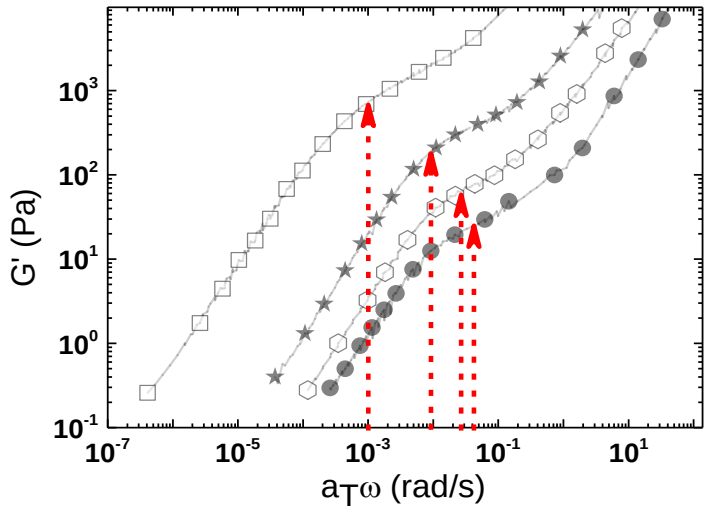

Figure IV-16: Low-frequency tails of the master curves $G'(\omega)$ represented in Figure IV-8 for the investigated DGEBA/SiO_2 samples (reference temperature $T_{ref} = 273K$). The dashed red arrows indicate the Peclet frequencies for the various silica fractions (see Table 5)

Equation (4.2.2.6) can alternatively also be exploited as a fit function for the Brownian relaxation times delivered by the experiment. Unfortunately the determination of the relaxation times is not straightforward. First the low-frequency relaxation is in competition with the α-process of the matrix. Secondly even if the Brownian relaxation can be deconvolved from the viscoelastic behaviour of the matrix (as done in Figure IV-15), the "high frequency" modulus $G_{BR,\infty}$ increasing with ω opposes the determination of the relaxation time by fitting the data to models like Maxwell or BSW. In this project operational methods as described in appendix VI.2 are used to determine the Brownian relaxation times. Table 5 lists the operational relaxation times τ as a function of the volume concentration x_V. As can be observed in Figure IV-17 the relaxation times τ increase with growing filler content. This behaviour is in agreement with the evolution of the Peclet time when the filler concentration changes. In order to use the Peclet time as a model function for a fit, an analytical function for the viscosity $\eta_{HI}(x_V)$ has to be introduced. In paragraph (i) of this section it has been shown that the viscosity $\eta_{HI}(x_V)$ can be described by the Krieger-Dougherty relation (equation (2.2.2.9)) with parameters $x_{V,max} = 0.28$ and $[\eta] \cdot x_{V,max} = 1.83$. Then equation (4.2.2.6) can be rewritten as

$$\tau_p(x_V) = \frac{\pi \eta_m a^3}{k_B T}\left(1 - \frac{x_V}{0.28}\right)^{-1.83}, \qquad (4.2.2.8)$$

where the particle radius is the only remaining fit parameter. The red line in Figure IV-17 represents the fit of equation (4.2.2.8) to the Brownian relaxation times. The fit yields a radius $a_{fit} = 17\ nm$. Obviously the relaxation times are adequately described by the Peclet-time although at the lowest filler fraction the fit value τ_P more substantially differs from the relaxation time obtained from the experiment.

Nevertheless it can be concluded that the Peclet time represents an appropriated timescale for the Brownian relaxation process observed in the DGEBA/SiO_2 suspensions with filler concentrations in the range $0.054 \leq x_V \leq 0.25$. The particle radius delivered by the fit perfectly matches the order of magnitude of the average particle radius $a = 12.5\ nm$ (see section III.1.2).

Table 5: Brownian relaxation time τ , Peclet-times τ_p and Peclet-frequencies ω_p at different volume concentrations x_V. The Peclet-times are calculated according to equation (4.2.2.6) using the high-frequency viscosities η_{HI} from Table 4 and a particle radius of 12.5 nm.

x_V (-)	τ (s)	τ_p (s)	ω_p (rad/s)
0.05	125	20.7	0.058
0.11	142	34.8	0.048
0.18	196	109	0.029
0.25	2325	937	0.009

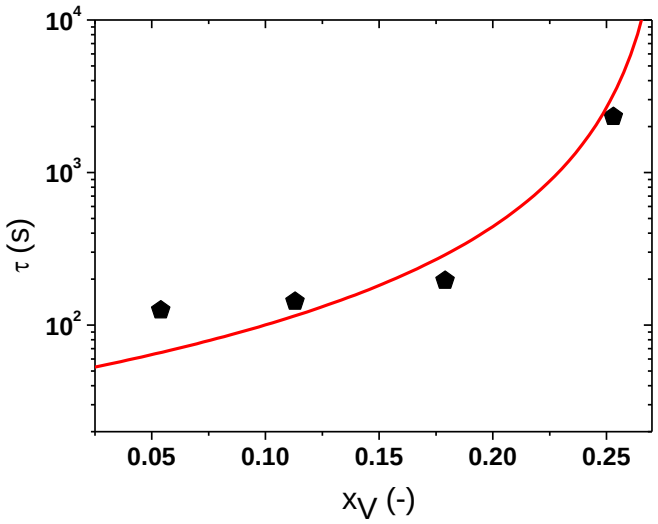

Figure IV-17: Operational Brownian relaxation times τ (data points) as a function of the filler volume concentration x_V . The τ values stem from Table 5. The red solid line corresponds to a least square fit of the Peclet time $\tau_p(x_V)$ (equation (4.2.2.8)) to the experimental relaxation time τ. The fit yields a particle radius $a_{fit} = 17\ nm$

Conclusion and outlook

So far evidences could be provided that the low-frequency process observed in DGEBA/SiO_2 suspensions can be interpreted as Brownian relaxation. Additionally it could be shown that the Peclet-time represents an appropriate timescale to describe the evolution of the Brownian relaxation times within the volume concentration range $0.054 \leq x_V \leq 0.25$.

Compared to findings on Brownian relaxation reported in literature the use of a matrix (DGEBA) with viscoelastic properties in the frequency range where the Brownian relaxation occurs represents a new result. The corresponding result have recently been published [80].

Moreover compared to suspensions known from literature to exhibit Brownian relaxation, the DGEBA/SiO_2 systems investigated in this project rely on nanoparticles with much smaller size. Indeed the smallest particles described in literature in the context of Brownian relaxation have sizes four times larger than those of the silica particles in this project [4, 50, 68]. However the particle size imposes limitations to the measurability of Brownian relaxation at low volume concentrations. Lionberger and Russel [45] found that the strength of the Brownian relaxator scales with the filler content and with a^{-3} (a: particle radius). Inspection of Figure IV-16 yields that the first prediction of Lionberger and Russel [45] holds true for the DGEBA/SiO_2 suspensions when one tentatively chooses the storage shear modulus $G^{'}$ at the onset of the quasi-plateau as a measure for the relaxation strength. As the relaxation strength also scales with a^{-3} it can be understood that the smallest filler fraction at which Brownian relaxation was observed in systems described in literature, is $x_V = 0.1$. Consequently the lowest volume concentration considered in this section ($x_V = 0.05$) is already smaller than the lowest filler fraction reported in literature. But still at this volume fraction the tentative Brownian relaxation strength is much higher than the resolution limit of the rheometer ($G^{'}(\omega), G^{''}(\omega) \approx 0.1Pa$). Therefore the investigation of Brownian relaxation in the DGEBA/SiO_2 suspensions can be extended to even smaller volume concentrations.

IV.2.3. Extension to ultra-dilute DGEBA/SiO_2 suspensions

In order to study Brownian relaxation in ultra-dilute colloidal DGEBA/SiO_2 suspensions, the same measurements as described in section IV.2.2 have been performed. The results from the frequency sweeps and the shift factors used to construct the master curves are represented in appendix VI.1. The temperature dependency of the shift factors applied for the construction of the master curves of the ultra-diluted suspensions is identical to the one obtained in case of the samples with higher filler fractions (Figure IV-9).

Figure IV-18 depicts the master curves $G'(\omega)$ and $G''(\omega)$ obtained for the DGEBA matrix and for DGEBA/SiO_2 suspensions with volume concentrations extending from 0.005 to 0.25 at a reference temperature $T_{ref} = 273K$. Obviously Brownian relaxation is observed for all of the investigated DGEBA/SiO_2 suspensions. In particular the phenomenon occurs in a DGEBA/SiO_2 suspension with $x_V = 0.005$, a filler content which is ten times smaller than in the most diluted DGEBA/SiO_2 suspension investigated so far and even reduced by a factor of 20 compared to the system with the smallest filler content reported in literature. However for samples with filler fractions smaller than $x_V = 0.005$ no trustable data for the low-frequency process could be obtained as the resolution limit of the rheometer has been reached.

Before tackling the discussion of the Brownian relaxation in ultra-dilute suspensions the influence of the silica particle on the dynamic glass transition of the DGEBA matrix is commented: As can be observed in Figure IV-18, at frequencies higher than *10 rad/s,* the suspensions with low volume concentrations ($0.005 \leq x_V \leq 0.026$)

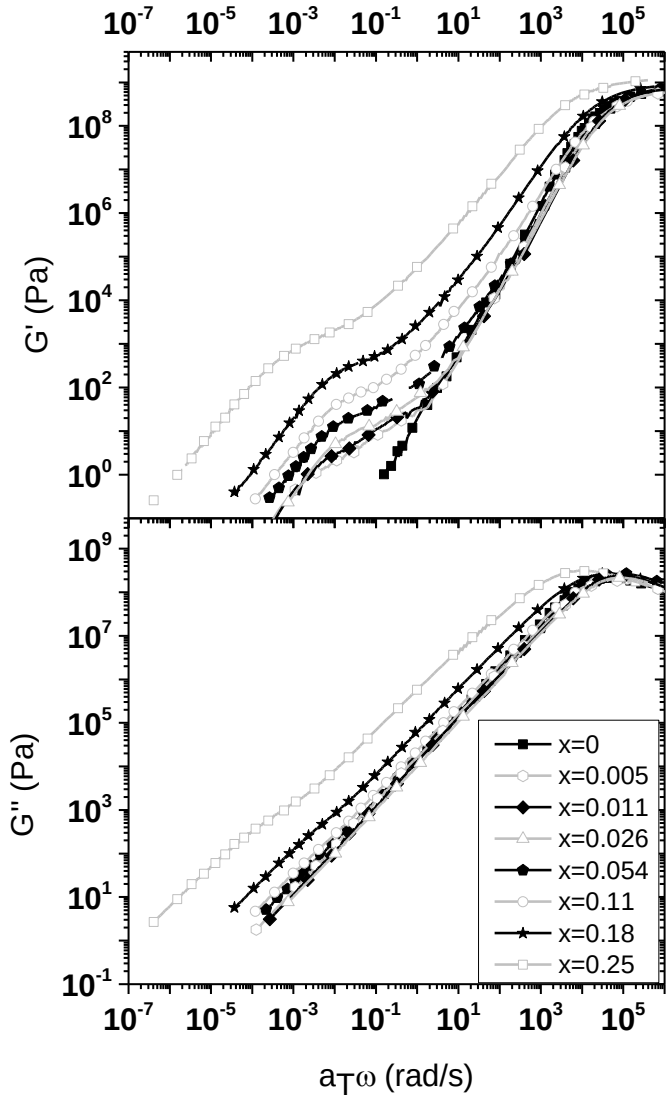

Figure IV-18: Master curves $G'(\omega)$ (upper figure) and $G''(\omega)$ (lower figure) for DGEBA/SiO_2 suspensions with different filler volume concentrations at the reference temperature $T_{ref} = 273K$. Symbols are only used for the sake of clarity; data points lie much closer and are here represented by solid lines.

exhibit exactly the same viscoelastic behaviour as the DGEBA matrix. This leads to the conclusion that, as expected, the dynamic glass transition is not affected by the nanoparticles in ultra-dilute suspensions.

A closer look at the low-frequency relaxation in Figure IV-18 yields a surprising feature: it seems that at the lowest filler concentrations, the operational onset frequency of the quasi-plateau regime does not decrease with the volume concentration (as it does in case of the suspensions with higher concentrations (see Figure IV-17)). The latter observation is corroborated by the representation in Figure IV-19. Here the low-frequency tails of the reduced storage moduli are shown for all of the filler fractions. The red arrows highlight the respective onsets of the quasi-plateau regimes.

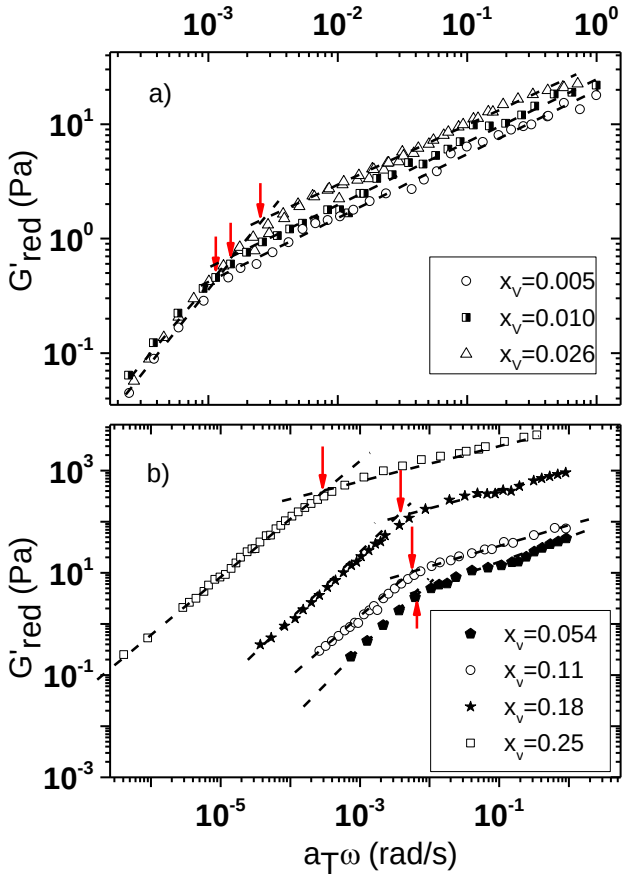

Figure IV-19: Low-frequency tails of the reduced storage shear moduli G'_{red} for a) $0.005 \leq x_V \leq 0.026$ and b) $0.054 \leq x_V \leq 0.25$ at the reference temperature $T_{ref} = 273K$. The arrows indicate the transition between terminal regime and quasi-plateau (and simultaneously the operational relaxation frequencies)

i) Non-monotonic concentration dependency of Brownian relaxation times

Table 6 lists the Brownian relaxation times obtained from the operational relaxation frequencies determined using Figure IV-18. Figure IV-20 depicts the evolution of the Brownian relaxation times as function of the filler fraction. Obviously, in case of the ultra-dilute suspensions, the relaxation times decrease with increasing filler content and pass through a minimum at a volume concentration located between $x_V = 0.05$ and $x_V = 0.1$. At higher concentrations the relaxation time monotonously increases. This non-monotonic behaviour of the relaxation time is clearly not in agreement with the evolution of the Peclet time (grey line in Figure IV-20), which monotonously increases with growing x_V.

The non-monotonic dependency of the Brownian relaxation times on the concentration is supported by theoretical models described in literature. In fact Banchio, et al. [57] applied mode-coupling theory to investigate the micro-viscoelastic behaviour of colloidal suspensions containing hard spheres.

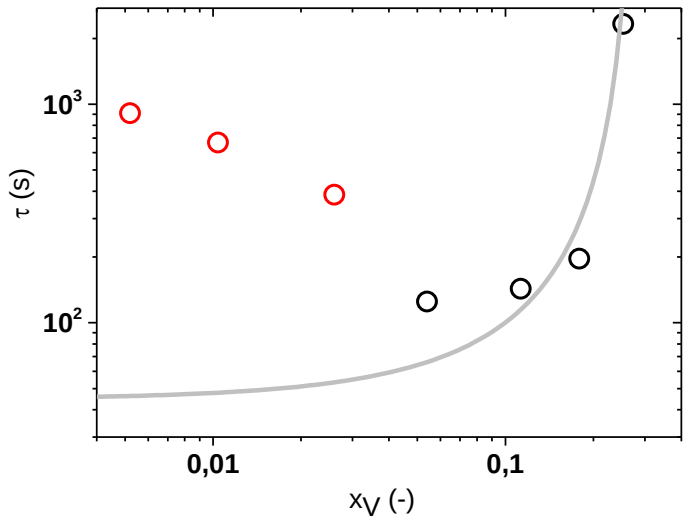

Figure IV-20: Operational Brownian relaxation times τ as a function of the volume concentration x_V. The red symbols represent the relaxation times determined for the ultra-diluted DGEBA/SiO_2 suspensions. The black symbols correspond to the relaxation times determined for the concentrated suspensions discussed in section IV.2.2. The grey line visualizes the evolution of the Peclet-time as a function of the filler content (equation (4.2.2.8)). The data rely on the particle radius $a_{fit} = 17\ nm$ delivered by the fit of equation (4.2.2.8)) to the operational relaxation times discussed in section IV.2.2

The authors could establish that the Brownian relaxation times non-monotonously depend on the filler fraction. In analogy to the results presented in the present thesis mode-coupling theory predicts relaxation times decreasing at low filler fractions and increasing at high volume concentrations. Hence the relaxation time passes through a minimum which is located at a concentration around $x_{V,min} \approx 0.3$. This value definitely does not coincide with the concentration at which the minimum occurs for the relaxation times determined for the DGEBA/SiO_2 suspensions. This deviation might be considered as a disagreement between the theoretical model established by Banchio, et al. [57] and the experimental data found for the DGEBA/SiO_2 suspensions. However in subsection iv) of this section it will be shown that the discrepancy has to be expected when one considers that the viscosity of the DGEBA/SiO_2 suspensions exhibits another concentration dependency as the one of the system studied by Banchio, et al. [57]. So far the theoretical model developed by Banchio, et al. [57] was only supported by experimental data obtained from higher concentrated suspensions [5]. As already mentioned, Brownian relaxation times obtained from experimental investigations of ultra-diluted suspensions are still missing. Thus there is so far no experimental evidence for the non-monotonous behaviour of the Brownian relaxation times when the filler concentration increases.

Table 6: Operational Brownian relaxation time τ as function of the volume concentrations x_V for DGEBA/SiO_2 suspensions

x_V (-)	τ (s)
0.005	909
0.01	666
0.026	384
0.05	125
0.11	142
0.18	196
0.25	2325

ii) Characteristic timescale for Brownian relaxation: generalization of the Peclet-time

Obviously, in order to be able to predict the behaviour of the Brownian relaxation time throughout the whole concentration range the definition of the Peclet-time needs to be reviewed.

Requirements for the characteristic timescale

In general the idea of using a diffusion time as a characteristic timescale for a process such as Brownian relaxation seems to be justified as the phenomenon is linked to intrinsic diffusion processes. In a suspension with spherical particles the diffusion time can be defined as the time needed by a particle to cover a characteristic length by diffusion i.e.

$$\tau_D(x_V) = \frac{k^2(x_V)}{6D(x_V)}, \qquad (4.2.3.1)$$

where $k(x_V)$ represents the characteristic length-scale and $D(x_V)$ an adequate self-diffusion coefficient. Equation (4.2.3.1) follows directly from Einstein's expression for the mean square displacement of a particle diffusing in a three dimensional space (equation (2.2.2.2)). Consequently the diffusion time τ_D is characterized by two parameters depending on the filler concentration $k(x_V)$ and $D(x_V)$.

In equation (4.2.3.1) the nature of the diffusion coefficient is not specified. Generally the short-time self-diffusion coefficient $D_s(x_V)$ or the long- time self-diffusion coefficient $D_L(x_V)$ can be used. Both of them decrease with increasing nanoparticle content. At low volume concentrations $D_s(x_V)$ and $D_L(x_V)$ are practically equal: Both coefficients can be used. However at high filler fractions the difference between the two diffusion coefficients becomes considerable. While the short-time self-diffusion coefficient $D_s(x_V)$ tends to zero at the maximum packing fraction $x_{V,rcp}$ [46, 57], the long-time self-diffusion coefficient $D_L(x_V)$ converges to zero at the filler fraction corresponding to the particle glass transition $x_{V,g}$ (see section II.2.2) [54]. In most of the contributions from literature related to Brownian relaxation phenomena there is a common understanding that the relaxation times diverge at the particle

glass transition [4, 84]. Hence the long-time self-diffusion coefficient seems to be the most appropriated for the description of the Brownian relaxation times[7]. As previously shown the Stokes-Einstein equation (equation (2.2.2.5)) relates the long-time self-diffusion coefficient to the zero-shear viscosity η_0. Consequently the diffusion time from equation (4.2.3.1) can be expressed by

$$\tau_D(x_V) = \frac{a\pi}{k_B T}\eta_0(x_V)\cdot k^2(x_V)\cdot \qquad (4.2.3.2)$$

The zero-shear viscosity monotonously increases with the filler fraction. If $k(x_V) = a$, the diffusion time τ_D corresponds to the Peclet-time and monotonously increases with the filler fraction. Obviously such a behaviour does not agree with the experimental findings presented in this thesis. In contrast a characteristic length $k(x_V)$, decreasing in an appropriate manner with growing volume concentration, would allow to explain the emergence of a minimum of the diffusion time τ_D. In fact, as the zero-shear viscosity of ultra-diluted suspensions can in a first approximation be considered as quasi-constant (see Figure IV-14), a characteristic length $k(x_V)$ decreasing with increasing filler fraction could be responsible for the reduction of the diffusion time τ_D. At high volume concentrations the zero-shear viscosity strongly increases. Therefore, if at high filler fractions $k(x_V)$ would decrease slower than $\eta_0(x_V)$ increases the diffusion time could be expected to increase. Hence this scenario would lead to a minimum in the diffusion time τ_D at a volume concentration $x_{V,min}$, depending on both, $\eta_0(x_V)$ and $k(x_V)$.

Characteristic length-scales

The mean distance $\langle r(x_V)\rangle$ between neighbouring particles is a characteristic length fulfilling the requirements described here above. Moreover it has been stated that interactions between particles are a prerequisite for Brownian relaxation. Common to all interactions is the fact that they get stronger (according to specific distance laws) when the distance between the particles decreases. In most of the cases the interactions are short-range and can only have an effect when the particles are relatively close. Hence the characteristic range that a suspended particle has to cover by diffusion before interaction forces with other particles start to get noticeable somehow scales with the average particle –particle distance. To get a first impression for the influence of a characteristic length on the filler fraction evolution of the diffusion time it is surmised that $k(x_V) = \langle r(x_V)\rangle$. Then the diffusion time τ_D in equation (4.2.3.2) can be written as

$$\tau_{\langle r\rangle}(x_V) = \frac{a\pi}{k_B T}\eta_0(x_V)\cdot\langle r(x_V)\rangle^2 \qquad (4.2.3.3)$$

[7] In the previous section IV.2.2 the short-time self-diffusion coefficient $D_s(x_V)$ was tentatively used for the calculation of the Peclet-time following the work of [4] T. Shikata and D. S. Pearson, "Viscoelastic behavior of concentrated spherical suspensions," *Journal of Rheology,* vol. 38, pp. 601-616, 1994. However since the most of findings from literature suggest the use $D_L(x_V)$ the latter will be used in the following.

In the last equation the index $\langle r \rangle$ is meant to highlight the assumption $k(x_V) = \langle r(x_V) \rangle$. The surface-to-surface mean particle distance represents a possible choice for $\langle r(x_V) \rangle$:

$$\left\langle r(x_V) \right\rangle_{SS} \approx 2a\left(\left(\frac{x_{V,rcp}}{x_V} \right)^{1/3} - 1 \right) \qquad (4.2.3.4)$$

where $x_{V,rcp} = 0.63$ is the maximum packing fraction for randomly dispersed particles (see section II.2.2).

With equation (4.2.3.4) and the zero-shear viscosity obeying to the semi-empirical Krieger-Dougherty model (see section IV.2.2) with parameters $x_{V,max} = 0.26$ and $[\eta] \cdot x_{V,max} = 1.83$ the diffusion time (equation (4.2.3.2)) can be expressed as

$$\tau_{\langle r \rangle,SS} = 4\frac{a^3 \pi \eta_m}{k_B T}\left(1 - \frac{x_V}{0.26}\right)^{-1.83} \cdot \left(\left(\frac{x_{V,rcp}}{x_V} \right)^{1/3} - 1 \right)^2, \qquad (4.2.3.5)$$

Here the additional index '*ss*' is meant to stress the use of the surface-to-surface mean particle distance as a characteristic length. Equation (4.2.3.5) can be fitted to the relaxation times depicted in Figure IV-20 (red line in Figure IV-21). Again the particle radius *a* is used as fit parameter. The model (equation (4.2.3.5)) not only fully describes the non-monotonic evolution of the Brownian relaxation times when the filler concentration varies but also yields a good particle radius $a_{fit} = 12.5nm$ (see section III.1.2). This finding has recently been published [85].

Banchio, et al. [57] illustrate that the relaxation times obtained by mode-coupling theory can properly be approximated by the diffusion times needed by a filler to cover distances comparable to the center-to-center mean-particle distance

$$\left\langle r(x_V) \right\rangle_{CC} = 0.3a\left(\frac{4\pi}{3x_V} \right)^{1/3}. \qquad (4.2.3.6)$$

Replacing $\langle r(x_V) \rangle_{SS}$ in equation (4.2.3.5) by $\langle r(x_V) \rangle_{CC}$ (equation (4.2.3.6)) yields

$$\tau_{\langle r \rangle,CC} = 0.09\frac{a^3 \pi \eta_m}{k_B T}\left(1 - \frac{x_V}{0.26}\right)^{-1.83} \cdot \left(\frac{4\pi}{x_V} \right)^{2/3}. \qquad (4.2.3.7)$$

The grey line in Figure IV-21 describes the fit of equation (4.2.3.7) to the experimental Brownian relaxation times. This time the fit delivers a particle radius $a_{fit} = 11.2nm$ which still matches the order of magnitude of the value given in section III.1.2. Even if the curves $\tau_{\langle r \rangle,SS}(x_V)$ and $\tau_{\langle r \rangle,CC}(x_V)$ do not coincide both of them sustain the experimental data. Consequently the mean particle distance seems to represent a good approach for the characteristic diffusion length in the colloidal suspensions under investigation.

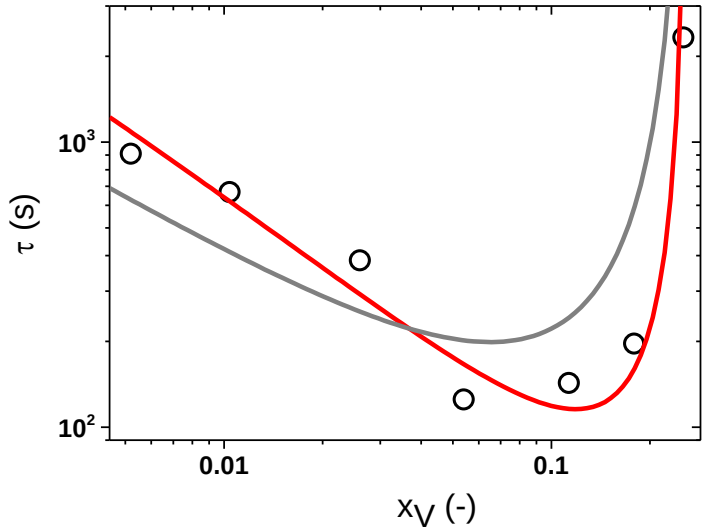

Figure IV-21: Brownian relaxation times in DGEBA/SiO_2 suspensions as a function of the filler fraction ($T_{ref} = 273K$). The black dots correspond to the relaxation times τ evaluated from experimental data gained from oscillatory shear measurements (see Table 6). The red line corresponds to a least square fit of equation (4.2.3.5) to the experimental relaxation times yielding a particle radius $a_{fit} = 12.5nm$. The grey line describes a least square fit of equation (4.2.3.7) to the experimental relaxation times ($a_{fit} = 11.2nm$)

iii) Link between Brownian relaxation times and characteristic transition times in the diffusion behaviour of colloidal suspensions

As previously mentioned Brownian relaxation can be considered as the macroscopic signature of the microscopic temporal fluctuation of the intrinsic stress which for sure is not shear induced. This argument has been corroborated by Sohn and Rajagopalan [42] who used passive microrheology to record the mean square displacement of a tagged particle suspended in a fluid matrix as a function of time. The authors found that the mean square displacement reveals three diffusive regimes: Short-time self-diffusion, sub-diffusion (cage effect) and long-time self-diffusion (as schematically shown in Figure IV-22). Following the local power-law method based on Mason's prescription [86] the authors could extract the complex shear modulus from the logarithmic time derivative of the measured mean square displacement. Most interestingly Sohn and Rajagopalan [42] could show that - in the time domain - the transition from short- to long-time self-diffusion behaviour goes along with Brownian relaxation in the frequency domain. Consequently characteristic transition times between short- to long-time self-diffusion behaviour should directly be linked to Brownian relaxation times.

In literature it has been shown that the cage effect becomes important when colloids have diffused over distances in the order of the mean interparticle distance $\langle r \rangle$ (see grey line in Figure IV-22) [43]. Hence the transition from short-time to long time diffusion is expected to occur at a time corresponding to the one needed by the particle to cover the distance $\langle r \rangle$. However, as can be seen in Figure IV-22, this specific time is ill-defined.

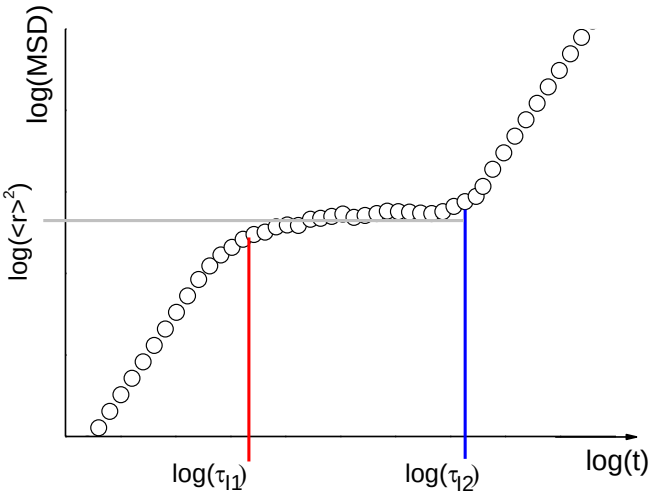

Figure IV-22: Schematic representation of the temporal evolution of the mean square displacement (MSD) in a double logarithmic representation. The horizontal grey line indicates that the cage effect appears at distances of order of the mean particle separation $\langle r \rangle$. The red and blue lines depict the transition τ_{I1} and τ_{I2} (see text)

Fortunately Sanchez-Miranda, et al. [44] have shown that the transition time between short-time self-diffusion and sub-diffusion behaviour (see red line in Figure IV-22) is given by

$$\tau_{I1} = \frac{\langle r(x_v) \rangle^2}{6D_S}, \qquad (4.2.3.8)$$

where D_S represents the short-time self-diffusion coefficient, while the transition from sub-diffusive to long-time self-diffusion behaviour (see blue line in Figure IV-22) is expressed by [43]

$$\tau_{I2} = \frac{\langle r(x_v) \rangle^2}{6D_L} \qquad (4.2.3.9)$$

with D_L the long-time self-diffusion coefficient. Obviously the expressions for both transition times τ_{I1} and τ_{I2} corroborate the choice of the characteristic diffusion timescale $\tau_{\langle r \rangle}$ (equation (4.2.3.3)) and hence of the length-scale $\langle r \rangle$. To summarize:

- Brownian relaxation times can be linked to diffusion times,
- Brownian relaxation times are directly related to characteristic transition times in the diffusion behaviour.
- the mean interparticle distance seems to be the adequate length-scale for the diffusion times.

iv) Discussion of the location of the minimum of Brownian relaxation times

Both, experimental investigations and theoretical modelling provide information on the evolution of the Brownian relaxation time τ when the particle fraction x_V in a colloidal suspension varies. It has been established that the curves $\tau(x_V)$ delivered by experiment and theory respectively share several common features (e. g. non-monotonic behaviour). However the locations of the minimum of $\tau(x_V)$ delivered by the experiment and predicted by theory deviate substantially: The experiment delivers a minimum of $\tau(x_V)$ located in the concentration interval $0.05 - 0.1$; mode-coupling theory predicts that the minimum has to be expected at a filler fraction $x_{V,min} = 0.3$.

As stated previously, $x_{V,min}$ depends on the competition between the monotonously increasing viscosity function $\eta_0(x_V)$ and the monotonously decreasing characteristic length function $k(x_V)$. In case of DGEBA/SiO_2 suspensions the zero-shear viscosity diverges at a volume concentration $x_{V,max} = 0.26$ (see section IV.2.2). Banchio, et al. [57] studied neutral hard sphere suspensions where $\eta_0(x_V)$ diverges at the particle glass transition ($x_{V,max} \approx 0.58$). Hence the location of the minimum of the Brownian relaxation times has to be different for both systems. Banchio, et al. [57] also investigated highly charged hard sphere suspensions. For this type of suspensions the viscosity diverges at a volume concentration $x_{V,max} \approx 0.1$ while $\tau(x_V)$ keeps its non-monotonic behaviour. In this case the minimum of the relaxation times appears around $x_{V,min} = 0.02$.

In the following it is assumed that, irrespective of the nature of the investigated system, the dependence of the suspension viscosity on the filler volume concentration can be described by the Krieger-Dougherty model (see section II.2.2):

$$\eta_0(x_V) = \eta_m \left(1 - \frac{x_V}{x_{V,\max}}\right)^{[\eta] \cdot x_{V,\max}} . \qquad (4.2.3.10)$$

To illustrate how $x_{V,max}$ in equation (4.2.3.10) takes influence on the location of the minimum $x_{V,min}$ of the diffusion or Brownian relaxation times (equation (4.2.3.2)) the equation

$$\frac{d\tau_{D,i}(x_{V,\min})}{dx_V} = 0 \qquad (4.2.3.11)$$

is solved ($i = ss$ or $i = cc$). In Figure IV-23 the volume concentration $x_{V,min}$ is represented as a function of $x_{V,max}$ for the exponent $\left[[\eta] \cdot x_{V,max}\right]_{theo} = 1.83$. Obviously for both characteristic lengths ($\langle r(x_V)\rangle_{SS}$ and $\langle r(x_V)\rangle_{CC}$ the location of the minimum $x_{V,min}$ is shifted towards higher concentrations when $x_{V,max}$ increases. In case of the DGEBA/SiO_2 suspensions the zero-shear viscosity diverges at $x_{V,max} = 0.26$. For this value an inspection of Figure IV-23 yields a minimum of the relaxation

time around $x_{V,min} = 0.12$ using $k(x_V) = \langle r(x_V)\rangle_{SS}$ and $x_{V,min} = 0.07$ for $k(x_V) = \langle r(x_V)\rangle_{CC}$. Both values are not in contradiction to the experimental result ($x_{V,min} \in [0.05; 0.1]$). Banchio, et al. [57] studied neutral hard sphere suspensions, for which $x_{V,max} = 0.58$. In this case the minimum of the relaxation time is expected at $x_{V,min} = 0.45$ when $k(x_V) = \langle r(x_V)\rangle_{SS}$ and $x_{V,min} = 0.17$ when $k(x_V) = \langle r(x_V)\rangle_{CC}$. It is worth noting that the value $x_{V,min} = 0.30$ reported by Banchio, et al. [57] ranges within the concentration interval $[0.17; 0.45]$. To summarize, for a given characteristic diffusion length, the location of the minimum of the Brownian relaxation times is controlled by the filler fraction at which the suspension viscosity diverges.

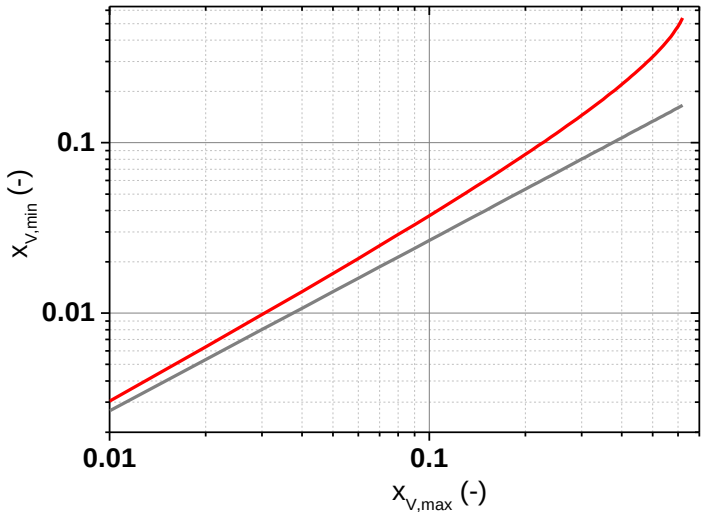

Figure IV-23: Location of the minimum $x_{V,min}$ of the diffusion times $\tau_{D,SS}$ and $\tau_{D,CC}$ (red and grey lines respectively) as a function of the filler fraction $x_{V,max}$ at which the suspension viscosity diverges. $x_{V,min}$ has been determined using equation (4.2.3.11) and the semi-empirical Krieger-Dougherty relation with $x_{V,max} \cdot [\eta] = 1.83$

IV.3. Influences of the nature of the suspended particles and the properties of the matrix on the dynamics of viscoelastic colloidal suspensions

In the last section it has been established that in colloidal DGEBA/SiO_2 suspensions the non-monotonic evolution of the Brownian relaxation times with changing filler content can be described by diffusion times which depend on the suspension viscosity and on the choice of a characteristic diffusion length-scale.

Generally it is assumed that the characteristic diffusion length depends on the nature of the particle-particle interactions. Taking into account the Krieger-Dougherty relation for the suspension viscosity the diffusion time τ_D can be written as

$$\tau_D = 4\frac{a\pi\eta_m}{k_B T}\left(1-\frac{x_V}{x_{V\max}}\right)^{-[\eta]x_{V\max}} \cdot k(x_V) \qquad (4.3.1.1)$$

At a given temperature the diffusion time τ_D depends on the filler concentration x_V, the matrix viscosity η_m, the particle radius a, the particle shape (via the intrinsic viscosity $[\eta]$) and the characteristic length-scale. Hence if the self-diffusion time (equation (4.3.1.1)) is supposed to be qualified to describe Brownian relaxation in a more general context, the Brownian relaxation times derived from experimental data have to scale with the characteristic self-diffusion time when one or more of the previously mentioned parameters vary.

In the following it will be tested whether the validity range of equation (4.3.1.1) can be extended to colloidal suspensions with modified matrices or being filled with a different type of nanoparticles. In a first step DGEBA/SiO2 suspensions with modified DGEBA matrices will be studied. In a second step the silica particles in the original DGEBA matrix will be replaced by alumina particles.

IV.3.1. Influence of the matrix viscosity

From equation (4.3.1.1) it gets clear that the diffusion time τ_D linearly increases with the matrix viscosity. Do the Brownian relaxation times exhibit the same behaviour? Two series of measurement will be described. First Brownian relaxation will be investigated on a set of DGEBA/SiO_2 suspensions with DGEBA matrices cured with different amounts of Bisphenol A. Thereby the concentration of the silica particles will be kept constant at $x_V = 0.05$. Second it will be checked whether the non-monotonic behaviour of the Brownian relaxation times found for DGEBA/SiO_2 suspensions with an uncured DGEBA matrix can be reproduced on a set with silica suspensions with a cured DGEBA matrix.

Before starting the investigation of the suspensions the DGEBA matrices cured with different amounts of Bisphenol A need to be characterized.

In section III.1.1 it has been shown that the degree of polymerization of DGEBA can be increased by curing the original oligomer with Bisphenol A. However from the distribution of the molecular weights shown in Figure III-3 it becomes clear that besides linearly polymerized DGEBA molecules, there are also branched molecules which are formed during the curing process. Consequently it is impossible to unambiguously characterize the chemically modified DGEBA by a degree of polymerization. Hence the mass ratio $r_{BPA} = m_{BPA}/m_{DGEBA}$ will be used to specify the different DGEBA matrices used in the following.

Figure IV-24 shows the master curves $G'(\omega)$ and $G''(\omega)$ for polymerized DGEBA matrices with mass ratios $0 \leq r_{BPA} \leq 0.7$ at the reference temperature $T_{ref} = 273K$. The master curves with $r_{BPA} = 0$ correspond to the neat DGEBA matrix used in the previously described investigations and already characterized in detail in section IV.1. Curing of DGEBA with BPA only leads to a horizontal shift of the master curves compared to those of neat DGEBA. This implies that:

i) The dynamic glass transition is shifted towards smaller frequencies with increasing mass ratio of cured Bisphenol A. The slowing down of the dynamic glass transition is correlated with an increase of the suspension

viscosity which can be determined from the loss modulus $G''(\omega)$ using equation (4.1.2.1). In fact, as can be seen in Table 7, the matrix viscosity increases by five orders of magnitude when the ratio r_{BPA} increases from 0 to 0.7.

ii) Besides the α-process no additional relaxation process is visible in the master curves. In fact all of the investigated matrices exhibit the same terminal regime scaling i.e. $G'(\omega) \propto \omega^{1.86}$and $G''(\omega) \propto \omega^{0.99}$. From the absence of rubbery plateau regimes it is concluded that even for the highest mass ratio $r_{BPA} = 0.7$ most of the molecules in the matrix possess molecular weights lower than $M_n \leq 1000\ g/mol$ [26]. It follows that all of the polymerized matrices can still be considered as low-molecular weight glass former.

To summarize curing of DGEBA with BPA allows to systematically change the viscosity of the matrix (slowing own of the α-process) without taking influence on the "shape" of the master curves.

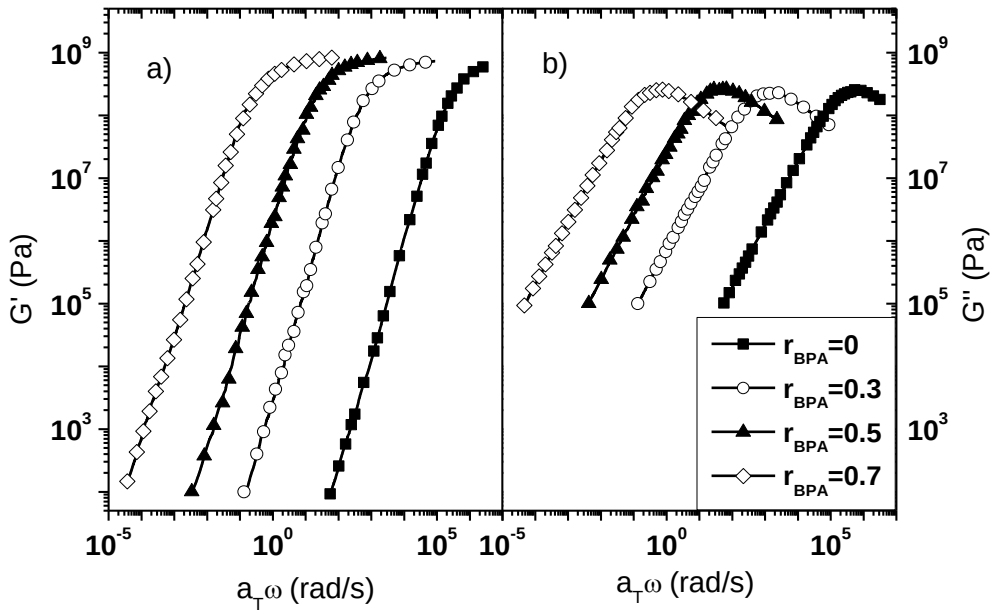

Figure IV-24: Master curves $G'(\omega)$ (a) and $G''(\omega)$ (b) obtained for DGEBA/BPA matrices with different mass ratios $r_{BPA} = m_{BPA}/m_{DGEBA}$ at the reference temperature $T_{ref} = 273K$.

i) Influence of the matrix viscosity on the linear viscoelastic behaviour of DGEBA+ 5 vol% SiO_2 suspensions

After characterizing the linear viscoelastic behaviour of the cured DGEBA matrices, the influence of the matrix viscosity on the Brownian relaxation phenomenon in DGEBA/SiO_2 suspensions can be studied. For this purpose first the linear viscoelastic behaviour of suspensions with a fixed volume concentration $x_V = 0.05$ of silica particles are investigated for different mass ratios r_{BPA}.

Figure IV-25 allows to compare the master curves $G'(\omega)$ and $G''(\omega)$ for the cured DGEBA matrices (closed symbols) to those of the corresponding DGEBA/SiO_2 suspensions with $x_V = 0.05$ (open symbols). The reference temperature is $T_{ref} = 273K$ and $0 \leq r_{BPA} \leq 0.7$. Obviously the master curves of the suspensions and the respective matrices shift identically to lower frequencies with increasing mass ratio r_{BPA}: the silica embedded in the various DGEBA matrices do not influence the dynamic glass transition.

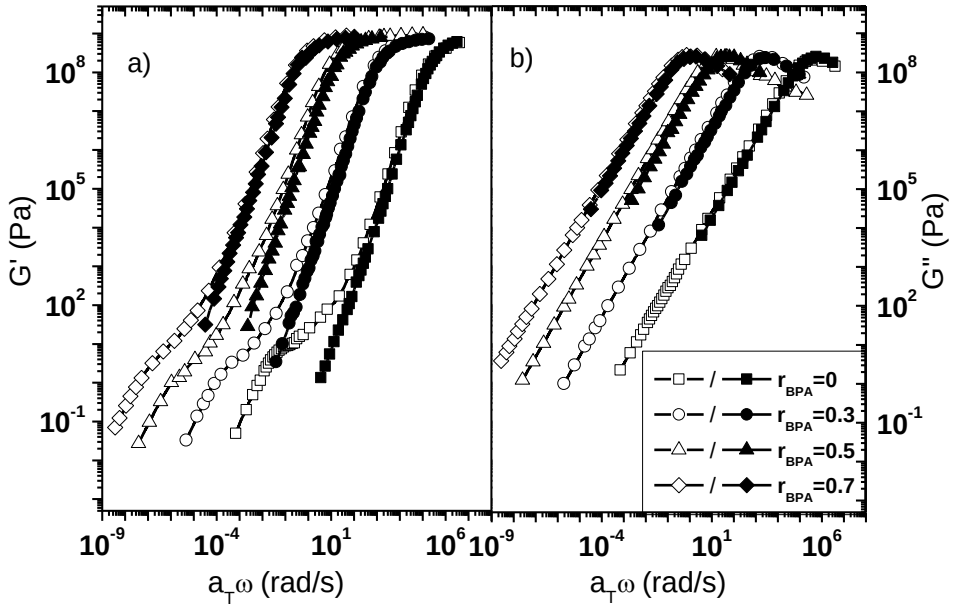

Figure IV-25: Master curves $G'(\omega)$ (a) and $G''(\omega)$ (b) for polymerized DGEBA matrices (closed symbols) as well as for the polymerized DGEBA/SiO_2 suspensions with $x_V = 0.05$ (open symbols) both for different mass ratios r_{BPA} at the reference temperature $T_{ref} = 273K$.

Irrespective of the mass ratio r_{BPA} Brownian relaxation manifests itself by the occurrence of a low-frequency plateau-like elastic behaviour of the storage shear moduli $G'(\omega)$. According to the Kramers-Kronig relation this feature should be accompanied by a transition of $G''(\omega)$ from a regime with zero-shear viscosity η_0 to "high-frequency" viscosity η_{HI}. For the samples discussed in this section the filler concentration is small to such an extent that the latter transition is not detectable in the loss shear moduli i. e. $\eta_0 \approx \eta_{HI}$. For the determination of the Brownian relaxation times τ the operational procedures presented in appendix VI.2 are used. The τ –values

are listed in Table 7 for the different mass ratios r_{BPA} and represented in Figure IV-25 as a function of the matrix viscosities η_m determined in the previous section (see Table 7).

In Figure IV-26 the Brownian relaxation times τ (open symbols) are represented as a function of the matrix viscosity η_m. The lines in Figure IV-26 depict the diffusion times $\tau_{\langle r\rangle,SS}$ (red line), $\tau_{\langle r\rangle,CC}$(grey line) and the Peclet-time τ_p (dashed line) calculated according to equation (4.3.1.1) using the different length-scales $k(x_V) = \langle r(x_V)\rangle_{SS}; \langle r(x_V)\rangle_{CC}; a$. For the calculations $a = 12.5\,nm$, the reference temperature $T_r = 273K$ and a volume concentration $x_V = 0.05$ have been used. Clearly the diffusion times calculated for the different characteristic length scales qualitatively agree with the Brownian relaxation times τ delivered by the experiment. Hence the Brownian relaxation times linearly increase with the matrix viscosity.

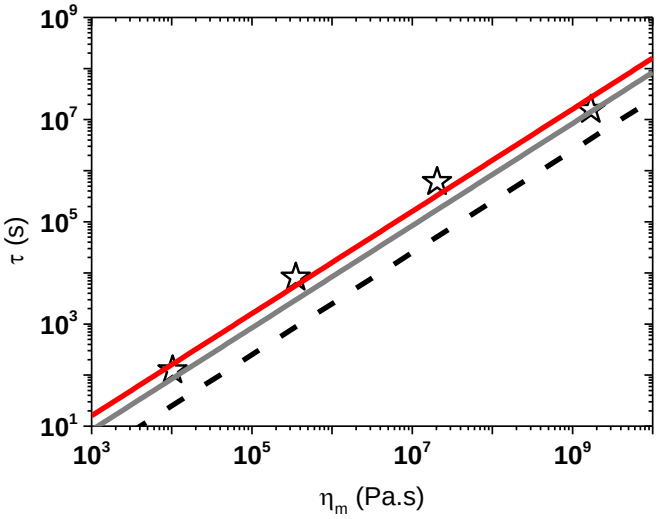

Figure IV-26: Relaxation times as a function of the matrix viscosity. All values are taken from Table 7. The solid lines correspond to the diffusion times $\tau_{\langle r\rangle,SS}$ (red line) and $\tau_{\langle r\rangle,CC}$ (grey line) from equation (4.2.3.5) respectively (4.2.3.7) using the parameters $a = 12.5\,nm$, $T = 273K$ and $x_V = 0.05$. The dashed line illustrates the variation of the Peclet-time (equation (4.2.2.8)) calculated for the same parameters.

Table 7: Matrix viscosities η_m and Brownian relaxation times τ at different mass ratios $r_{BPA} = 0; 0.3; 0.5; 0.7$. The viscosities and the relaxation times are determined using equation (4.1.2.1) and applying the operational procedure presented in appendix VI.2.

r_{BPA} (-)	η_m (Pa.s)	τ (s)
0	$1.03 \cdot 10^4$	125
0.3	$3.52 \cdot 10^5$	$8.13 \cdot 10^4$
0.5	$2.40 \cdot 10^7$	$6.05 \cdot 10^5$
0.7	$1.70 \cdot 10^9$	$1.55 \cdot 10^7$

ii) Influence of the nanoparticle concentration on the linear viscoelastic behaviour of polymerized DGEBA/SiO_2 suspensions

Obviously the Peclet-time yields a fair description of the evolution of the Brownian relaxation times when the matrix viscosity changes. In the following it will be shown that the Peclet-time fails again when an adequate characterization of $\tau(x_V)$ is required in case of a DGEBA/SiO_2 suspension with a cured matrix. The investigation will be carried out on a set of DGEBA/SiO_2 suspensions with a cured DGEBA matrix ($r_{BPA} = 0.3$) and filler concentrations $0 \leq x_V \leq 0.18$. The matrix used in the current study has a viscosity which is by a factor 70 higher than for the system studied in section IV.2.3 (see Table 7).

Figure IV-27 depicts the master curves $G'(\omega)$ and $G''(\omega)$ for the cured DGEBA/SiO_2 suspensions with a cured matrix at a reference temperature $T_{ref} = 273K$. As expected the dynamic glass transition is only slightly affected by the silica particles and Brownian relaxation manifests itself by the emergence of a plateau-like elastic behaviour of the storage shear moduli $G'(\omega)$.

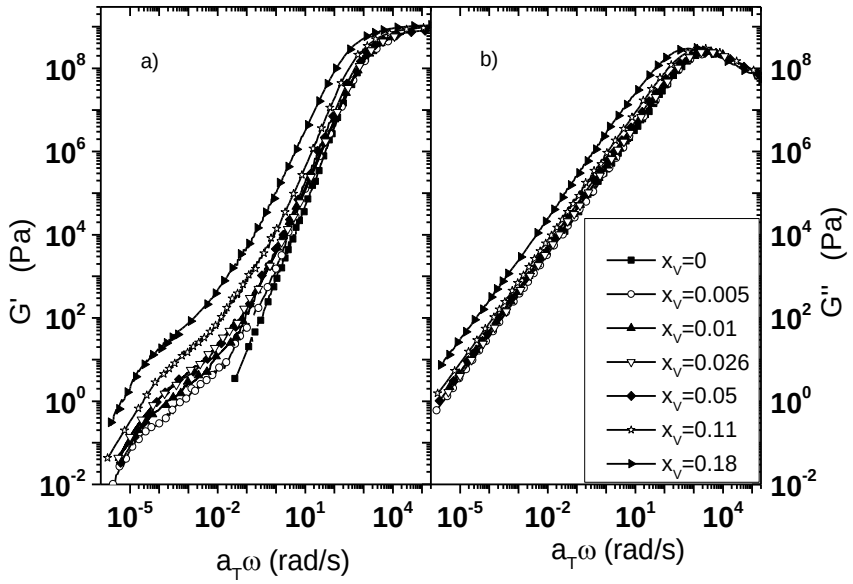

Figure IV-27: Master curves $G'(\omega)$ (a) and $G''(\omega)$ (b) for cured DGEBA/SiO_2 suspensions (r_{BPA} =0.3) with various filler volume concentration x_V at the reference temperature $T_{ref} = 273K$. Symbols are only used for the sake of clarity; data points lie much closer and are represented by solid lines.

The Brownian relaxation times are determined using the operational procedures described in appendix VI.2. The τ-values are listed in Table 8 for all volume concentrations. In Figure IV-28 the relaxations times $\tau(x_V)$ are shown for both the DGEBA/SiO_2 suspensions with the uncured DGEBA matrix (open symbols) and with the cured matrix (closed symbols). Obviously both systems exhibit an identical, non-monotonic variation of the Brownian relaxation times with the filler content. In both systems a minimum of the Brownian relaxation time occurs at a volume concentration x_V located between 0.05 and 0.1. Moreover, irrespective of the filler volume concentration, the relaxation times found for the modified suspensions lie about two orders of magnitude higher compared to those of the uncured suspensions. This

means that the increased viscosity of the matrix does not qualitatively affect the evolution of the relaxation times as a function of the filler content but only shifts the curves vertically. Before using the analytical functions of the diffusion times from equations (4.2.3.5) and (4.2.3.7) the concentration dependency of the zero-shear viscosity needs to be checked.

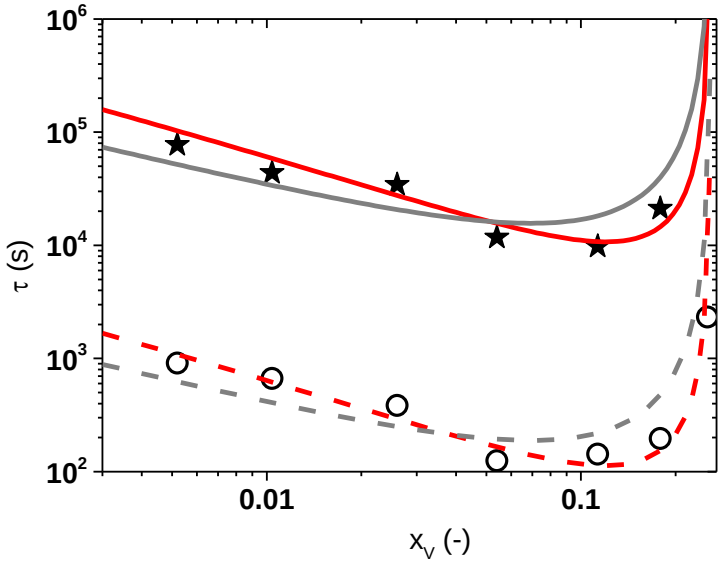

Figure IV-28: Operational Brownian relaxation times τ for suspensions with an uncured DGEBA matrix (open symbols, from Table 6) and for suspensions with a cured DGEBA matrix (closed symbols, from Table 8; $r_{BPA} = 0.3$) as a function of the filler volume concentration x_V. The red solid and dashed lines correspond to least square fits of the data using the diffusion time $\tau_{\langle r\rangle,SS}$ and a matrix viscosity of $3.52 \cdot 10^5 Pa.s$ (see Table 8) and 10275 Pa.s respectively(see Table 6). The grey lines represent the least square fit of the diffusion time $\tau_{\langle r\rangle,CC}$ using the same matrix viscosities as introduced above

For the DGEBA/SiO_2 suspensions with uncured DGEBA matrices it has been shown that the viscosities η_0 and η_{HI} obey to Krieger-Dougherty relations with the parameters $x_{V,max} = 0.26, \quad [\eta].x_{V,max} = 1.83$ and $x_{V,max} = 0.28, [\eta].x_{V,max} = 1.83$ respectively. The only difference between the DGEBA/SiO_2 suspensions with an uncured DGEBA matrix and the DGEBA/SiO_2 dispersions with a DGEBA matrix cured with Bisphenol A is the increased matrix viscosity when switching from uncured to cured. Referring to the Krieger-Dougherty relation (equation (2.2.2.9)) the evolution of the relative suspension viscosities ($\eta_r = \eta_0/\eta_m$ and $\eta_r = \eta_{HI}/\eta_m$) as a function of the filler fraction are expected to be independent of the matrix viscosity when (i) the same nanoparticles are embedded in the matrix and (ii) it is assumed that the matrix-filler interactions are not influenced when the matrix molecules change. In Figure IV-29, the relative viscosities $\eta_r = \eta_0/\eta_m$ and $\eta_r = \eta_{HI}/\eta_m$ for the systems with cured matrices are represented as a function of the volume concentration and compared to the evolution of the relative viscosities obtained from the Krieger-Dougherty relations using the same parameters as in case of the DGEBA/SiO_2 system with uncured matrices. Obviously the Krieger-Dougherty data adequately match the data delivered by the experiment. Consequently the equations (4.2.3.5) and (4.2.3.7) for the

diffusion times $\tau_{\langle r\rangle,SS}$ and $\tau_{\langle r\rangle,CC}$ can be used as fit functions for the experimental data corresponding to the modified DGEBA/SiO_2 suspensions. The solid lines in Figure IV-28 illustrate the fits of the diffusion times $\tau_{\langle r\rangle,SS}$ (red line) and $\tau_{\langle r\rangle,CC}$ (grey line) to the Brownian relaxation times found for the modified DGEBA/SiO_2 suspensions. The fits yield the particle radii $a_{fit} = 17.5\,nm$ and $a_{fit} = 15\,nm$ respectively for a matrix viscosity $\eta_m = 3.52 \cdot 10^5 Pa.s$ at $T_r = 273K$. Obviously the non-monotonic behaviour of the Brownian relaxation times $\tau(x_V)$ adequately fits to the diffusion times calculated from equation (4.3.1.1) when the length-scale $k(x_V)$ corresponds either to surface-to-surface or to centre-to-centre inter-particle distance.

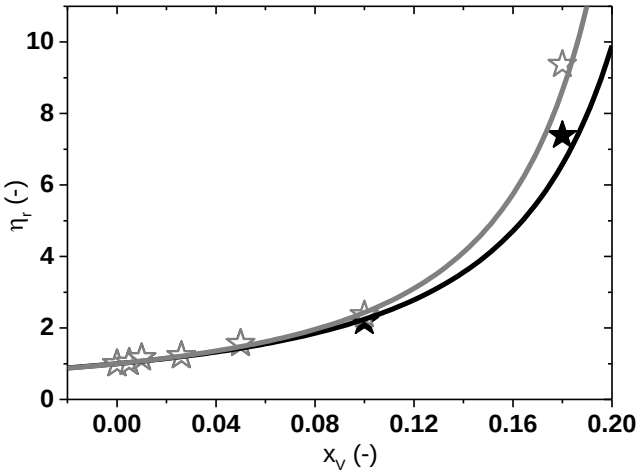

Figure IV-29: Relative viscosities $\eta_r = \eta_{HI}/\eta_m$ (closed symbols) and $\eta_r = \eta_0/\eta_m$(open symbols) for DGEBA/SiO_2 suspensions with a DGEBA matrix cured with BPA ($r_{BPA} = 0.3$) as a function of the volume concentration x_V. The black and grey lines represent relative viscosities calculated from the Krieger-Dougherty relation (equation (2.2.2.9)) using the same parameters as for the DGEBA/SiO_2 suspensions with an uncured DGEBA matrix, i.e. $x_{V,max} = 0.28$; $[\eta] \cdot x_{V,max} = 1.83$ for η'_∞ and $x_{V,max} = 0.26$; $[\eta] \cdot x_{V,max} = 1.83$ for η'_0 respectively

Table 8: High frequency viscosity $\eta_{HI'}$ zero-shear viscosity η_0 and operational Brownian relaxation times τ for the DGEBA/SiO_2 suspensions with a cured DGEBA matrix for different volume concentrations x_V of silica particles.The values of the viscosities were determined using equations (4.2.2.2) and (4.2.2.3).

x_v	η_{HI} ($.10^5$Pa.s)	η_0 ($.10^5$Pa.s)[8]	τ ($.10^4 s$)
0	3.52	3.52	---
0.005	3.65	3.65	7.75
0.01	4.1	4.1	4.38
0.026	4.3	4.3	3.42
0.05	5.1	5.5	1.17
0.1	7.6	8.3	0.98
0.18	26	33	2.11

[8] These viscosity has been determined using a different method (see appendix VI.3) than this described by equations (4.2.2.2) and (4.2.2.3)

IV.3.2. Influence of the type of nanoparticles

In the introduction of this chapter it has been stated that the diffusion time τ_D (equation (4.3.1.1)) correlates also with the particle size, the particle shape and the particle-particle interactions. Striving for an extension of the validity range of equation (4.3.1.1) for the description of Brownian relaxation, investigations on DGEBA/Al_2O_3 colloidal suspensions will be described. The change of the type of nanoparticles allows testing the combined influence of the particle size and shape, particle-matrix and inter-particle interactions on Brownian relaxation. As described in the material section III.1.2, the mechanical dispersion of alumina particles in a DGEBA matrix leads to fractal clusters with radii in the range $50 - 100\ nm$. Thus, compared to the silica nanoparticles, the size of the alumina fillers is considerably increased, and their particle shape is no longer spherical. Changed size and shape of the fillers are not the only features to be considered when studying the DGEBA/Al_2O_3 suspensions. Calorimetric and dielectric measurements have revealed that for DGEBA/ Al_2O_3 suspensions the glass transition temperature T_g depends on the nanoparticle concentration indicating that, in contrast to the silica particles, the alumina clusters are interacting with the DGEBA matrix.

Figure IV-30 shows the master curves $G'(\omega)$ and $G''(\omega)$ for the DGEBA/Al_2O_3 suspensions with volume concentrations $0 \leq x_V \leq 0.117$ at a reference temperature $T_{ref} = 273K$[9]. The general evolution observed for the DGEBA/Al_2O_3 suspensions is similar to the one described for the DGEBA/SiO_2 dispersions: besides the dynamic glass transition occurring at high frequencies Brownian relaxation manifests itself at low frequencies by plateau-like elastic behaviour of the storage shear moduli going along with transitions of the loss modulus from a zero-shear to a high-frequency viscosity regime (only observable at the three highest filler concentrations). The horizontal shift factors $log(a_T)$ used for the construction of the master curves are represented in Figure IV-31 as a function of the temperature. Similar to the situation encountered for the DGEBA/SiO_2 suspensions, all of the $log(a_T)$-curves are continuous. Thus the TTS-principle is applicable to the DGEBA/Al_2O_3 suspensions in the temperature and frequency ranges where the isothermal frequency sweeps have been carried out. In addition the $log(a_T)$-curves obtained for the various filler fractions superimpose and can be described by a single WLF-function (red solid line in Figure IV-31). From these observations it can be concluded that the low-frequency process in the DGEBA/Al_2O_3 suspensions can again be interpreted as Brownian relaxation process. However before Brownian relaxation in DGEBA/Al_2O_3 dispersions can be discussed, information on the particle-matrix interactions and on the evolution of the suspension viscosity with the filler content is requested.

[9] The frequency sweeps used for the construction of the master curves in Figure IV-30 can be found in appendix VI.1.2

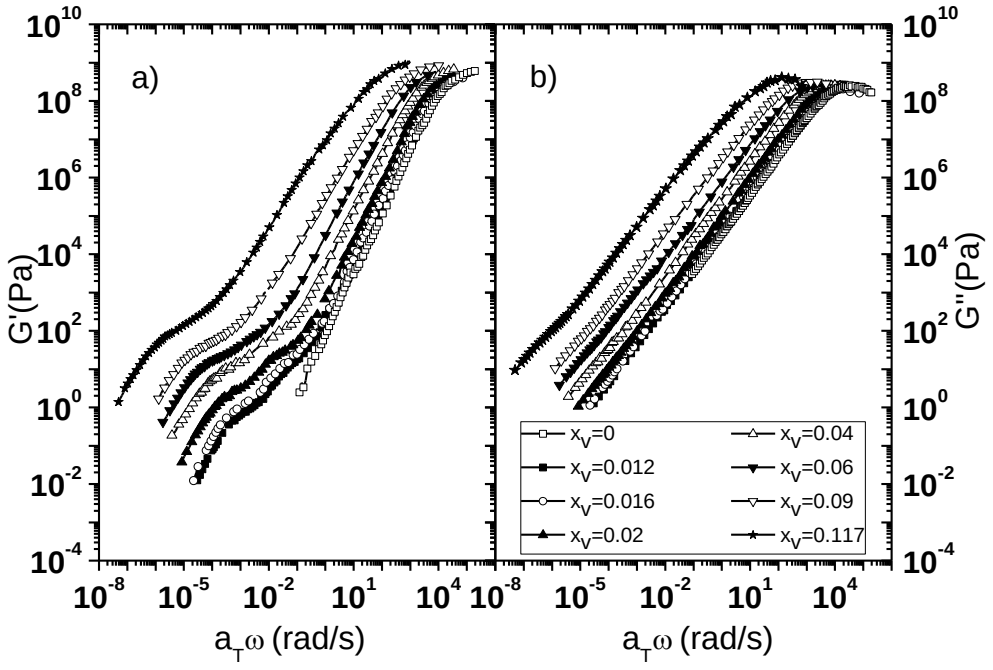

Figure IV-30: Master curves $G'(\omega)$ (a) and $G''(\omega)$ (b) for DGEBA/Al_2O_3 suspensions for various filler volume concentration x_V at the reference temperature $T_{ref} = 273K$.

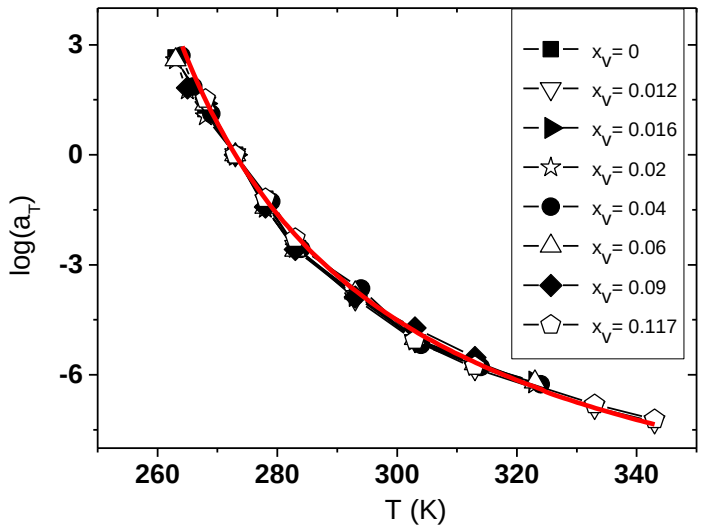

Figure IV-31: Temperature dependency of the horizontal shift factors $log(a_T)$ used for the construction of the master curves in Figure IV-30. The red line represents a WLF-plot (equation 2.1.4.11) with parameters $C_1 = 8.63$ and $C_2 = 44.08\ K$.

i) Influence of the alumina nanoparticles on the glass transition of DGEBA

The master curves $G'(\omega)$ and $G''(\omega)$ in Figure IV-30 reveal that the alumina nanoparticles strongly affect the dynamic glass transition of DGEBA. Contrary to the behaviour of the DGEBA/SiO_2 systems, the dynamic glass transition in the DGEBA/ Al_2O_3 suspensions is shifted towards lower frequencies when the filler content increases. This observation agrees with the finding that the glass transition temperature of the DGEBA/Al_2O_3 suspensions increases with the filler content [19] (see Figure IV-33). The glass transition temperature T_g can be defined as the temperature, at which the suspension viscosity takes the value of $10^{12.3}\ Pa.s$ (see section IV.2.2, equation (4.2.2.4)). As already practiced for the DGEBA/SiO_2 suspensions, the suspension viscosity η_{HI} of the DGEBA/ Al_2O_3 systems can be obtained from the loss shear moduli (using equation (4.2.2.3)) provided by the frequency sweeps shown in appendix VI.1. In Figure IV-32 the viscosities are represented as a function of the temperature[10]. Obviously all of the considered suspensions obey to Vogel-Fulcher-Tammann behaviour (red lines in Figure IV-32).

The corresponding fit parameters are listed in Table 9. By solving the Vogel-Fulcher-Tammann equation for the temperature $T = f(\eta_{HI})$, using the parameters from Table 9 and replacing the viscosity by $10^{12.3} Pa.s$ (equation (4.2.2.4)) the glass transition temperature T_g can be obtained for the different volume concentrations.

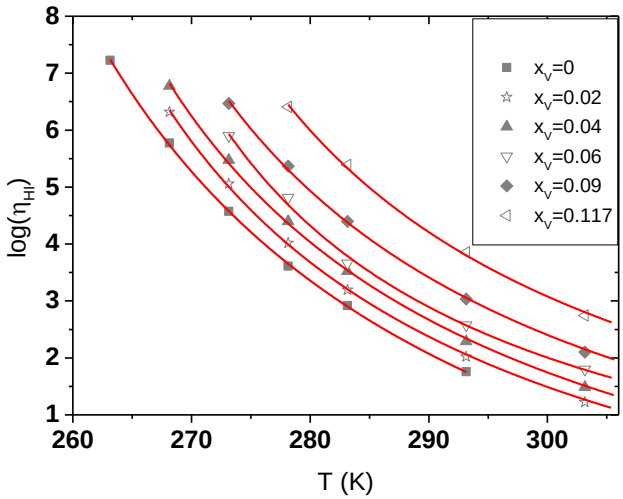

Figure IV-32: Temperature dependency of the high-frequency viscosities (equation (4.2.2.3)) of DGEBA and DGEBA/Al_2O_3 suspensions at different volume concentrations. The data are obtained from loss shear moduli delivered by isothermal frequency sweeps documented in appendix VI.1. The red lines represent Vogel-Fulcher-Tammann fits (equation (2.1.2.11)). The corresponding parameters of the VFT-fits are listed in Table 9

[10] In order to avoid an overload of Figure IV-32 the investigation is restricted to the concentration range $0.02 \leq x_V \leq 0.117$. Outside of this concentration interval, there are no T_g –values from calorimetry and dielectric spectroscopy available.

Table 9: Parameters obtained by fitting the VFT-law (equation (2.1.2.11)) to the viscosity data in Figure IV-32: $\eta_{HI,0}$ is the viscosity at $T \to \infty$; $\Delta G/k_B$ represents the free enthalpy normalized by k_B and T_V the Vogel-temperature. The values are listed for the DGEBA/Al_2O_3 suspensions with different volume concentrations x_V.

x_V (-)	$\eta_{HI,0}$ (Pa.s)	$\Delta G/k_B$ (K)	T_V (K)	T_g (K)
0	$3.7 \cdot 10^{-5}$	908	231	254.9
0.02	$7.8 \cdot 10^{-4}$	656	238	256.5
0.04	$8.4 \cdot 10^{-4}$	689	237	257.4
0.06	$9.8 \cdot 10^{-4}$	681	238	258.7
0.09	$2 \cdot 10^{-3}$	687	240	260.3
0.117	$1.1 \cdot 10^{-2}$	628	245	264.7

The glass transition temperatures $T_g(x_V)$ obtained from the oscillatory shear measurements are represented in Figure IV-33 together with the results provided by calorimetry and dielectric spectroscopy. All of the experimental probes deliver the same result: the glass transition temperature of the DGEBA/Al_2O_3 suspensions increases with increasing filler content. Obviously the data provided by rheology confirms the general trend of the glass transition behaviour of the DGEBA/Al_2O_3 suspensions found by calorimetry and dielectric spectroscopy of the evolution of the glass transition temperature. According to Baller, et al. [19] the increase of T_g can be attributed to physical interactions between alumina particles and DGEBA molecules.

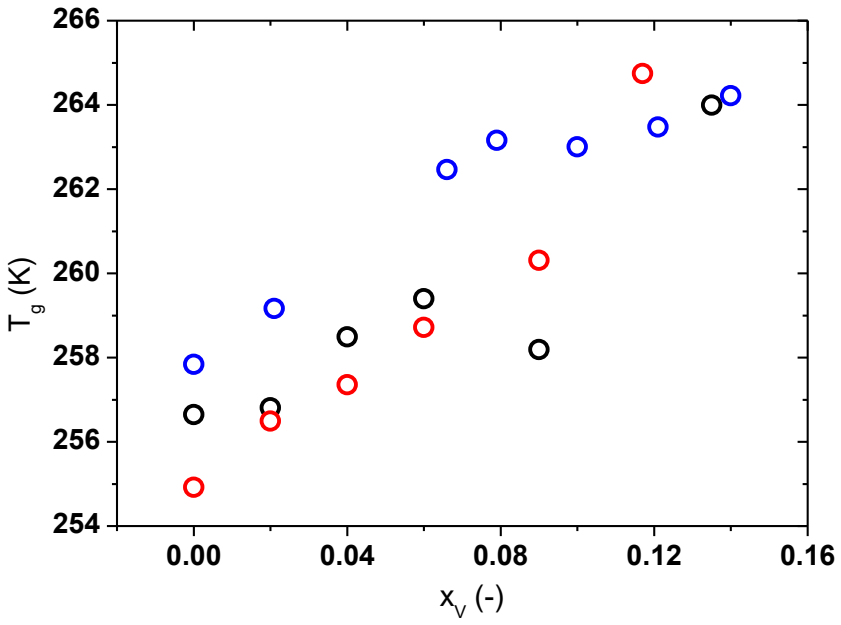

Figure IV-33: Glass transition temperature T_g of DGEBA/Al_2O_3 suspensions as a function of the filler fraction. The T_g-values have been obtained by different experimental methods. The red, black and blue symbols represent the data from rheology, dielectric spectroscopy and calorimetry respectively

ii) Influence of the alumina particles on the matrix viscosity

The viscosities of the alumina suspensions at the reference temperature are listed in Table 10. The relative viscosities η_0/η_m and η_{HI}/η_m are represented in Figure IV-34 as a function of the concentration of the alumina fillers. It has to be stressed that the relative viscosities of the DGEBA/Al_2O_3 suspensions increase much faster than those of the DGEBA/SiO_2 systems (for comparison see Figure IV-14). In fact while in case of a DGEBA/SiO_2 dispersion with $x_V = 0.11$ the zero-shear viscosity is *3.7* times higher than the matrix viscosity, in a DGEBA/Al_2O_3 suspension with a comparable volume concentration η_0 is *5000* times higher than the matrix viscosity. As in case of the DGEBA/SiO_2 suspensions the relative viscosities of the DGEBA/Al_2O_3 systems can be described by the Krieger-Dougherty relation (equation (2.2.2.9)) as depicted by the solid lines in Figure IV-34. The fits yield the parameters $x_{V,max} = 0.16$; $[\eta] \cdot x_{V,max} = 5.71$ for the high-frequency viscosity η_{HI} and $x_{V,max} = 0.15$ and $[\eta] \cdot x_{V,max} = 5.71$ for the zero-shear viscosity η_0 respectively. Similar to the situation encountered for the DGEBA/SiO_2 suspensions, the maximum filler fractions $x_{V,max}$ of the DGEBA/Al_2O_3 systems are very small compared to the theoretically expected values $0.58 - 0.63$. But while for the DGEBA/SiO_2 dispersions the difference was explained by repulsive interparticle interactions, the latter probably arises due to the clustering of the alumina particles (see section II.2.2). The aggregation of the alumina particles is also responsible for the relative high exponent $[\eta] \cdot x_{V,max} = 5.71$, which clearly reflects that the aggregates can no longer be considered as perfect spheres, since in this case the exponent is expected to be equal to 2.5.

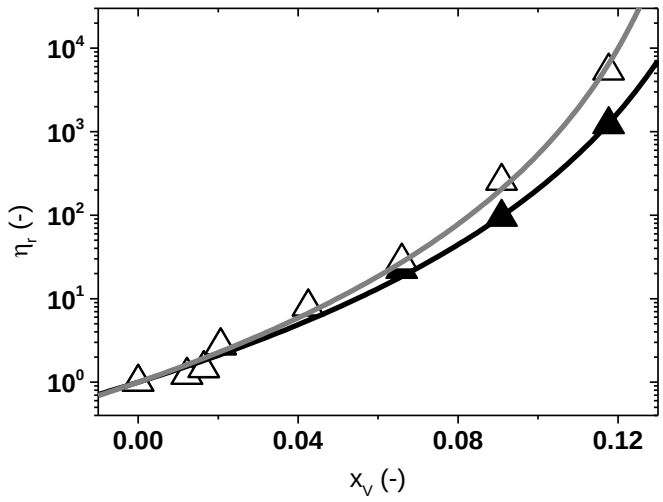

Figure IV-34: Relative viscosities $\eta_r = \eta_{HI}/\eta_m$ (closed symbols) and $\eta_r = \eta_0/\eta_m$(open symbols) for DGEBA/Al_2O_3 suspensions as a function of the volume concentration x_V. The black and grey lines correspond to fits of the Krieger-Dougherty relation (equation (2.2.2.9)) to the experimental data. The fit parameters are $x_{V,max} = 0.16$ and $[\eta] \cdot x_{V,max} = 5.71$ for η_{HI} and $x_{V,max} = 0.15$ and $[\eta] \cdot x_{V,max} = 5.71$ for η_0

Table 10: High frequency viscosity, zero-shear viscosity (η_{HI}, η_0) as well as the Brownian relaxation times τ for DGEBA/Al_2O_3 suspensions with different volume concentrations x_V ($T_{ref} = 273K$). The values of the viscosities are determined using equations (4.2.2.2) and (4.2.2.3)

x_v	η_{HI} ($.10^4$Pa.s)	η_0 ($.10^4$Pa.s)[11]	τ ($.10^4 s$)
0	3.36	3.36	---
0.012	4.07	4.07	0.767
0.016	4.89	4.89	0.712
0.02	9.22	9.22	0.806
0.04	26.9	26.9	1.63
0.06	75.6	95.4	3.45
0.09	319	860	7.87
0.117	4092	18000	30.6

iii) Brownian relaxations in DGEBA/Alumina suspensions

As discussed in the introduction of this section the DGEBA/Al_2O_3 suspensions behave differently compared to the DGEBA/SiO_2 dispersions. In contrast to the DGEBA/SiO_2 suspensions, the fillers take influence on the glass transition in the DGEBA/Al_2O_3 systems. Furthermore, compared to the DGEBA/SiO_2 suspensions, the viscosity changes are by orders of magnitude larger when the filler content increases. The specific behaviour of the suspensions with alumina fillers is attributed to particle-matrix interactions and also to clustering of the fillers. Consequently the question arises how these specific properties influence the Brownian relaxation process (especially the corresponding relaxation times).

Brownian relaxation can be observed for all alumina suspensions under study. However compared to the DGEBA/SiO_2 dispersions the smallest filler concentration for which Brownian relaxation can be resolved ($x_V = 0.012$) is twice higher. This difference is not surprising when one relies on the theoretical work of Lionberger and Russel [45]. According to the theoretical predictions of these authors the strength of the Brownian relaxation scales with a^{-3} where *a* is the particle size. Hence, for the same filler fraction, the relaxator strength is expected to be smaller for the system with the alumina fillers than for the DGEBA/SiO_2 suspension (due to the different particle sizes).

The Brownian relaxation times are determined using the operational method described in appendix VI.2. The values are listed in Table 10 and represented in Figure IV-35 as a function of the volume concentration. Surprisingly the evolution of the Brownian relaxation times determined for the DGEBA/Al_2O_3 suspensions does not allow to unambiguously conclude on a non-monotonic variation. As a matter of fact the changes of the Brownian relaxation times at the lowest filler contents (see Table 10) could be interpreted as data scattering. In this case the behaviour of the Brownian relaxation times (see Figure IV-35) could be described by the classical Peclet self-diffusion times ($k(x_V) = a$ in equation (4.3.1.1)).

[11] These viscosity has been determined using a different method (see appendix VI.3) than the one based on equations (4.2.2.2) and (4.2.2.3)

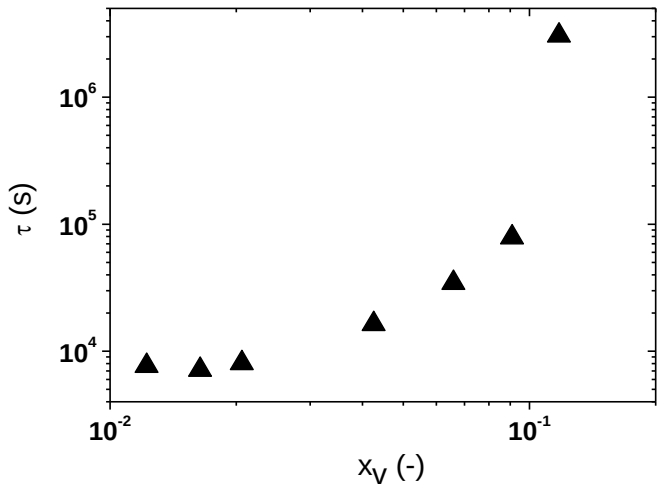

Figure IV-35: Operational Brownian relaxation times for DGEBA/Al_2O_3 suspensions as function of the volume concentration x_V ($T_{ref} = 273K$)

Hence it is legitimate to question the general applicability of the diffusion times $\tau_{\langle r \rangle}$ (equation (4.2.3.3)), which have been found to be appropriate for the description of Brownian relaxation in the DGEBA/SiO_2 suspensions.

As discussed in section IV.2.3 the non-monotonic evolution of the relaxation times/characteristic diffusion times is expected to strongly depend on the variation of the zero-shear viscosity when the filler fraction varies (for a given characteristic particle-particle interaction length). As a matter of fact, for a growing filler concentration, the competition between the decreasing characteristic self-diffusion length and the increasing suspension viscosity defines the location of the minimum of the relaxation times (see Figure IV-23). Since the zero-shear viscosity of the DGEBA/Al_2O_3 suspensions diverges at a lower volume concentration ($x_{V,max} = 0.15$) than the one of the DGEBA/SiO_2 dispersions ($x_{V,max} = 0.26$), the minimum of the Brownian relaxation times determined for the DGEBA/Al_2O_3 samples is expected to be shifted to a smaller volume concentration. In fact for a Krieger-Dougherty exponent $[\eta] \cdot x_{V,max} = 5.71$ the minimum of the relaxation times is expected to occur at $x_{V,min} = 0.028$ for $k(x_V) = \langle r(x_V) \rangle_{CC}$ respectively $x_{V,min} = 0.023$ for $k(x_V) = \langle r(x_V) \rangle_{SS}$[12]. Therefore both concentrations $x_{V,min}$ are close to the lowest filler content used for the DGEBA/Al_2O_3 suspensions which could explain why the minimum in the relaxation times is not clearly identifiable.

A more efficient approach to describe the evolution of the Brownian relaxation times found for the DGEBA/Al_2O_3 suspensions consists in fitting equation (4.3.1.1) for the characteristic self-diffusion times to the Brownian relaxation times. Thereby $k(x_V)$ can tentatively be chosen to correspond either to center-to-center or to surface-to-surface interparticle distance (see also equations (4.2.3.4) and (4.2.3.6)). Moreover the zero-shear viscosity η_0 needs to be adapted to the DGEBA/ Al_2O_3 systems by

[12] for the determination procedure of the minimum see section IV.2.3.iv)

considering the parameters $x_{V,max} = 0.15$ $[\eta] \cdot x_{V,max} = 5.71$ in the Krieger-Dougherty relation. Figure IV-36 depicts the evolution of the Brownian relaxation times (closed symbols) together with the fits (solid lines) of equation (4.3.1.1) to the data. While the red solid line illustrates the fit obtained for $k(x_V) = \langle r(x_V) \rangle_{CC}$ corresponding to center-to-center inter-particle distance, the grey solid line depicts the fit results when the characteristic length scale is related to the surface-to-surface inter-particle distance i.e. $k(x_V) = \langle r(x_V) \rangle_{SS}$. While in the first case the fit yields a particle radius $a_{fit} = 18\,nm$ in the second case $a_{fit} = 25\,nm$. Obviously, the characteristic self-diffusion times (calculated for the two chosen $k(x_V)$ functions) adequately describe the behaviour of the Brownian relaxation times when the filler content changes.

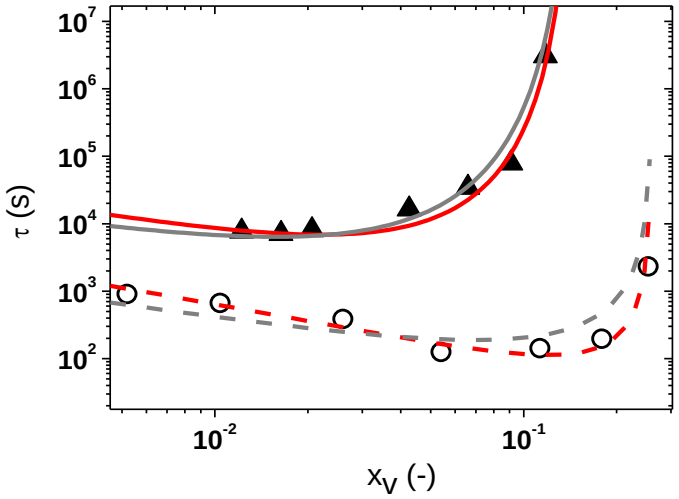

Figure IV-36: Operational Brownian relaxation times τ determined for DGEBA/Al_2O_3 suspensions (black symbols) and uncured DGEBA/SiO_2 dispersions (open symbols) as a function of the filler volume concentration x_V. The red solid and red dashed lines correspond to least square fits of equation (4.3.1.1) to the Brownian relaxation times with $k(x_V)$ corresponding to surface-to-surface interparticle distance. The grey lines represent least square fits of equation (4.3.1.1) to the Brownian relaxation times with $k(x_V)$ corresponding to the center-to-center interparticle distance

However it has to be emphasized that the particle radii provided by the fits substantially deviate from the expected values $(50 - 100\,nm)$. To explain this deviation the assumptions made to formulate the equation for the characteristic self-diffusion time $\tau_{\langle r \rangle}$ need to be revised. Basically $\tau_{\langle r \rangle}$ corresponds to the ratio of a characteristic length and a self-diffusion diffusion constant (see equation (4.2.3.1)). Both parameters are based on models which are restricted to spherical particles. In a first approach the fractal alumina clusters in the DGEBA/Al_2O_3 suspensions can be assimilated to spheres (see section II.2.2). Relying on this approach, e. g. center-to-center or surface-to-surface inter-particle distances continue to make sense. In contrast the applicability of the Stokes-Einstein relation used for expressing the self-diffusion coefficient in terms of the suspension viscosity (see equation (2.2.2.5)) is somehow doubtful. In fact, in case of the DGEBA/Al_2O_3 suspensions, the Krieger Dougherty exponent $[\eta] \cdot x_{V,max}$ takes a value of *5.17* which does not correspond to

a sphere-like shape of the particles ($[\eta] \cdot x_{V,max} = 2$). From all these considerations it follows that the particle radii provided by the fit are certainly not representative for the alumina clusters.

A particular feature of the master curves represented in Figure IV-30, is the appearance of a double-step-like behaviour of the storage shear moduli at low frequencies. This specific evolution of the storage shear moduli has only be observed for low a concentrations of alumina particles. The double-step-like behaviour can clearly be observed in Figure IV-37, where the reduced storage moduli[13] have been represented for the DGEBA/Al_2O_3 suspensions with volume concentrations $0.012 \leq x_V \leq 0.06$. The additional process occurs at higher frequencies than the Brownian relaxation and seems to disappear at higher volume concentrations (see $x_V = 0.06$ in Figure IV-30). Furthermore the feature seems to be characteristic for the DGEBA/Al_2O_3 suspensions. In fact, in the equivalent representation of the reduced storage shear moduli of the DGEBA/SiO_2 dispersions the two-step behaviour at low frequencies could not be observed (see Figure IV-19). Further investigations are necessary before coming up with a final interpretation of the phenomenon.

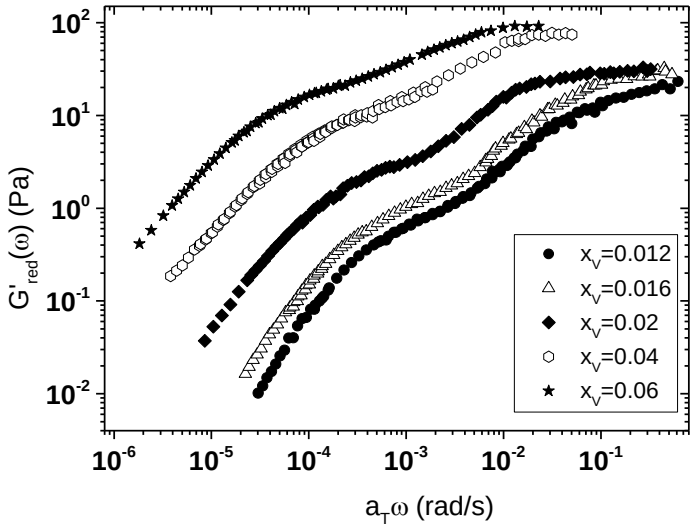

Figure IV-37: Reduced storage shear moduli $G'_{red}(\omega)$ for DGEBA/Al_2O_3 suspensions with volume concentrations $0.012 \leq x_V \leq 0.06$ at the reference temperature $T_{ref} = 273K$.

[13] The reduced storage moduli are obtained by subtracting the elasticity of the DGEBA matrix from the master curves in Figure IV-30.

IV.4. Characteristic length-scales for Brownian relaxation times: Comparison to literature and generalized representation

In the previous chapters the linear viscoelastic behaviour of several types of colloidal suspensions has been studied. All of the investigated suspensions use the oligomer DGEBA (uncured or cured with Bisphenol A) as a matrix. It could be shown that all of the investigated systems share the property that besides the α-process Brownian relaxation manifests itself in in shear experiments. Irrespective of the composition of the suspension the evolution of the Brownian relaxation times can adequately be described by the behaviour of characteristic diffusion times depending on the suspension viscosity and a characteristic diffusion length. The suspension viscosity is well known to increase with the filler content. An important achievement of the present project is that it could be shown that the Brownian relaxation times can correctly be described by characteristic self-diffusion times only if the characteristic diffusion length adequately depends on the filler content. Until now, in literature, Brownian relaxation was generally described by Peclet-times where the characteristic diffusion length is defined as the radius of the suspended particles. However it has to be stressed that the validity of the characteristic diffusion time as it has been defined in the present thesis is so far restricted to DGEBA/SiO_2 –Al_2O_3 suspensions.

The final part of the present PhD project deals with the generalization of the model which has been used for the description of Brownian relaxation occurring in DGEBA/SiO_2 and DGEBA/Al_2O_3 samples. Results on Brownian relaxation times known from literature will be compared to self-diffusion times calculated according to the model developed in the present work. A comparison of all of the data is only possible in a generalized representation.

IV.4.1. Brownian relaxation times: Results and corresponding length-scales reported in literature

As described in the previous chapters Brownian relaxation manifests itself in the shear moduli $G'(\omega)$ and $G''(\omega)$ obtained from small amplitude oscillatory shear experiments. In this context literature provides results from experiments [4, 68] and from theoretical investigations [43, 57]. Shear moduli are directly linked to complex viscosities (see equations (2.1.3.8) and (2.1.3.9)). Brownian relaxations have also been detected in experiments yielding the real and imaginary parts of the complex viscosity ([5]) .

Moreover Brownian relaxation has also been reported for investigations of the time dependent diffusion behaviour of colloidal suspensions using dynamic light scattering [87] and computer simulations [88].

All of these works have in common that:

- the investigated suspensions can be considered as dispersions of hard spheres,

- the authors studied the relaxation or transition times as function of the volume concentration of the fillers,
- the relaxation or transition times are compared to characteristic diffusion times whereby different characteristic diffusion length-scales have been used.

In Table 11 the cited works, the methods and the characteristic lengths are listed.

Table 11: List of published contributions related to Brownian relaxation. The methods and the characteristic lengths $k(x_V)$ used by the authors are detailed. Further information can be found in the text

Work	method	length scale
Dannert, et al. [85]	SAOS	$k(x_V)=2a\left(\left(\frac{0.63}{x_V}\right)^{1/3}-1\right)$
Banchio, et al. [57]	MCT	$k(x_V)=0.3a\left(\frac{4\pi}{3x_V}\right)^{1/3}$
van der Werff, et al. [5]	torsional rheometry	$k(x_V)=a$
Cichocki and Hinsen [88]	simulations	$k(x_V)=a$
Shikata and Pearson [4]	SAOS	$k(x_V)=a$
Foss and Brady [84]	BD	$k(x_V)=a$
Sohn and Rajagopalan [42]	passive microrheology	$k(x_V)=a$
Aoki, et al. [68]	SAOS	$k(x_V)=a$
Weeks and Weitz [43]	DLS	$k(x_V)=4a\left(\left(\frac{0.63}{x_V}\right)^{1/3}-1\right)$

IV.4.2. Brownian relaxation times: generalized representation

There is a major problem regarding the comparison of the Brownian relaxation times provided by the various contributions listed in Table 11: the various authors have worked on systems with different types of matrices and suspended particles. Matrix viscosity and particle size are two parameters which take influence on the Brownian relaxation times and the characteristic self-diffusion times. Therefore a common representation of the reported relaxation times is not possible.

However by scaling the relaxation times τ in units of the Peclet-time τ_p (equation (4.2.2.5)) the dimensionless normalized relaxation time

$$\tau_{norm} = \frac{\tau}{\tau_p} \tag{4.4.2.1}$$

becomes independent of the particle size and suspension viscosity. Consequently, by using τ_{norm}, all of the reported data (from literature and this work) are expected to fit into a common representation as a function of the filler content. With equation (4.3.1.1) for the characteristic diffusion time τ_D the normalized relaxation times

$$\tau_{norm}(x_V) = \frac{\tau_D}{\tau_p} = \left(\frac{k(x_V)}{a} \right)^2 \tag{4.4.2.2}$$

only depend on the choice of the characteristic length scale $k(x_V)$. Figure IV-38 shows the normalized relaxation times τ_{norm} obtained from the relaxation times reported in literature (see Table 11 and from the study presented in this thesis). It is important to note that in contrast to the previous chapters the normalized relaxations times for the uncured and cured DGEBA/SiO_2 and for the DGEBA/Al_2O_3 suspensions are represented in terms of effective volume concentrations $x_{V,eff}$ instead of nominal filler fractions x_V. The switch from x_V to $x_{V,eff}$ is necessary due to the observation that in the suspensions DGEBA/SiO_2 and DGEBA/Al_2O_3 the respective viscosities diverge at much too small filler fractions compared to the viscosities of similar hard sphere suspensions discussed in literature. The applied procedure used to convert x_V into $x_{V,eff}$ and its justification are presented in appendix VI.4.

It has to be emphasized that for the representation in Figure IV-38 no additional shifting was applied to the data. Obviously all of the considered normalized relaxation times behave in a fairly similar way especially from a qualitative point of view. As a matter of fact most of the represented data [4, 43, 54] monotonously decreases with increasing filler content. Only the data of Foss and Brady [84] and of van der Werff, et al. [5] seem to be independent of the filler content in the concentration range where data points are available.

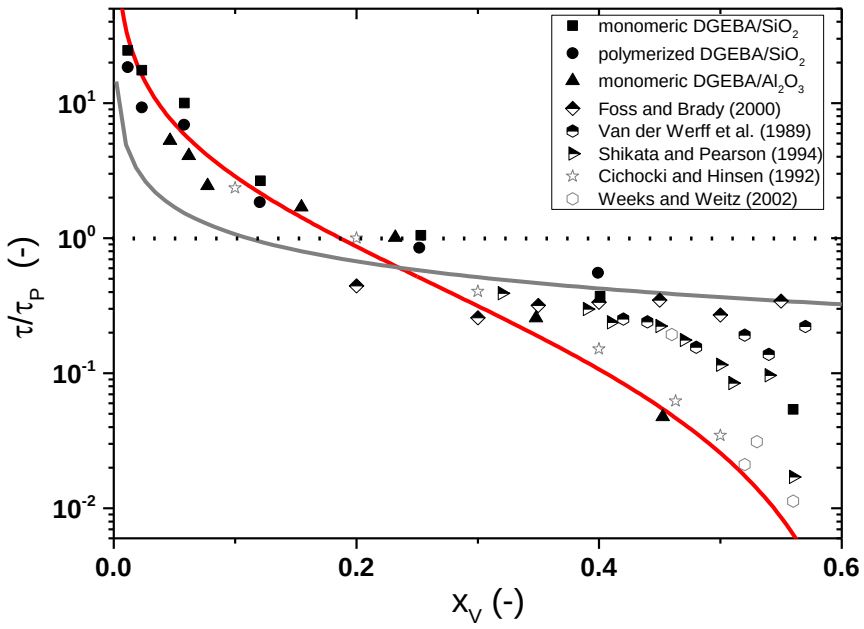

Figure IV-38: Reduced Brownian relaxation times τ_{norm} as a function of the filler volume fraction x_V for the suspensions studied in this work and data known from literature (see Table 11). The black dotted line corresponds to $\tau_{norm} = 1$. The red and grey solid lines describe the functions $\tau_{norm}(x_V)_{SS}$ (equation (4.5.2.3)) and $\tau_{norm}(x_V)_{CC}$ (equation (4.5.2.4)) respectively

Often in literature (e. g. contributions relying on $k(x_V) = a$ (see Table 11)) the Peclet-time τ_p is used as a characteristic diffusion time (or Brownian relaxation time). In such cases $\tau_{norm} = 1$, i. e. the normalized relaxation time becomes independent of the volume concentration. In Figure IV-38 $\tau_{norm} = 1$ is represented by the horizontal dotted line. Obviously all of the represented data substantially deviates from$\tau_{norm} = 1$: while at low concentrations the τ_{norm} values are higher than unity, they tend to get smaller than unity at high concentrations. Although the normalized relaxation times calculated from the results of Foss and Brady [84] and van der Werff, et al. [5] are nearly constant they are by around one decade smaller than unity [89].

To properly describe most of the data in Figure IV-38 a function $k(x_V)$ which monotonously decreases with increasing filler content is needed (see equation (4.4.2.2)). Such a behaviour is in line with the concentration dependent behaviour of the mean particle distance $\langle r \rangle$.

In case that the surface-to-surface interparticle distance (equation (4.2.3.4)) is used the normalized relaxation time τ_{norm} reduces to

$$\tau_{norm}(x_V)_{SS} = 4\left(\left(\frac{0.63}{x_V}\right)^{\frac{1}{3}} - 1\right)^2, \qquad (4.4.2.3)$$

while if the center-to-center mean particle distance is used as characteristic length-scale (equation (4.2.3.6)) τ_{norm} can be expressed by

$$\tau_{norm}(x_V)_{CC} = 0.09\left(\frac{4\pi}{3x_V}\right)^{\frac{2}{3}}. \qquad (4.4.2.4)$$

The functions $\tau_{norm}(x_V)_{SS}$ and $\tau_{norm}(x_V)_{CC}$ are represented in Figure IV-38 by the red and grey solid lines respectively. Obviously, at low concentrations, $\tau_{norm}(x_V)_{CC}$ yields lower values than $\tau_{norm}(x_V)_{SS}$, while at high concentrations the opposite behaviour is observed. Clearly the deviation at high concentrations is explained by the fact that the center-to-center mean particle distance approaches a certain fraction of the particle radius while the surface-to-surface interparticle separation tends towards zero. As can be observed in Figure IV-38 all results obtained from the here studied suspensions perfectly fit to the $\tau_{norm}(x_V)_{SS}$ values at small filler contents, while they lie between both models ($\tau_{norm}(x_V)_{SS}$ and $\tau_{norm}(x_V)_{CC}$) at high volume concentrations. Astonishingly the data obtained from the work of Cichocki and Hinsen [88] perfectly fits to $\tau_{norm}(x_V)_{SS}$ over the whole concentration range. The data published by Foss and Brady [84] and van der Werff, et al. [5] which, at first sight, seemed to be independent of the volume concentration fairly coincide with $\tau_{norm}(x_V)_{CC}$. The τ_{norm} -values determined from contributions by Shikata and Pearson [4] or Weeks and Weitz [43] are located between both models.

Finally it can be concluded that a characteristic self-diffusion length which somehow scales with the particle distance seems to be appropriated for the description of the Brownian relaxation times. While at low filler fractions the surface-to-surface mean particle distance correctly describe all available data, at high volume concentrations the two characteristic length scales, on the one hand the average particle center-to-center distance and on the other the average surface-to-surface distance can be considered as upper respectively as lower limit for τ_{norm}. For sure the classical Peclet-time, which is generally used in literature, is certainly not the adequate timescale for Brownian relaxation since none data well agree with the predictions of τ_p.

V. Conclusion and Outlook

In the framework of this thesis, colloidal suspensions consisting of low molecular weight glass formers as matrices and two types of nanoparticles as colloidal fillers have been investigated. The dynamics of these systems have been studied by measuring mechanical susceptibilities namely shear moduli and viscosities by Small Amplitude Oscillatory Shear Rheology (SAOS). As expected a strong relaxation process spanning over many decades could be evidenced in the frequency dependency of the shear moduli. This relaxation process can be identified as the structural relaxation process (α-process) of the glass-forming matrix. Classical canonical glass formers can show additional relaxation processes (e.g. secondary relaxations of molecular side groups etc.) but for low molecular weight glass formers as the ones used here as matrix material, the α-process is the relaxation process with the slowest dynamics visible in mechanical susceptibilities. The low-frequency tail of the α-process leads to terminal regime behaviour in the frequency dependency of the shear moduli. The starting point for the investigations preformed during this PhD project was the detection of an additional relaxation process which turns up when the matrices are filled with nanoparticles. This additional process is evidenced as a weak deviation of the shear moduli's frequency dependency from terminal regime behaviour. It is centred at low frequencies very close to the resolution limit of modern rheometers. To the author's best knowledge, a similar process has never been reported for viscoelastic suspensions. For Newtonian liquids as matrix material, studies with micro-scaled fillers exist which exhibit a low-frequency process attributed to the Brownian movement of the fillers. A direct link to the observed low-frequency process in viscoelastic suspensions with nano-scaled fillers is complicated by the occurrence of the broad structural relaxation process which superposes the weak low-frequency process. Therefore a different approach has been used during this PhD project. The low-frequency process has been studied by varying the concentration of nanoparticles, by changing the viscosity of the matrices and by using two types of nanoparticles with different sizes, shapes and interaction potential. This methodology led to the following main findings:

- The low-frequency process can be identified as Brownian relaxation of the nanoparticles.
- The timescale of the relaxation process scales with the matrix viscosity and with the types of nanoparticles.
- The dependency of the relaxation times on the concentration of nano-scaled fillers is non-monotonic, it shows a minimum.

These experimental results allowed to develop a phenomenological model which is capable to quantitatively describe the dependency of the relaxation times on matrix viscosity and filler content. It is based on the assumption that interaction between filler particles is a perquisite for Brownian relaxation. Therefore a characteristic length scale related to the distance between the particles has been introduced. The diffusion

time corresponding to this length scale has been identified as the relevant time scale for Brownian relaxation.

In addition to the quantitative analysis of own experimental data, the introduction of a characteristic length scale allowed to include data from literature into this phenomenological description. This comprises Brownian relaxation times for Newtonian liquids stemming from different sources such as rheological measurements in the frequency domain, diffusion measurements in the time domain, theoretical calculations based on mode coupling theory and data from computer simulations.

Besides the clarified queries concerning Brownian relaxation in viscoelastic colloidal suspensions several open questions persist on this topic. To cite some of the most important:

- How the matrix viscoelasticity influences Brownian relaxation?
- Are the introduced length- and time-scales characteristic parameters for colloidal suspensions?

To answer these questions altered suspensions have to be studied. Concerning the influence of the matrix viscoelasticity one can imagine to cure DGEBA with an agent possessing several amino groups like Diethylenetriamine (DETA). The resulting matrix should possess highly branched molecules resulting in a complex viscoelastic behaviour (appearance of a rubbery plateau). Regarding the generalization of the here introduced length- and time-scale measurements on suspensions with even smaller particles and particles possessing different types of interparticle interactions should be performed.

VI. Appendix

VI.1. Raw data

VI.1.1. DGEBA/SiO_2

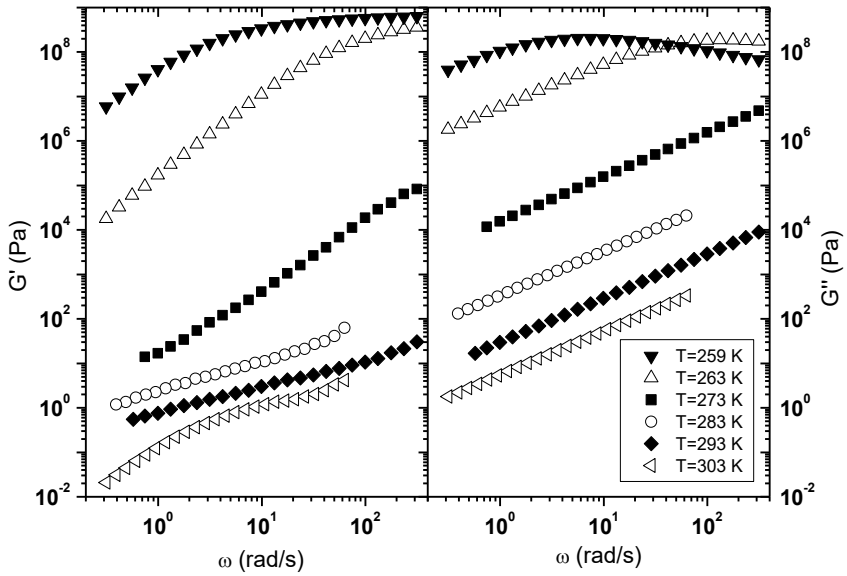

Figure VI-1: Storage modulus $G'(\omega)$ (left) and loss modulus $G''(\omega)$ (right) of a DGEBA/SiO_2 suspension with $x_V = 0.005$ for different temperatures

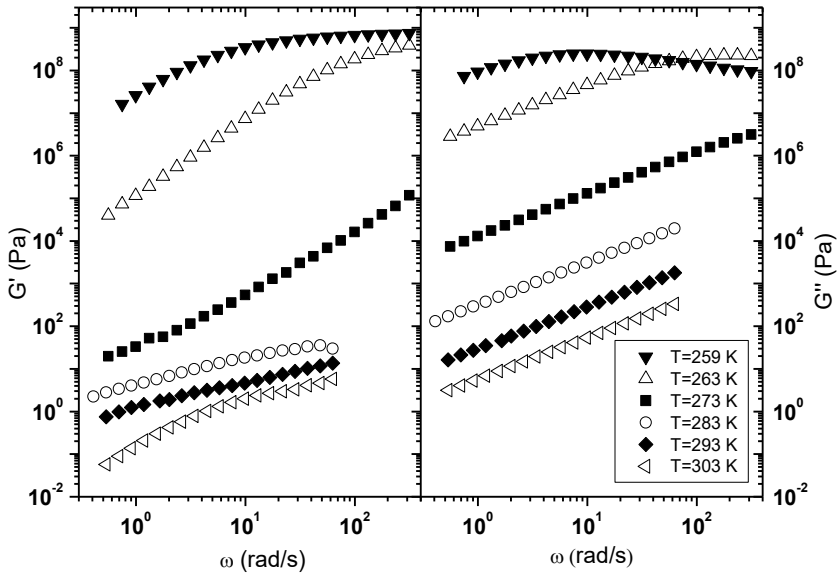

Figure VI-2: Storage modulus $G'(\omega)$ (left) and loss modulus $G''(\omega)$ (right) of a DGEBA/SiO_2 suspension with $x_V = 0.01$ for different temperatures

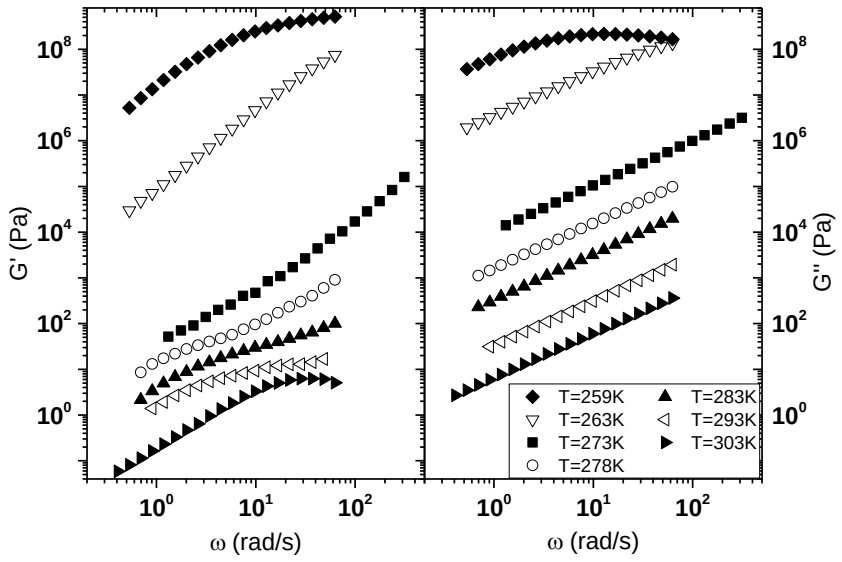

Figure VI-3: Storage modulus $G'(\omega)$ (left) and loss modulus $G''(\omega)$ (right) of a DGEBA/SiO_2 suspension with $x_V = 0.026$ for different temperatures

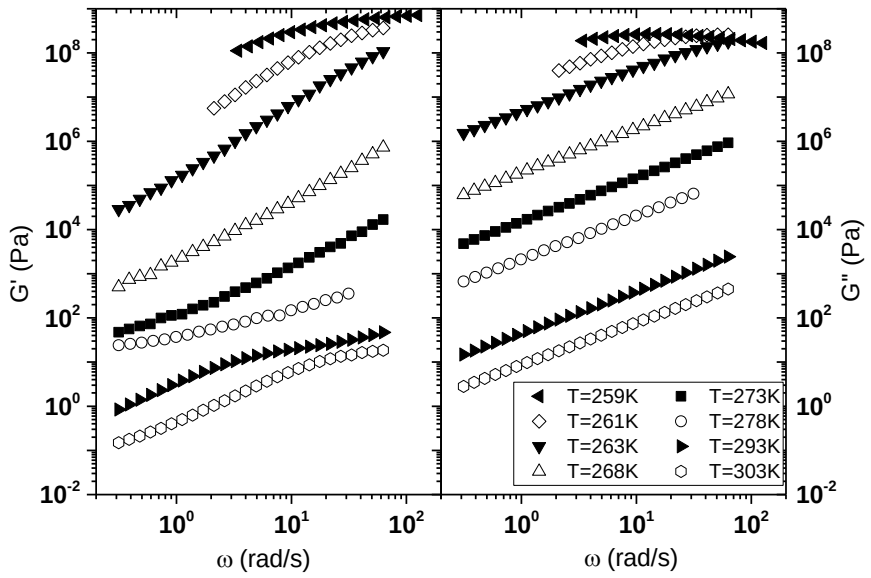

Figure VI-4: Storage modulus $G'(\omega)$ (left) and loss modulus $G''(\omega)$ (right) of a DGEBA/SiO_2 suspension with $x_V = 0.054$ for different temperatures

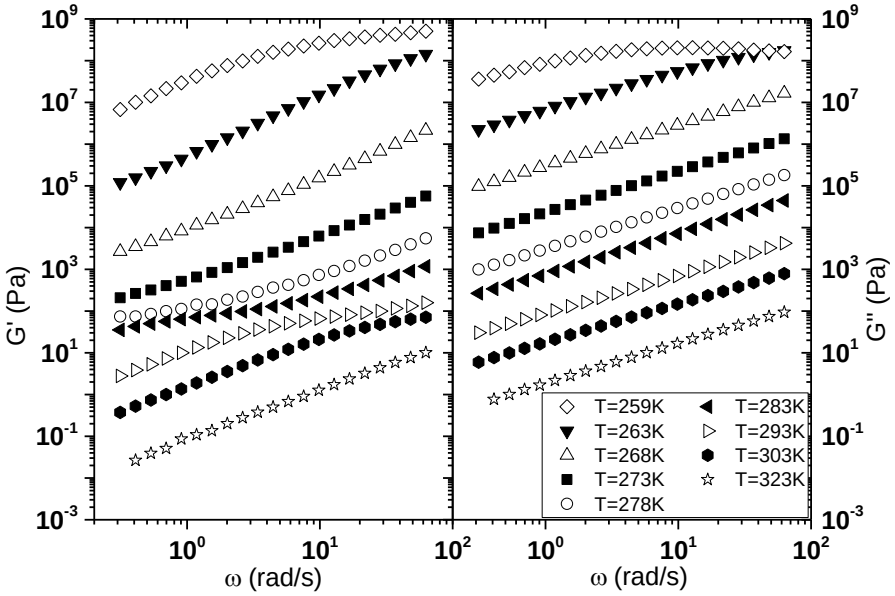

Figure VI-5: Storage modulus $G'(\omega)$ (left) and loss modulus $G''(\omega)$ (right) of a DGEBA/SiO_2 suspension with $x_V = 0.113$ for different temperatures

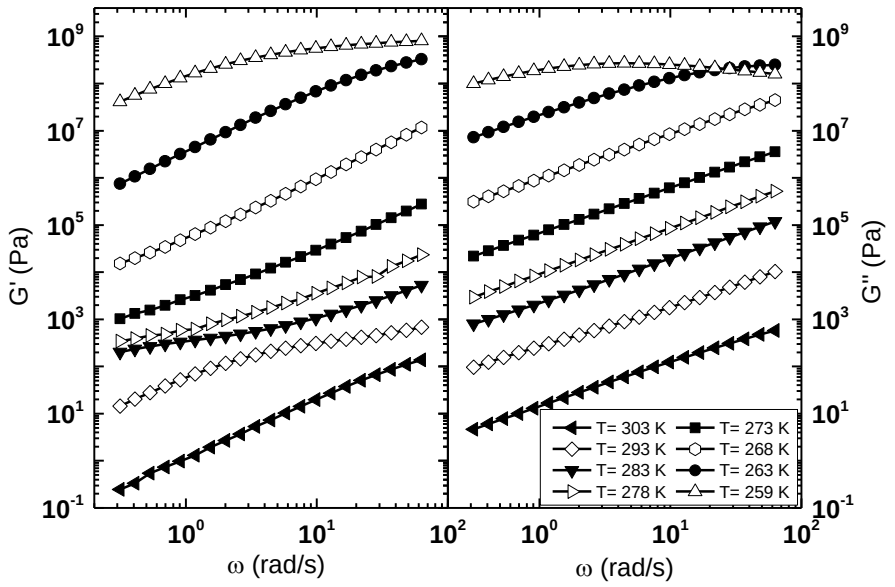

Figure VI-6: Storage modulus $G'(\omega)$ (left) and loss modulus $G''(\omega)$ (right) of a DGEBA/SiO_2 suspension with $x_V = 0.18$ for different temperatures

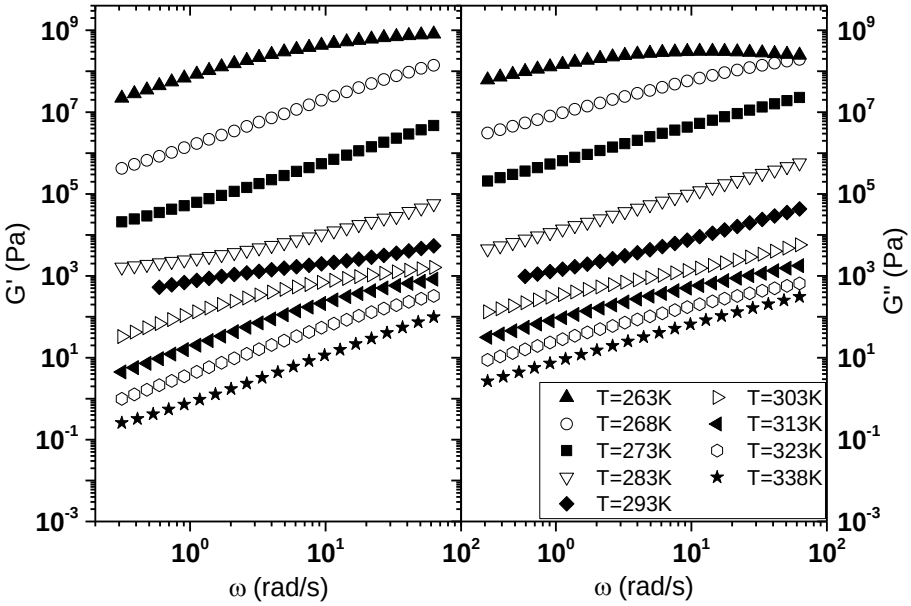

Figure VI-7: Storage modulus $G'(\omega)$ (left) and loss modulus $G''(\omega)$ (right) of a DGEBA/SiO_2 suspension with $x_V = 0.25$ for different temperatures

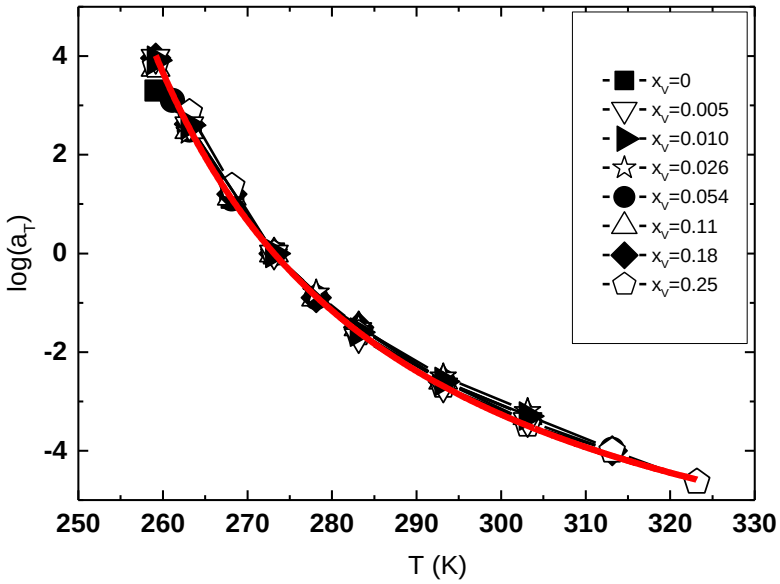

Figure VI-8: Horizontal shift factors $log(a_T)$ used for the construction of the master curves (Figure IV-18). The red line represents a WLF-plot (equation 2.1.4.11) with parameters $C_1 = 8.63$ and $C_2 = 44.08\ K$.

VI.1.2. DGEBA/Al_2O_3

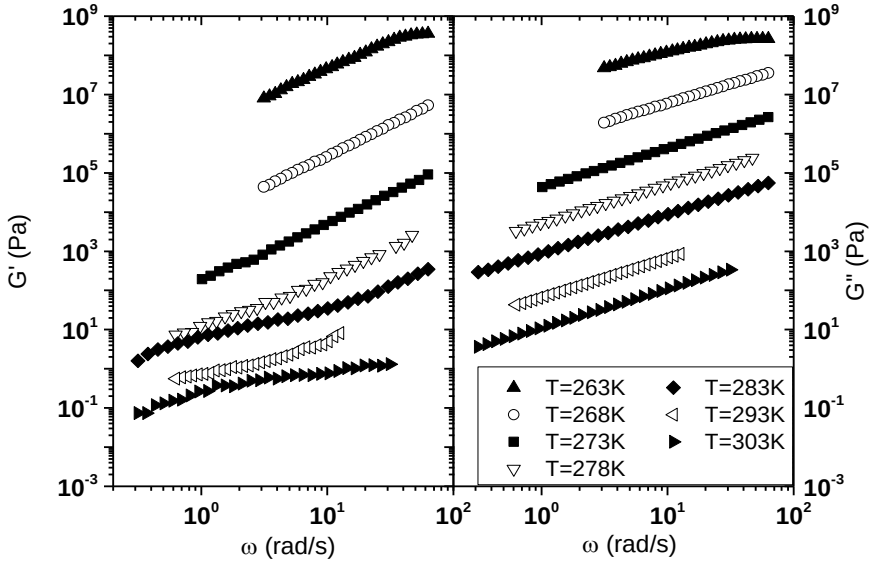

Figure VI-9: Storage modulus $G'(\omega)$ (left) and loss modulus $G''(\omega)$ (right) of a DGEBA/Al_2O_3 suspension with $x_V = 0.012$ for different temperatures

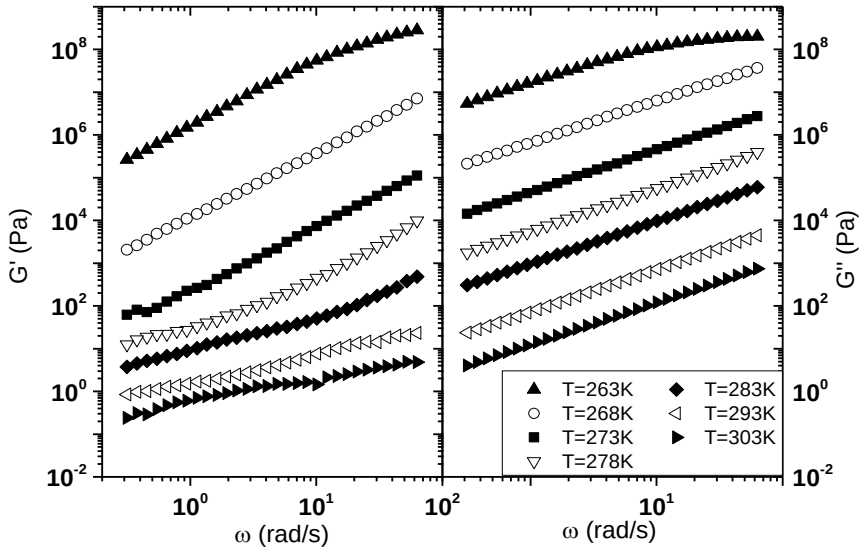

Figure VI-10: Storage modulus $G'(\omega)$ (left) and loss modulus $G''(\omega)$ (right) of a DGEBA/Al_2O_3 suspension with $x_V = 0.016$ for different temperatures

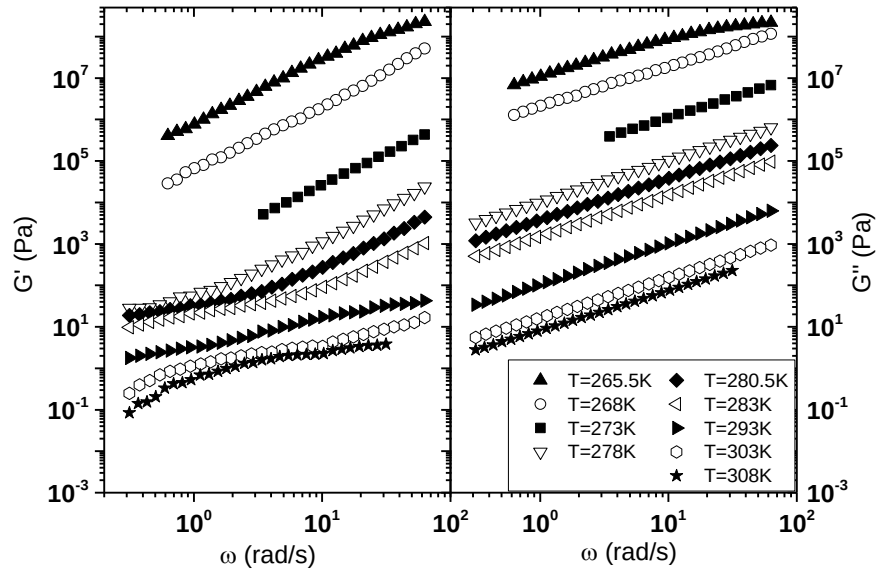

Figure VI-11: Storage modulus $G'(\omega)$ (left) and loss modulus $G''(\omega)$ (right) of a DGEBA/Al_2O_3 suspension with $x_V = 0.02$ for different temperatures

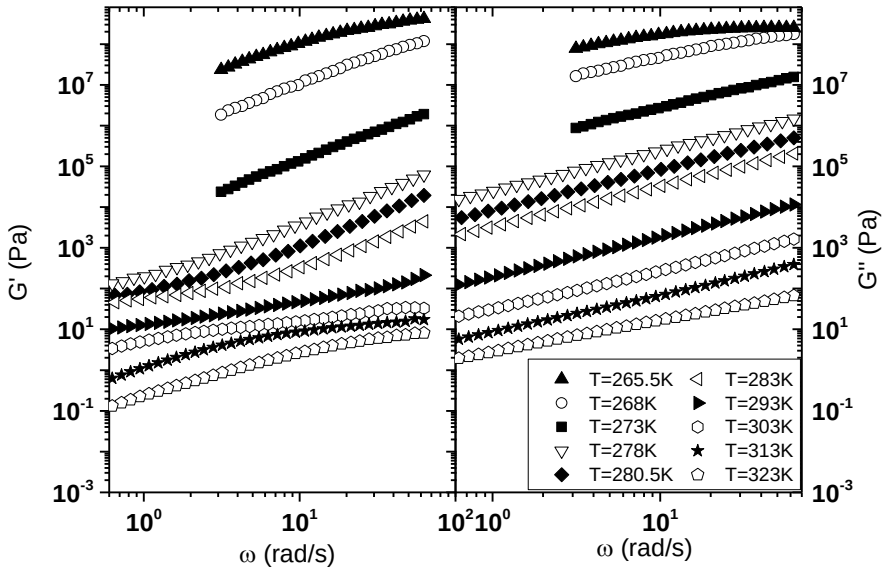

Figure VI-12: Storage modulus $G'(\omega)$ (left) and loss modulus $G''(\omega)$ (right) of a DGEBA/Al_2O_3 suspension with $x_V = 0.04$ for different temperatures

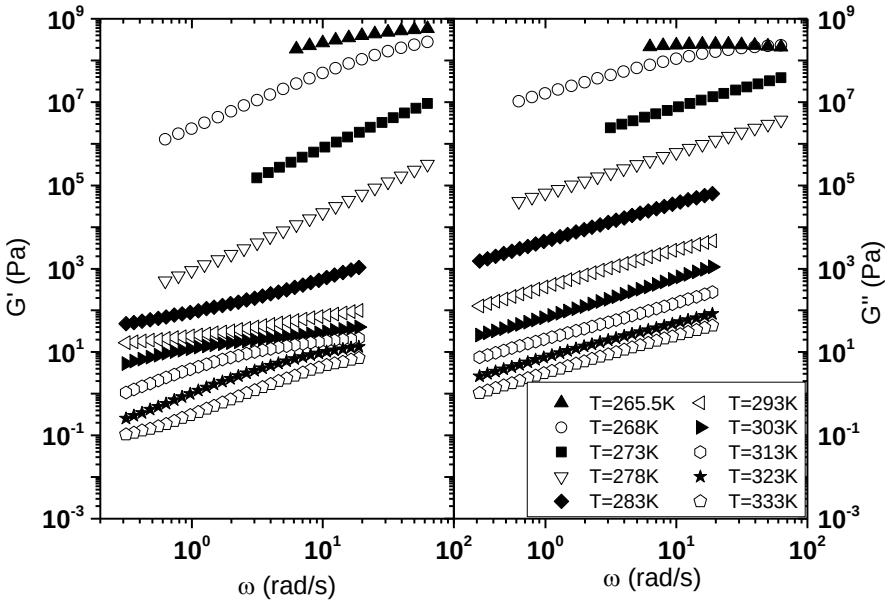

Figure VI-13: Storage modulus $G'(\omega)$ (left) and loss modulus $G''(\omega)$ (right) of a DGEBA/Al_2O_3 suspension with $x_V = 0.06$ for different temperatures

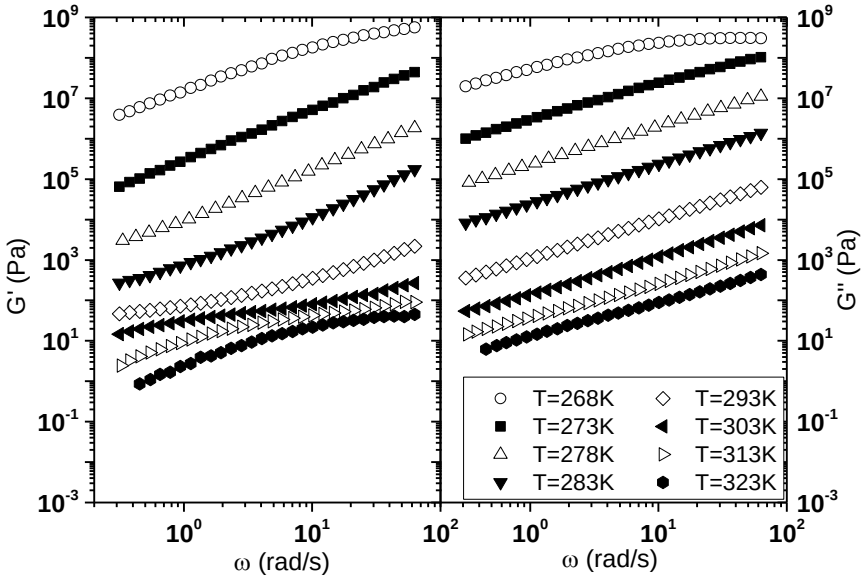

Figure VI-14: Storage modulus $G'(\omega)$ (left) and loss modulus $G''(\omega)$ (right) of a DGEBA/Al_2O_3 suspension with $x_V = 0.09$ for different temperatures

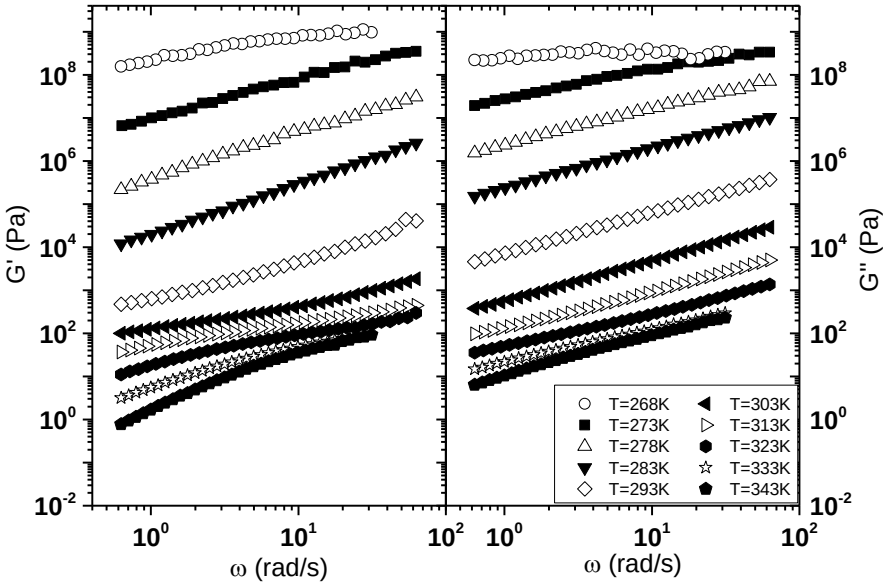

Figure VI-15: Storage modulus $G'(\omega)$ (left) and loss modulus $G''(\omega)$ (right) of a DGEBA/Al_2O_3 suspension with $x_V = 0.117$ for different temperatures

VI.2. Determination of Brownian relaxation times

The determination of the Brownian relaxation times is difficult as the corresponding process is in concurrence to the dynamic glass transition of the matrix. In fact for all considered suspensions Brownian relaxation manifest themselves by transitions in the storage moduli and for high volume concentrations in the loss moduli. In general for independent Maxwell-like relaxation processes the determination of the relaxation times could be performed:

- by fitting the measured data to the Maxwell or BSW-Model
- by tentatively using the intersection frequency of the shear moduli. The relaxation time is then defined as the inverse of the intersection frequency.

Unfortunately since Brownian relaxation can only be isolated from the matrix for high volume concentrations (see Figure IV-15) the determination of the intersection frequency is restricted to these concentrations. The fit to known models is not possible at all as even for isolated Brownian relaxation the increasing high frequency modulus $G'_{\infty,BR}$ (see section IV.2.2) deviates from Maxwell-like behaviour.

Consequently the relaxation times have to be determined via alternative methods. From the master curves shown in this dissertation becomes clear that Brownian relaxation are observed for each concentration in the storage modulus. Therefore a first method consists in subtracting the matrix elasticity from the master curves $G'(\omega)$ and fitting the terminal regime behaviour as well as the high frequency modulus $G'_{\infty,BR}$ by linear regression. The intersection of these linear regressions leads to an operational frequency ω_{op}, which can be converted into a relaxation time τ using

$$\tau = \frac{1}{\omega_{\text{int}}} . \qquad \text{(A. 1)}$$

The method is illustrated in Figure VI-16 (DGEBA/SiO_2 suspension with $x_V = 0.18$). As can be seen the so obtained operational frequency ω_{op} is similar to the intersection frequency ω_{int}, which deliver an argument for the applicability of the operational method. However it is worth to mention that compared to the determination of the intersection frequency ω_{int} the operational method delivering ω_{op} can be applied to all types of suspensions and volume concentration as long as Brownian relaxation are visible in the storage moduli.

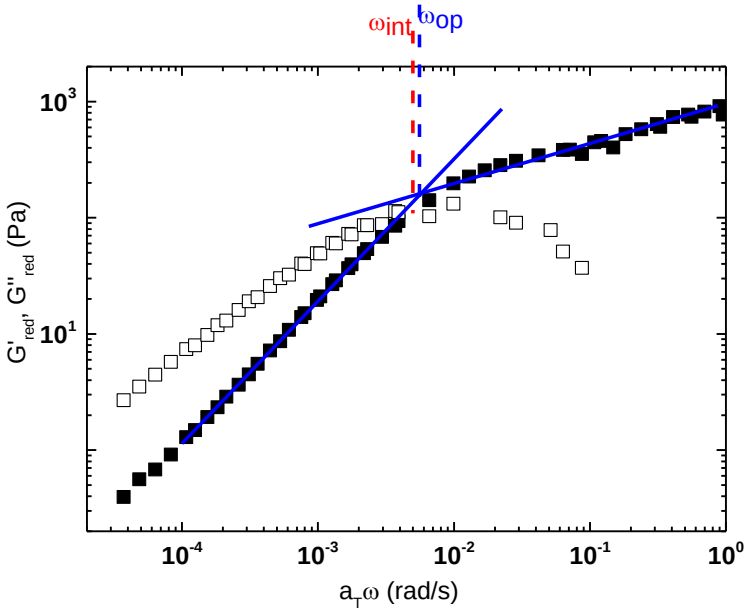

Figure VI-16: Representation of reduced shear moduli $G'_{red}(\omega)$ and $G''_{red}(\omega)$ at a reference temperature of T_{ref} = 273K for DGEBA/SiO_2 suspensions with $x_V = 0.18$. The blue solid lines indicate the linear fits of the terminal regime and high-frequency part of the reduced storage modulus. The intersection point of these regressions leads to the operational frequency ω_{op} (blue dashed line), which is not too far of from the interaction frequency ω_{int} of the reduced shear moduli

The operational method can also be applied to the imaginary part of the complex viscosity, which is related to the storage modulus via

$$\eta''(\omega) = \frac{G'(\omega)}{\omega} = \int_0^{+\infty} g(s)\sin(\omega s)ds . \qquad \text{(A.2)}$$

In Figure the imaginary part of the complex viscosity is exemplarily represented together with the real part

$$\eta'(\omega) = \frac{G''(\omega)}{\omega} = \int_0^{+\infty} g(s)\cos(\omega s)ds \qquad \text{(A.3)}$$

for a DGEBA/SiO_2 suspension with $x_V = 0.18$. As can be seen the real part of the complex viscosity follows a transition from the zero-shear viscosity η_0 to the high-

frequency viscosity η_{HI}, while the imaginary part exhibit a peak like behaviour with constant slopes left and right from the maximum. Therefore the left side (corresponding to the terminal regime of $G'(\omega)$) and the right part (corresponding to the high-frequency modulus $G'_{\infty,BR}$) can both be fitted by a linear regression. The intersection point of these regressions corresponds again to the operational frequency ω_{op}, which is fairly in agreement with the reversal point of $\eta'(\omega)$ (see first derivative of $\eta'(\omega)$ in Figure VI-17), a property which fortify again the applicability of the operational method.

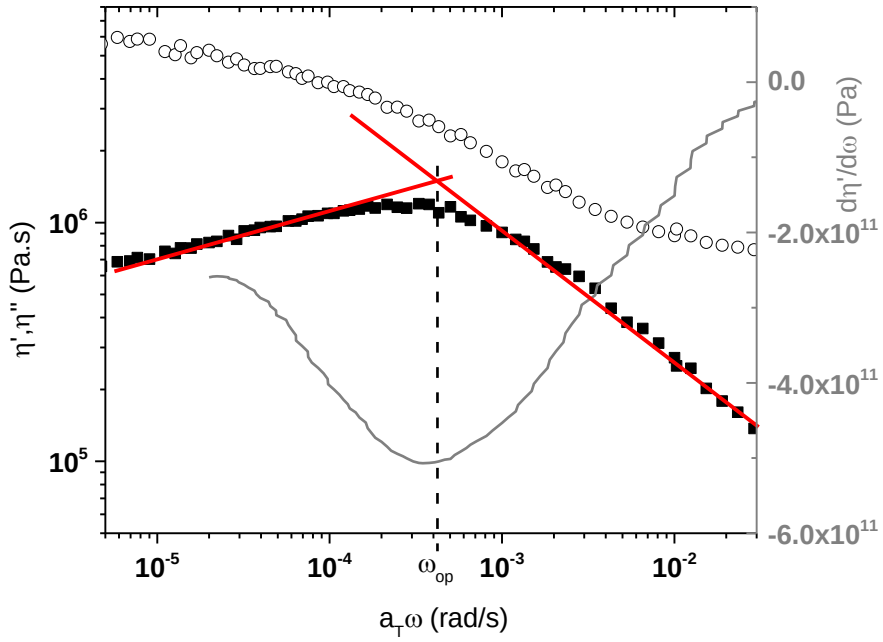

Figure VI-17: Real part (open symbols) and imaginary part (closed symbols) of the complex viscosity at a reference temperature of T_{ref} = 273K for DGEBA/SiO_2 suspensions with $x_V = 0.25$. The corresponding viscosities have been determined from the shear moduli $G'_{red}(\omega)$ and $G''(\omega)$ using equations (A.3) respectively (A.2). The grey solid line depicts the first derivative of $\eta'(\omega)$, which indicates at his minimum the reversal point of $\eta'(\omega)$. The dashed line illustrate the operational frequency ω_{op} obtained via the intersection point of two linear regressions (red solid lines)

VI.3. Particularity in the determination of the zero-shear viscosity

In general the suspension viscosities η_0 and η_{HI} are determined by linear fits of the terminal regime of the loss modulus when the latter is represented in a log-log scale as function of the frequency ω. Mathematically this procedure is described by

$$\log(\omega) + log(\eta_{HI}) = log(G'') \qquad \text{(A.4)}$$

and

$$\log(\omega) + log(\eta_0) = log(G''). \qquad \text{(A.5)}$$

In other words the viscosities are somehow related to the loss modulus at $\log(\omega) = 0$. For the determination of η_{HI} this procedure is applicable (see Figure VI-18). However for some measurements the calculation of η_0 from equation (A.5) is not possible since the measurements could not be performed down to such low frequencies that the loss modulus achieves the second terminal regime (on the left side of the low-frequency process). The situation is visualized in Figure VI-18 where the real part of the viscosity is represented as function of the frequency. While η' is nearly constant at high frequencies leading to a well-defined high-frequency viscosity η_{HI} (see red solid line), η' is still depending on the frequency for frequencies below the transition from η_0 to η_{HI} (see blue solid line). Consequently the experimental determined viscosity $\eta_{0,exp}$ (see Figure VI-18) is smaller than the theoretical one $\eta_{0,theo}$ (see blue dashed line).

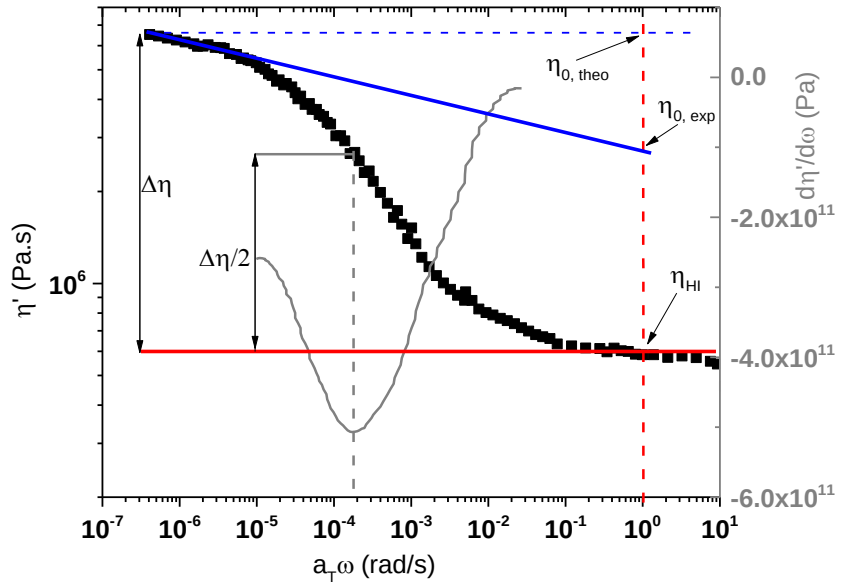

Figure VI-18: Real part of the complex viscosity as function of the frequency. The red solid line illustrates the fit of the high-frequency part leading to the viscosity η_{HI}. In contrast the blue solid line depicts that η' still depends on the frequency at low frequencies. As a consequence different values of η_0 are found depending on the method ($\eta_{0,exp}$ and $\eta_{0,theo}$). The grey curve shows the first derivative of η' and by his minimum the inflection point of η'. From the inflection point the difference $\Delta\eta$ and thus η_0 can be determined (see text).

Thus for these cases an alternative method has to be used. One possibility consists in the determination of the difference $\Delta\eta = \eta_0 - \eta_{HI}$ using the first derivative of η'. As can be seen in Figure VI-18 the first derivative of η' yield a minimum, which reflects the inflection point of η'. As a first approximation the difference between the viscosity corresponding to this point and the high-frequency viscosity η_{HI} can be considered as $\Delta\eta/2$. With this information the zero-shear viscosity can be determined via $\eta_0 = \Delta\eta + \eta_{HI}$. Values of η_0 which are determined by this method are labelled in the manuscript.

VI.4. Normalized Brownian relaxation times for the studied colloidal suspensions

In section IV.4 the Brownian relaxation times found for all here investigated types of suspensions have been normalized by corresponding Peclet-times and represented as function of effective volume concentrations $x_{V,eff}$ instead of nominal filler fractions x_V. For reasons of clarity in section IV.4 neither the conversion from nominal to effective volume concentrations nor the explicit calculation of the normalized relaxation times have been shown. These points will be addressed in the following.

VI.4.1. Conversion from nominal to effective volume concentrations

For all of the studied types of suspensions e.g DGEBA/SiO_2, polymerized DGEBA/SiO_2 and DGEBA/Al_2O_3 the zero-shear viscosities have been shown to diverge at nominal filler fractions ($x_{V,max} = 0.26$ for DGEBA/SiO_2, polymerized DGEBA/SiO_2 respectively $x_{V,max} = 0.15$ for DGEBA/ Al_2O_3) which are small compared to the expected value ($x_{V,g} = 0.58$ for colloidal suspensions of neutral hard spheres). While for the suspensions with silica particles the deviation was explained by small repulsive interaction layers around the particles, for the alumina dispersions the clustering of the primary particles has been mentioned to be responsible for the difference in the diverging concentration of the zero-shear viscosity. In fact as shown in section II.2.2 both effects affect the nominal volume concentrations (obtained for the studied suspensions from the mass concentration x_m , see section III.1.2). Therefore in order to include these effects and compare the found results to data from literature the nominal volume concentrations x_V need to adapted to effective filler fractions $x_{V,eff}$. For all suspensions the expression

$$\frac{x_{V,eff}}{x_V} = \frac{x_{V,g}}{x_{V,max}} \qquad \text{(A.6)}$$

can be used, where $x_{V,max}$ stands for the volume concentration at which the zero-shear viscosity diverges in the studied suspensions and $x_{V,g} = 0.58$ for particle glass transition fraction at which $\eta_0(x_V)$ should diverge. Consequently for the silica dispersions equation (A.6) leads to $\frac{x_{V,eff}}{x_V} = 2.23$, while for the alumina suspensions $\frac{x_{V,eff}}{x_V} = 3.87$. The resulting effective volume concentrations are listed in Table 12 and Table 13 for the different types of suspensions. In case of silica particles the repulsive interaction layers increase the particle size leading to an effective particle radii, which can be calculated from equation (2.2.2.11). As the nominal mean particle radius of the silica colloids is given by $a = 12.5\,nm$ the corresponding effective particle radius is expected to be $a_{eff} = 16\,nm$. For the alumina particles the transition from nominal to effective volume concentrations can give a hint of the cluster sizes. Using equation (2.2.2.13), together with the information that the aggregates are chemical linked clusters composed of primary alumina particles with radii around $a = 12\,nm$ the cluster radii R is expected to be $35\,nm$.

In this context it is important to note that the non-monotonic nature of the relaxation times is not affected by converting the nominal volume concentrations into effective

filler fractions. In fact only the location of the minimum in the relaxation times is shifted to higher concentrations.

Table 12: Nominal volume concentrations x_V and corresponding effective volume concentrations $x_{V,eff}$ for the studied suspensions based on silica particles

x_V	$x_{V,eff}$
0.005	0,011
0.01	0,023
0.026	0,06
0.054	0,12
0.113	0,25
0.18	0,4
0.25	0,56

Table 13: Nominal volume concentrations x_V and corresponding effective volume concentrations $x_{V,eff}$ for the studied suspensions based on alumina particles

x_V	$x_{V,eff}$
0.012	0,046
0.016	0,061
0.02	0,077
0.04	0,15
0.06	0,23
0.09	0,35
0.117	0,45

VI.4.2. Calculations of normalized Brownian relaxation times

Once that the nominal volume concentrations have been converted into effective filler fractions the experimentally determined relaxation times can be normalized by dividing them by the Peclet-time using equation (4.2.2.5). However two particularities have to be considered:

- In equation (4.2.2.5) no explicit diffusion coefficient is specified. However as shown in section IV.2.3 the long-time self-diffusion coefficient seems to be adequate for Brownian relaxation times.
- The used length-scale of the Peclet-time is the particle radius. In case of the suspensions based on silica particles, the sizes of the latter could be determined via the fit of the diffusion time $\tau_{\langle r \rangle,CC}$ to the Brownian relaxation times τ. This procedure leaded to fit radii of $a_{fit} = 12.5\,nm$ for the DGEBA/SiO_2 samples and $a_{fit} = 17\,nm$ for the polymerized DGEBA/SiO_2 suspensions. However as shown in the last section the conversion from nominal to effective volume concentrations yield effective particle radii, which can be calculated using equation (2.2.2.11). Consequently the particle radii to use for the normalization procedure are $a_{fit,eff} = 16\,nm$ for the DGEBA/SiO_2 samples and $a_{fit,eff} = 24\,nm$ for the polymerized DGEBA/SiO_2 suspensions. In contrast for the dispersions based on alumina particles no

reliable information on the particle sizes are available. Also the radius obtained from the fit of diffusion time $\tau_{\langle r\rangle,CC}$ ($a_{fit} = 18\ nm$) seems not to be well justified. Therefore the radius of the clusters $R = 35\ nm$ found from the conversion from nominal to effective volume concentrations is used

Using these properties the used Peclet-time can be written as

$$\tau_P = \frac{\pi \eta_0 a_{fit,eff}^3}{k_B T} \tag{A.7}$$

for the silica suspensions and

$$\tau_P = \frac{\pi \eta_0 R^3}{k_B T} \tag{A.8}$$

for the alumina based dispersions. In the Table 14-

Table *16* all needed quantities for the calculation of the normalized relaxation times are listed for the different effective volume concentrations.

Table 14: Zero-shear viscosity η_0, expected Peclet-time τ_p, experimentally determined relaxation time τ and normalized relaxation time $\tau_{norm} = \tau/\tau_P$ for the corresponding effective volume concentrations $x_{V,eff}$ for the DGEBA/SiO_2 suspensions

$x_{V,eff}$(-)	η_0 (.10^5Pa.s)	τ_p (s)	τ (.10^3s)	τ_{norm} (-)
0,011	1.02	34	0.91	26
0,023	1.04	35	0.66	18
0,06	1.06	36	0.38	10
0,12	1.28	43	0.13	2.3
0,25	3.74	127	0.14	1.1
0,4	14.5	496	0.19	0.39
0,56	127.4	43533	2.32	0.053

Table 15: Zero-shear viscosity η_0, expected Peclet-time τ_p, experimentally determined relaxation time τ and normalized relaxation time $\tau_{norm} = \tau/\tau_P$ for the corresponding effective volume concentrations $x_{V,eff}$ for the polymerized DGEBA/SiO_2 suspensions

$x_{V,eff}$(-)	η_0 (.10^5Pa.s)	τ_P (.$10^4 s$)	τ (.$10^4 s$)	τ_{norm} (-)
0,011	3.65	0.42	7.75	18
0,023	4.1	0.47	4.38	9.4
0,06	4.3	0.49	3.42	6.2
0,12	5.5	0.63	1.17	1.8
0,25	8.3	0.95	0.98	1.02
0,4	33	3.8	2.11	0.55

Table 16: Zero-shear viscosity η_0, expected Peclet-time τ_p, experimentally determined relaxation time τ and normalized relaxation time $\tau_{norm} = \tau/\tau_P$ for the corresponding effective volume concentrations $x_{V,eff}$ for the DGEBA/Al_2O_3 suspensions

$x_{V,eff}$(-)	η_0 (. 10^4Pa.s)	τ_p (s)	τ (.10^4 s)	τ_{norm} (-)
0,046	4.07	34	0.767	5.2
0,061	4.89	35	0.712	4.0
0,077	9.22	36	0.806	2.4
0,15	26.9	43	1.63	1.7
0,23	95.4	127	3.45	1.01
0,35	860	496	7.87	0.25
0,45	18000	5604	30.6	0.048

VII. References

[1] J. Mewis and N. J. Wagner, *Colloidal suspension rheology*: Cambridge University Press, 2012.

[2] G. K. Batchelor, "Effect of Brownian motion on bulk stress in a suspension of spherical particles," *Journal of Fluid Mechanics,* vol. 83, pp. 97-117, 1977 1977.

[3] J. Morris, "A review of microstructure in concentrated suspensions and its implications for rheology and bulk flow," *Rheologica Acta,* vol. 48, pp. 909-923, 2009/10/01 2009.

[4] T. Shikata and D. S. Pearson, "Viscoelastic behavior of concentrated spherical suspensions," *Journal of Rheology,* vol. 38, pp. 601-616, 1994.

[5] J. van der Werff, C. de Kruif, C. Blom, and J. Mellema, "Linear viscoelastic behavior of dense hard-sphere dispersions," *Physical Review A,* vol. 39, pp. 795-807, 1989.

[6] T. N. Phung, J. F. Brady, and G. Bossis, "Stokesian Dynamics simulation of Brownian suspensions," *Journal of Fluid Mechanics,* vol. 313, pp. 181-207, 1996.

[7] N. J. Wagner and J. F. Brady, "Shear thickening in colloidal dispersions," *Physics Today,* vol. 62, pp. 27-32, 2009.

[8] R. Lionberger and W. Russel, "High frequency modulus of hard sphere colloids," *Journal of Rheology,* vol. 38, pp. 1885-1908, 1994.

[9] B. Dudkin, G. Zainullin, P. Krivoshapkin, E. Krivoshapkina, and M. Ryazanov, "Influence of nanoparticles and nanofibers of aluminum oxide on the properties of epoxy composites," *Glass Physics and Chemistry,* vol. 34, pp. 187-191, 2008.

[10] B. Johnsen, A. Kinloch, R. Mohammed, A. Taylor, and S. Sprenger, "Toughening mechanisms of nanoparticle-modified epoxy polymers," *Polymer,* vol. 48, pp. 530-541, 2007.

[11] A. Kinloch, K. Masania, A. Taylor, S. Sprenger, and D. Egan, "The fracture of glass-fibre-reinforced epoxy composites using nanoparticle-modified matrices," *Journal of Materials Science,* vol. 43, pp. 1151-1154, 2008.

[12] A. Kinloch and A. Taylor, "The mechanical properties and fracture behaviour of epoxy-inorganic micro-and nano-composites," *Journal of Materials Science,* vol. 41, pp. 3271-3297, 2006.

[13] B. Wetzel, F. Haupert, and M. Q. Zhang, "Epoxy nanocomposites with high mechanical and tribological performance," *Composites Science and Technology,* vol. 63, pp. 2055-2067, 2003.

[14] N. Suzuki, M. Ito, and F. Yatsuyanagi, "Effects of rubber/filler interactions on deformation behavior of silica filled SBR systems," *Polymer,* vol. 46, pp. 193-201, 2005.

[15] E. Chabert, M. Bornert, E. Bourgeat-Lami, J.-Y. Cavaillé, R. Dendievel, C. Gauthier*, et al.*, "Filler–filler interactions and viscoelastic behavior of polymer nanocomposites," *Materials Science and Engineering: A,* vol. 381, pp. 320-330, 2004.

[16] E. Jaber, H. Luo, W. Li, and D. Gersappe, "Network formation in polymer nanocomposites under shear," *Soft Matter,* vol. 7, pp. 3852-3860, 2011.

[17] N. Alberola, K. Benzarti, C. Bas, and Y. Bomal, "Interface effects in elastomers reinforced by modified precipitated silica," *Polymer Composites,* vol. 22, pp. 312-325, 2001.
[18] J. Baller, N. Becker, M. Ziehmer, M. Thomassey, B. Zielinski, U. Müller*, et al.*, "Interactions between silica nanoparticles and an epoxy resin before and during network formation," *Polymer,* vol. 50, pp. 3211-3219, 2009.
[19] J. Baller, M. Thomassey, M. Ziehmer, and R. Sanctuary, "Thermal and chemical glass transition of thermosets in the presence of two types of inorganic nanoparticles," in *Thermoplastic and thermosetting polymers and composites*, L. D. Tsai and M. R. Hwang, Eds., ed Hauppauge: Nova Science Publishers, 2011, pp. 197-212.
[20] R. Sanctuary, J. Baller, J.-K. Krüger, D. Schaefer, R. Bactavatchalou, B. Wetzel*, et al.*, "Complex specific heat capacity of two nanocomposite systems," *Thermochimica acta,* vol. 445, pp. 111-115, 2006.
[21] R. Sanctuary, J. Baller, B. Zielinski, N. Becker, J. K. Kruger, M. Philipp*, et al.*, "Influence of Al2O3 nanoparticles on the isothermal cure of an epoxy resin," *Journal of Physics: Condensed Matter,* vol. 21, p. 035118, 2009.
[22] K. Schröter and E. Donth, "Comparison of shear response with other properties at the dynamic glass transition of different glassformers," *Journal of Non-Crystalline Solids,* vol. 307, pp. 270-280, 2002.
[23] H. A. Barnes, J. F. Hutton, and K. Walters, *An introduction to rheology* vol. 3: Elsevier, 1989.
[24] C. Macosko and P. Rheology, "Measurements and Applications," *VCH, New York,* 1994.
[25] R. S. Lakes, *Viscoelastic materials*: Cambridge University Press, 2009.
[26] J. D. Ferry, *Viscoelastic properties of polymers*: John Wiley & Sons, 1980.
[27] N. W. Tschoegl, *The phenomenological theory of linear viscoelastic behavior: an introduction*: Springer Science & Business Media, 2012.
[28] M. Thomassey, "Etude de propriétés dynamiques linéaires et non-linéaires de deux liquides colloïdaux modèles par rhéologie : DGEBA/Al2O3 et DGEBA/SiO2," Faculté des Sciences, de la Technologie et de la Communication, Université du Luxembourg, 2012.
[29] C. A. Angell, "The glass transition," *Current opinion in solid state and Materials Science,* vol. 1, pp. 578-585, 1996.
[30] J. K. Dhont, *An introduction to dynamics of colloids*: Elsevier, 1996.
[31] E.-J. Donth, *The glass transition: relaxation dynamics in liquids and disordered materials* vol. 48: Springer Science & Business Media, 2013.
[32] M. Baumgaertel and H. H. Winter, "Determination of discrete relaxation and retardation time spectra from dynamic mechanical data," *Rheologica Acta,* vol. 28, pp. 511-519, Nov-Dec 1989.
[33] M. Baumgaertel and H. H. Winter, "Interrelation between continuous and discrete relaxation time spectra," *Journal of Non-Newtonian Fluid Mechanics,* vol. 44, pp. 15-36, 1992.
[34] H. H. Winter, "Analysis of dynamic mechanical data: Inversion into a relaxation time spectrum and consistency check," *Journal of Non-Newtonian Fluid Mechanics,* vol. 68, pp. 225-239, Feb 1997.
[35] H. H. Winter, M. Siebenbuerger, D. Hajnal, O. Henrich, M. Fuchs, and M. Ballauff, "An empirical constitutive law for concentrated colloidal suspensions in the approach of the glass transition," *Rheologica Acta,* vol. 48, pp. 747-753, Aug 2009.

[36] H. H. Winter, "Glass Transition as the Rheological Inverse of Gelation," *Macromolecules,* vol. 46, pp. 2425-2432, Mar 26 2013.
[37] C. Liang, W. Sun, T. Wang, X. Liu, and Z. Tong, "Rheological inversion of the universal aging dynamics of hectorite clay suspensions," *Colloids and Surfaces A: Physicochemical and Engineering Aspects,* vol. 490, pp. 300-306, 2016.
[38] J. Dealy and D. Plazek, "Time-temperature superposition—a users guide," *Rheol. Bull,* vol. 78, pp. 16-31, 2009.
[39] M. Van Gurp and J. Palmen, "Time-temperature superposition for polymeric blends," *Rheol Bull,* vol. 67, pp. 5-8, 1998.
[40] A. Einstein, "The theory of the brownian movement," *Ann. der Physik,* vol. 17, p. 549, 1905.
[41] A. Einstein, "Über die von der molekularkinetischen Theorie der Wärme geforderte Bewegung von in ruhenden Flüssigkeiten suspendierten Teilchen," *Annalen der physik,* vol. 322, pp. 549-560, 1905.
[42] I. Sohn and R. Rajagopalan, "Microrheology of model quasi-hard-sphere dispersions," *Journal of Rheology (1978-present),* vol. 48, pp. 117-142, 2004.
[43] E. R. Weeks and D. Weitz, "Properties of cage rearrangements observed near the colloidal glass transition," *Physical review letters,* vol. 89, p. 095704, 2002.
[44] M. J. Sanchez-Miranda, B. Bonilla-Capilla, E. Sarmiento-Gomez, E. Lazaro-Lazaro, A. Ramirez-Saito, M. Medina-Noyola*, et al.*, "Transition from diffusive to subdiffusive motion in colloidal liquids," *Soft Matter,* vol. 11, pp. 655-658, 2015.
[45] R. Lionberger and W. Russel, "A Smoluchowski theory with simple approximations for hydrodynamic interactions in concentrated dispersions," *Journal of Rheology (1978-present),* vol. 41, pp. 399-425, 1997.
[46] C. Beenakker and P. Mazur, "Diffusion of spheres in a concentrated suspension: Resummation of many-body hydrodynamic interactions," *Physics Letters A,* vol. 98, pp. 22-24, 1983.
[47] M. Tokuyama and I. Oppenheim, "On the theory of concentrated hard-sphere suspensions," *Physica A: Statistical Mechanics and its Applications,* vol. 216, pp. 85-119, 1995.
[48] X. Qiu, X. Wu, J. Xue, D. Pine, D. Weitz, and P. Chaikin, "Hydrodynamic interactions in concentrated suspensions," *Physical review letters,* vol. 65, p. 516, 1990.
[49] J. Zhu, D. Durian, J. Müller, D. Weitz, and D. Pine, "Scaling of transient hydrodynamic interactions in concentrated suspensions," *Physical review letters,* vol. 68, p. 2559, 1992.
[50] J. Mellema, J. van der Werff, C. Blom, and C. de Kruif, "Interpretation of the complex viscosity of dense hard-sphere dispersions," *Physical Review A,* vol. 39, pp. 3696-3699, 1989.
[51] D. B. Genovese, "Shear rheology of hard-sphere, dispersed, and aggregated suspensions, and filler-matrix composites," *Advances in Colloid and Interface Science,* vol. 171-172, 2012.
[52] I. M. Krieger and T. J. Dougherty, "A Mechanism for Non-Newtonian Flow in Suspensions of Rigid Spheres," *Transactions of the Society of Rheology,* vol. 3, pp. 137-152, 1959.
[53] J. Bergenholtz, F. Horn, W. Richtering, N. Willenbacher, and N. Wagner, "Relationship between short-time self-diffusion and high-frequency viscosity in charge-stabilized dispersions," *Physical Review E,* vol. 58, p. R4088, 1998.

[54] B. Cichocki and B. Felderhof, "Long-time self-diffusion coefficient and zero-frequency viscosity of dilute suspensions of spherical Brownian particles," *The Journal of chemical physics,* vol. 89, pp. 3705-3709, 1988.
[55] W. Van Megen and S. Underwood, "Tracer diffusion in concentrated colloidal dispersions. III. Mean squared displacements and self-diffusion coefficients," *The Journal of chemical physics,* vol. 91, pp. 552-559, 1989.
[56] M. Medina-Noyola, "Long-time self-diffusion in concentrated colloidal dispersions," *Physical review letters,* vol. 60, p. 2705, 1988.
[57] A. J. Banchio, G. Nägele, and J. Bergenholtz, "Viscoelasticity and generalized Stokes–Einstein relations of colloidal dispersions," *The Journal of chemical physics,* vol. 111, pp. 8721-8740, 1999.
[58] G. K. Batchelor, "BROWNIAN DIFFUSION OF PARTICLES WITH HYDRODYNAMIC INTERACTION," *Journal of Fluid Mechanics,* vol. 74, pp. 1-29, 1976 1976.
[59] R. A. Lionberger and W. Russel, "Microscopic theories of the rheology of stable colloidal dispersions," *Advances in Chemical Physics,* vol. 111, pp. 399-474, 2000.
[60] A. Banchio, J. Bergenholtz, and G. Nägele, "Rheology and dynamics of colloidal suspensions," *Physical review letters,* vol. 82, p. 1792, 1999.
[61] P. Pusey and W. Van Megen, "Phase behaviour of concentrated suspensions of nearly hard colloidal spheres," *Nature,* vol. 320, pp. 340-342, 1986.
[62] J. F. Brady, "The rheological behavior of concentrated colloidal dispersions," *The Journal of Chemical Physics,* vol. 99, pp. 567-581, 1993.
[63] S. Mueller, E. Llewellin, and H. Mader, "The rheology of suspensions of solid particles," in *Proceedings of the Royal Society of London A: Mathematical, Physical and Engineering Sciences*, 2009, p. rspa20090445.
[64] T. F. Tadros, "Correlation of viscoelastic properties of stable and flocculated suspensions with their interparticle interactions," *Advances in Colloid and Interface Science,* vol. 68, pp. 97-200, 1996.
[65] M. J. Vold, "The effect of adsorption on the van der Waals interaction of spherical colloidal particles," *Journal of colloid science,* vol. 16, pp. 1-12, 1961.
[66] Y. Min, M. Akbulut, K. Kristiansen, Y. Golan, and J. Israelachvili, "The role of interparticle and external forces in nanoparticle assembly," *Nature materials,* vol. 7, pp. 527-538, 2008.
[67] F. Rubio-Hernández, M. Ayucar-Rubio, J. Velazquez-Navarro, and F. Galindo-Rosales, "Intrinsic viscosity of SiO 2, Al 2 O 3 and TiO 2 aqueous suspensions," *Journal of colloid and interface science,* vol. 298, pp. 967-972, 2006.
[68] Y. Aoki, A. Hatano, and H. Watanabe, "Rheology of carbon black suspensions. II. Well dispersed system," *Rheologica Acta,* vol. 42, pp. 321-325, 2003.
[69] L. Landau and E. Lifshitz, "Fluid mechanics, vol. 6," *Course of Theoretical Physics,* pp. 227-229, 1987.
[70] M. E. Smith and H. Ishida, "Kinetics of the condensation reaction of epoxide with phenol: Linear chain growth versus branching," *Macromolecules,* vol. 27, pp. 2701-2707, 1994.
[71] P. Elens, "Dynamical rheological properties of DGEBA-SiO2 colloidal suspensions," Bachelor, Laboratory for the Physics of Advanced Materials, University of Luxembourg, 2014.
[72] A. Paar, "The Modular Compact Rheometer Series," A. Paar, Ed., ed, 2016.
[73] R. H. Ewoldt, M. T. Johnston, and L. M. Caretta, "Experimental challenges of shear rheology: how to avoid bad data," in *Complex Fluids in Biological Systems*, ed: Springer, 2015, pp. 207-241.

[74] J. F. Steffe, *Rheological methods in food process engineering*: Freeman press, 1996.
[75] D. S. Pearson and E. Helfand, "Viscoelastic properties of star-shaped polymers," *Macromolecules,* vol. 17, pp. 888-895, 1984.
[76] H. Watanabe, "Viscoelasticity and dynamics of entangled polymers," *Progress in Polymer Science,* vol. 24, pp. 1253-1403, 1999.
[77] S. Matsuoka, *Relaxation phenomena in polymers*: Hanser Munich etc., 1992.
[78] M. T. Shaw and W. J. MacKnight, *Introduction to polymer viscoelasticity*: John Wiley & Sons, 2005.
[79] L. Fetters, D. Lohse, D. Richter, T. Witten, and A. Zirkel, "Connection between polymer molecular weight, density, chain dimensions, and melt viscoelastic properties," *Macromolecules,* vol. 27, pp. 4639-4647, 1994.
[80] R. Dannert, R. Sanctuary, M. Thomassey, P. Elens, J. K. Krüger, and J. Baller, "Strain-induced low-frequency relaxation in colloidal DGEBA/SiO2 suspensions," *Rheologica Acta,* vol. 53, pp. 715-723, 2014.
[81] H. Watanabe, M.-L. Yao, T. Sato, and K. Osaki, "Non-Newtonian flow behavior of diblock copolymer micelles: Shear-thinning in a nonentangling matrix," *Macromolecules,* vol. 30, pp. 5905-5912, 1997.
[82] V. Vignaux-Nassiet, A. Allal, and J. P. Montfort, "Emulsion models and rheology of filled polymers," *European Polymer Journal,* vol. 34, pp. 309-322, Mar-Apr 1998.
[83] R. M. D. Graebling, and J. F. Palierne, "Linear Viscoelastic Behavior of Some Incompatible Polymer Blends in the Melt. Interpretation of Data with a Model of Emulsion of Viscoelastic Liquids," *Macromolecules,* vol. 26, 1993.
[84] D. R. Foss and J. F. Brady, "Brownian dynamics simulation of hard-sphere colloidal dispersions," *Journal of Rheology (1978-present),* vol. 44, pp. 629-651, 2000.
[85] R. Dannert, R. Sanctuary, and J. Baller, "Unexpected maximum in the concentration dependency of the relaxation frequency of Brownian stress in a colloidal suspension," *Journal of Rheology* vol. 59, pp. 391-404, 2015.
[86] T. G. Mason, "Estimating the viscoelastic moduli of complex fluids using the generalized Stokes-Einstein equation," *Rheologica Acta,* vol. 39, pp. 371-378, Aug 2000.
[87] E. R. Weeks and D. A. Weitz, "Properties of Cage Rearrangements Observed near the Colloidal Glass Transition," *Physical Review Letters,* vol. 89, p. 095704, 08/12/ 2002.
[88] B. Cichocki and K. Hinsen, "Dynamic computer simulation of concentrated hard sphere suspensions: II. Re-analysis of mean square displacement data," *Physica A: Statistical Mechanics and its Applications,* vol. 187, pp. 133-144, 1992.
[89] A. S. Khair and J. F. Brady, "“Microviscoelasticity” of colloidal dispersions," *Journal of Rheology,* vol. 49, pp. 1449-1481, 2005.

Danksagung

„Es ist ein lobenswerter Brauch:

Wer was Gutes bekommt,

der bedankt sich auch.“

Wilhelm Busch

Ich bedanke mich von ganzen Herzen bei meinen Betreuern Prof. Dr. Roland Sanctuary und Dr. Jörg Baller für die unermüdliche Unterstützung, die sie mir über die letzten Jahre gegeben haben. Euer wissenschaftliches Know-How sowie eure Geduld waren der Schlüssel für diese Arbeit. Ihr habt es verstanden mir das Ziel aufzuzeigen und mich gleichzeitig wissenschaftlich frei entfalten zu lassen. Dafür gilt euch mein tiefster Dank.

Zudem möchte ich mich bei Prof. Dr. Christian Wagner bedanken, der - neben der fortlaufenden Betreuung als CET-Mitglied - meine Entwicklung durch seine Funktion als Programmbeauftragter des deutsch-französischen Physikstudienganges seit meinem ersten Studienjahr entscheident mitgeprägt hat. Ihre Tür stand zu jeder Zeit offen und dafür möchte ich mich ganz herzlich bedanken.

Natürlich möchte ich mich bei allen Mitarbeitern der AG Sanctuary bedanken. Die angenehme und lustige Arbeitsatmosphäre hat es leicht gemacht Tag für Tag motiviert zur Arbeit zu kommen. Ein spezieller Dank gilt Dr. Carlo Di Giambattista für die unzähligen lustigen und wissenschaftlichen Gespräche. Auch Dr. Marlena Filimon möchte ich ganz herzlich danken, welche mir zu jeder Zeit mit Rat und Tat zur Seite stand. Danke auch an Mathias für die angenehme Pausenbegleitung.

Ich möchte mich auch bei all meinen Freunden bedanken, die mir den nötigen Ausgleich gegeben haben und dadurch grossen Anteil am Erfolg dieser Arbeit haben. Vielen Dank an Lisa, Daniel, Ludwig, Ralf, Steffen, Sebastian, Adrian, Gianna, Johannes, Florimond, Adnan, Tarek, Janine, Daniela, Marthe, Malte sowie Matthieu für die lustigen Abende und vor allem Nächte. Vielen Dank auch an meine tollen Nachbarn Sena, Leo, Sina, Eva, Ben, Julian, Ursula und Corina: Die Grillabende sind und bleiben unvergessen.

Ich möchte vor allem meiner gesamten Familie danken. Ich danke dir liebe Mama und lieber Fabien für die immense Unterstützung. Ein ganz spezieller Dank gilt meiner Oma. Ihr habe ich auch diese Arbeit gewidmet, weil sie ein ganz besonderer Mensch ist. Auch Kristin und Nico möchte ich für unvergessliche Momente danken.